Neddylation-dependent protein degradation is a nexus between the metabolic syndrome, synaptic insulin resistance and Alzheimer's Disease

Dissertation

zur Erlangung des akademischen Grades

Doctor rerum naturalium (Dr.rer.nat.)

genehmigt durch die Fakultät für Naturwissenschaften der Otto-von-Guericke-Universität Magdeburg

von M.Sc. Alessandro Dario Confettura
geb. am 23/07/1988 in Catania (ITA)

Gutachter: Prof. Dr. rer. nat. Eckart D. Gundelfinger
Prof. Dr. Andreas Grabrucker

Eingereicht am: 27/05/2019
Verteidigt am: 19/11/2019

Table of contents

Summary

The metabolic syndrome (MetS) is a "lifestyle disease" characterized by heterogeneous factors comprising overweight, high blood pressure, lipid metabolism's disorder and insulin resistance (IR). Neurons are insulin sensitive cells, where the hormone normally plays fundamental roles ranging from glucose uptake to cell survival and synaptic plasticity. Prolonged exposure to insulin as well as neuroinflammation drive neurons to IR via down regulation of the activity of the Insulin Receptor Substrates (IRS), a protein family that organizes the cytosolic insulin signaling. Disruption of the insulin signal in the brain, especially in the hippocampus, has been extensively linked to cognitive impairments. Moreover, it is well established that IR and MetS have a functional link with amyloid-β deposition: this is believed to be a major risk factor for sporadic Alzheimer's disease (AD). This thesis tried to elucidate the topology of synaptic insulin signaling pathways in the hippocampus in order to understand the molecular basis of IR.

Inactivation of IRSs can occur via an abnormal phosphorylation or via protein degradation. In the first part of the thesis, we developed an *in vitro* model for synaptic IR that we could use to understand the basis of IR in neurons and generate hypotheses about the molecular mechanism. The results indicated that exposure to high concentration of insulin and the pro-inflammatory cytokine TNFα efficiently induces synaptic IR in cultured neurons. However, insulin and TNFα seem to have dual effects: neuroinflammation promotes synaptic IR via alteration of IRS phosphorylation, while prolonged exposure to insulin causes IRSs degradation. The combination of the two detrimental effects worsens neuronal IR, enhancing the down-regulation of the insulin pathway. Interestingly, we found that NEDD8 and the neddylation cascade may carry out a crucial role in the degradation of IRSs. NEDD8 is a small molecule, analogous to Ubiquitin, which is conjugated to target proteins via a similar enzymatic cascade. Most established target proteins of neddylation are ubiquitous proteins belonging to the family of cullins. Once neddylated, cullins act as E3-ubiquitin ligase, which ubiquitinate proteins leading to their proteasomal degradation.

In the second part of the thesis we developed a mouse model for a high-risk population with the combination of genetically driven amyloid-β deposition and high fat diet (HFD)-induced MetS. These mice, called TBA2.1, express in the brain pyro-glutamylated Aβ3(pE)-42, a post-translational-modified species of amyloid-β, known to be highly neurotoxic and inducing efficiently TNFα release from astroglia. This allowed us to study the combinatory effects of MetS and neuroinflammation also *in vivo*. We found that Aβ3(pE)-42-expressing animals, fed with an HFD undergo synaptic plasticity and memory impairments. This is also accompanied by protein degradation of neuronal IRSs and astroglia activation in CA1 hippocampal region.

Lastly, we sought whether inhibition of neddylation counteracts synaptic IR also *in vivo*. Although preliminary, the data showed that a pharmacological intervention that selectively blocks neddylation improves insulin sensitivity in neurons, ameliorating synaptic plasticity and memory performances.

Zusammenfassung

Das Metabolische Syndrom (MetS) ist eine Lebensstil-Erkrankung charakterisiert durch folgende heterogene Faktoren: Übergewicht, Bluthochdruck, eine Störung im Lipidstoffwechsel und Insulinresistenz (IR). In Neuronen als insulinsensitive Zellen spielt das Hormon eine fundamentale Rolle bei der Glukoseaufnahme, für das Überleben der Zellen und bei der synaptischen Plastizität. Eine anhaltende Exposition mit Insulin sowie neuroinflammatorische Prozesse führen zu einer Herabregulation von Insulin-Rezeptor-Substraten (IRS). Die IRS gehören zu einer Proteinfamilie, welche die Insulin-Signalkaskade steuern. Nachgewiesen ist, dass eine Störung bzw. Unterbrechung des Insulin-Signalweges im Gehirn, insbesondere im Hippocampus, zu ausgeprägten kognitiven Beeinträchtigungen führt. Des Weiteren ist bekannt, dass IR und MetS im Zusammenhang mit der Ablagerung von β-Amyloid-Peptiden stehen – einer der Hauptrisikofaktoren für das Auftreten einer Alzheimer Erkrankung (AD). Die vorliegende Arbeit beleuchtet die Topologie synaptischer Insulin-Signalwege im Hippocampus, um die molekularen Grundlagen dieser Prozesse genauer zu verstehen. Die Inaktivierung der IRS kann durch eine abnormale Phosphorylierung oder durch Proteinabbau geschehen. Ein im ersten Abschnitt der Arbeit entwickeltes *in vitro* Modell für synaptische IR liefert die Grundlage zum Verständnis von IR in Neuronen. Zusätzlich werden damit neue Hypothesen über deren molekulare Mechanismen aufgestellt. Vorliegende Ergebnisse deuten darauf hin, dass eine lange Exposition mit hohen Konzentrationen an Insulin und pro-inflammatorischem TNFα synaptische IR in Neuronen-Kulturen auslöst. Allerdings scheinen Insulin und TNFα zweierlei Effekte zu haben: (I) Neuroinflammatorische Prozesse fördern die Ausprägung einer synaptischen IR über eine veränderte IRS-Phosphorylierung, während (II) eine verlängerte Exposition mit Insulin zu einer Reduktion von IRS führt. Die Kombination beider negativer Effekte verschlechtert die neuronale IR und verstärkt gleichzeitig die Herabregulation des Insulin-Signalweges. In dieser Arbeit konnte gezeigt werden, dass bemerkenswerterweise die Neddylierung von Proteinen mit NEDD8 eine entscheidende Rolle für den Funktionsverlust von IRS spielt. Analog zu Ubiquitin ist NEDD8 ein kleines Molekül, welches über eine ähnliche Enzymkaskade mit entsprechenden Zielproteinen konjugiert ist. Bekannteste Zielproteine der Neddylierung sind ubiquitäre, zur Familie der Culline gehörende Proteine. Nach erfolgter Neddylierung agieren Culline als E3-Ubiquitin-Ligasen, ubiquitinieren Proteine und führen zu einem Proteasom-abhängigen Abbau. Im zweiten Abschnitt der Arbeit wurde ein Maus-Modell für besonders gefährdete Personengruppen mit folgender Faktorenkombination entwickelt: (I) genetisch bedingtes Risiko der Amyloid-β-Ablagerung und (II) MetS, induziert durch fettreiche Ernährung (Hoch-Fett-Diät; HFD). Dieses Mausmodell (TBA2.1) exprimiert im Hirn pyro-glutaminiertes Aβ3(pE)-42, eine post-translational modifizierte und in hohem Maße neurotoxische Variante von Amyloid-β, welche zudem effizient die Abgabe von TNFα aus Astroglia induziert. Dadurch konnten gleichzeitig Kombinationseffekte von MetS und neuroentzündlichen Prozessen *in vivo* untersucht werden. Aβ3(pE)-42-exprimierende mit fetthaltiger Kost ernährte Tiere zeigen gestörte synaptische Plastizität und eingeschränkte Gedächtnisfunktion. Begleitet wird dies von der Degradation von neuronalem IRS und Astroglia-Aktivierung in CA1-Regionen des Hippocampus. Zusätzliche stellte sich die Frage, ob auch *in vivo* eine Inhibition der Neddylierung synaptischer IR entgegenwirkt. Vorläufige Daten zeigen, dass eine pharmakologische

Intervention, welche selektiv Neddylierung blockiert, die neuronale Insulinsensitivität, synaptische Plastizität und Gedächtnisleistungen verbessert.

1. Introduction

1.1. Insulin signaling in the brain

Insulin is a small peptide hormone, consisting of two 21 and 30 long amino acidic chains, bound to each other via two disulfide bonds. Insulin is mainly produced by β-cells in pancreatic islets, released into the blood and once bound to its receptors in liver, muscle or fat tissue, promotes glucose uptake and regulates the metabolism of carbohydrates and fatty acids (Cheng et al., 2010). Normally, insulin induces the translocation at the cell surface of glucose transporters (GLUT), a family of uniporter proteins that facilitates the internalization of glucose across the plasma membrane. Insulin plays a fundamental role also in the brain, one of the highest energy demand organs (Raichle & Gusnard, 2002). The source of brain insulin is not yet known and it is essentially unclear whether it is synthesized locally in some brain regions or whether it is actively transported through the blood-brain barrier (Ghasemi et al., 2013). However, neurons abundantly express the glucose transporter GLUT3, considered as the main but not the exclusive neuronal glucose transporter (Leino et al., 1997; McCall, Van Bueren et al., 1994). GLUT3 is predominantly found in axons and dendrites and, to a lesser degree, in the cell body (Vannucci et al., 1997) (Figure 1A). Insulin promotes GLUT3 translocation to the plasma membrane in neurons (Uemura & Greenlee, 2006). The monomeric glucose can be either straightly catabolized by the cells or stored in glycogen deposits. Neurons accumulate minute amount of deposits (Saez et al., 2014); glia cells essentially carry out this role in the brain (Sinadinos et al., 2014).

It is nowadays well established that neurons are responsive to insulin since they express high levels of Insulin receptors (InsR) and their downstream effectors (Adamo et al, 1989; Blázquez et al, 2014; Plum et al, 2005) (Figure 1A). It has been shown, for instance, that insulin signaling in the hypothalamus contributes to food intake regulation (Baskin et al., 1999), metabolism and body energy balance (Hoyer et al, 1996). One of the most insulin-responsive areas of the brain is the hippocampus (McNay & Recknagel, 2011), where insulin signaling has been described to be required for synaptic plasticity, memory formation (Zhao et al, 2010) and neurotransmitter release (Jonas et al., 1997;

Wan et al., 1997). In addition, insulin seems to have neuroprotective functions (Apostolatos et al., 2012; Lee et al, 2011).

1.1.1. Insulin pathway and Insulin Receptor Substrate (IRSs) proteins

Insulin acts canonically via binding to the InsR as well as the insulin-like growth factor receptor (IGFR). Both InsR and IGFR are transmembrane receptors belonging to the large class of tyrosine kinase receptors. They are heterodimers composed of two extracellular α-subunits and two intracellular β-subunits. Insulin and insulin-like growth factor bind to the α-subunit of the receptor triggering the intrinsic tyrosine kinase activity of the receptor β-subunit. At the cellular level, InsR is enriched in neurons as compared to glia (Chiu & Cline, 2010; Unger et al., 1989), while at the subcellular level, InsR is expressed all along the plasmatic membrane and enriched in the postsynaptic density (PSD) of hippocampal neurons (Abbott et al, 1999; Chiu & Cline, 2010).

Activated InsR and IGFR recruit a family of scaffold proteins called Insulin receptor substrates (IRSs) and induce their phosphorylation. Mammals express different isoforms of IRSs proteins: IRS1, IRS2, IRS3, IRS4 and the more distantly related IRS5 and IRS6 (Cai et al., 2003). IRS1 and IRS2 are ubiquitously expressed and are the primary mediators of insulin-dependent regulation of glucose metabolism in most cell types (Mardilovich et al, 2002); IRS3, which is expressed in rodents, is largely restricted to adipose tissue (White, 2002). Both humans and rodents express also IRS4, found primarily in brain, kidney, thymus and liver (Lavan et al., 1997), where it constitutively induces insulin pathway activation in the absence of growth factors (Hoxhaj et al, 2013; Ikink et al, 2016). IRSp53, another member of the family also named Brain-specific angiogenesis inhibitor 1-associated protein 2 (BAIAP2), is highly enriched in the PSD of excitatory and inhibitory neurons (Burette et al., 2014) band works in the activity-dependent reorganization of the actin cytoskeleton (Heung et al, 2008). IRSp53 is a mobile scaffold protein that translocates to synapses in response to enhanced activity (Hori et al., 2005) (Figure 1B).

IRS1 and IRS2 are the most abundant and the best studied components of the IRS family in neurons and are the main adaptors of InsR/IGFR in brain (Yamada et al., 1997). Although IRS1 and IRS2 have a similar structure, IRS1 activity has been mainly

associated with InsR signaling whereas IRS2 is associated with IGFR signal (Talbot et al., 2012). Both IRS1 and IRS2 contain a phospho-tyrosine binding (PTB) and a pleckstrin homology (PH) domain; and include several sites of phosphorylation on tyrosine, threonine and serine residues. IRS proteins do not contain any intrinsic kinase activity, but once tyrosine-phosphorylated, rather serve as a docking site for several SH2 domain-containing proteins, including phosphatidylinositol 3-kinase (PI3K). The PH domain of IRS is responsible for the bound to Class I PI3K, which become active and in turn regulate several other proteins such as the RAC-alpha serine/threonine protein kinase (AKT), Ikk-β kinase (IKK), c-Jun-N-terminal kinase (JNK), protein kinase C (PKC), glycogen synthase kinase 3 β (GSK3β), extracellular signal-regulated kinase (ERK) and the mammalian target for rapamycin (mTOR) (Taniguchi et al, 2006) (Figure 1A).

Active IRS1 and IRS2 typically bind to PI3K at the SH2-domain of its p85 regulatory subunit, releasing the p110 catalytic subunit of PI3K which converts phosphatidylinositol (4,5)-bisphosphate ($PI(3,4)P_2$) into phosphatidylinositol (3,4,5)-triphosphate ($PI(3,4,5)P_3$). This secondary messenger is recognized by PDK1 protein and is important for the activation of a signaling cascade of phosphorylation in which AKT is a nodal point. AKT is phosphorylated by PDK1 and therefore regulate downstream effectors such as GSK3β, mTOR, as well as transcription factors important for survival and gene expression involved in homeostasis of dendritic and synaptic circuits (Agostinone et al., 2018). mTOR is another crucial protein in the cytoplasm which integrates signals from nutrients and various hormones. mTOR can be assembled into two distinct complexes: mTOR protein complex 1 (mTORC1) and complex 2 (mTORC2) (Kim et al., 2012). mTORC1 is directly phosphorylated by insulin-activated AKT and regulates the translational regulator S6K leading to increased protein synthesis (Zoncu et al, 2011). On the other hand, mTORC2, responds to insulin and other growth factors (Oh & Jacinto, 2011). Together with PDK1, mTORC2 phosphorylates AKT after insulin stimulation. Active AKT mediates the metabolic action of insulin initiating the release of glucose transporter containing vesicles and promoting mTORC1 signaling to drive protein synthesis (Zoncu et al., 2011) (Figure 1A).

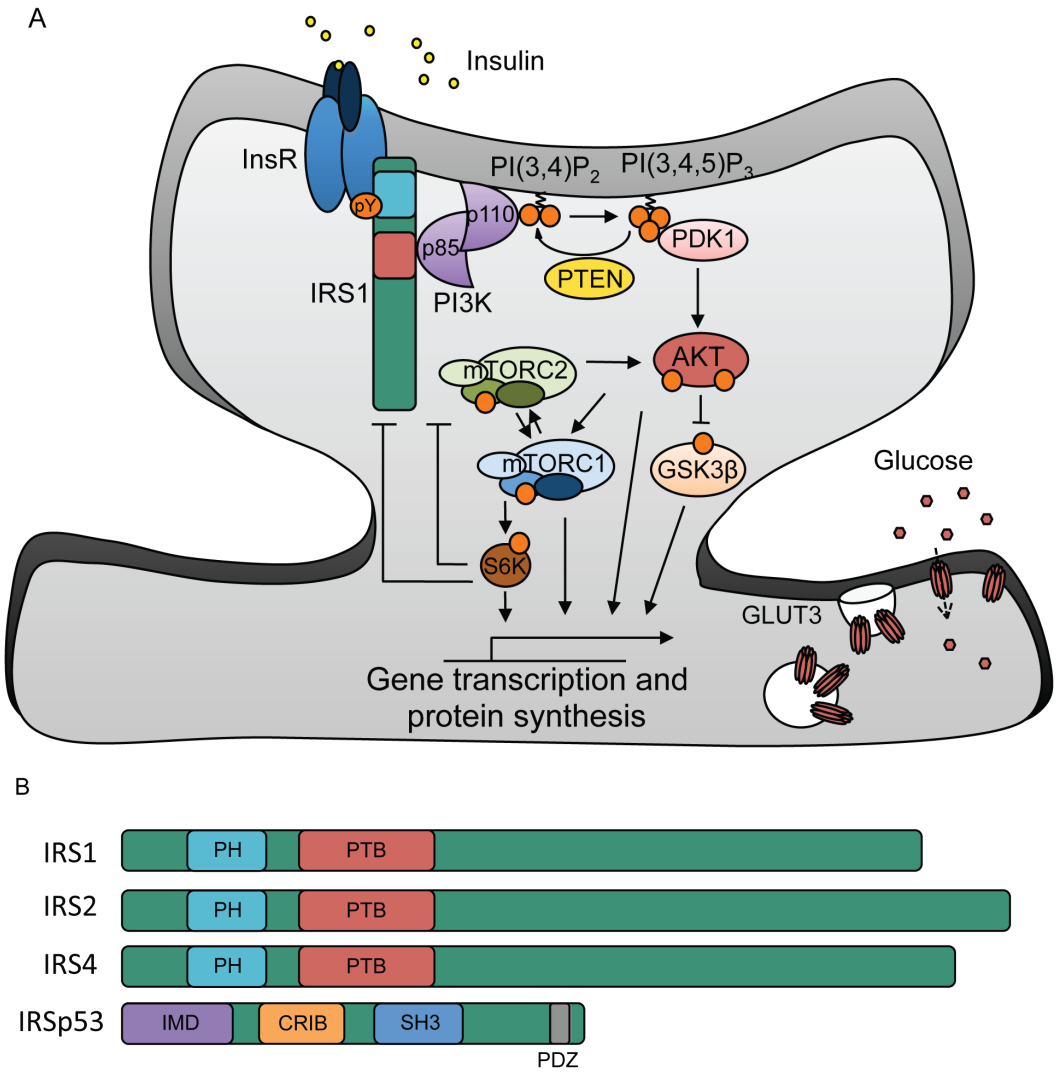

Figure 1: Insulin and Insulin receptor substrate family proteins. Insulin pathway at the post-synaptic terminal. (A) Insulin binds the InsR inducing the tyrosine phosphorylation of the IRS1 at tyrosine (pY). IRS1 interacts now with the receptor via its PH domain. The resulting conformational change makes IRS1 able to bind to the regulatory subunit (p85) of PI3K protein via IRS1 phosphotyrosine-binding (PTB) domain. The catalytic subunit of PI3K p110 is released and converts the membranous lipid $PI(3,4)P_2$ into $PI(3,4,5)P_3$. $PI(3,4,5)P_3$ is the second messenger that acts as an activator of PDK1. PDK1 phosphorylates AKT, which regulates many other pathways: release of GLUT3 containing vesicles, de-phosphorylation of GSK3β, induction of the assembly of the mTORC1 complex. mTORC2 is another mTOR-containing complex that also phosphorylates AKT. S6K kinase is one of the target proteins of mTORC1, important for activation of the protein translation and that can de-phosphorylate IRS1 in a negative feedback mechanism. Orange circles depict phosphorylation sites. (B) Insulin receptor substrate family in neurons. Interaction domains of the IRS proteins are indicated. Pleckstrin homology domain (PH); phosphotyrosine binding domain (PTB), IRSp53/MIM Homology Domain (IMD); Cdc42 and Rac-interacting binding domain (CRIB); Src-homology domain 3 (SH3); Post-synaptic Density 95/Disc Large/Zonula Occludens-1 domain (PDZ).

1.2. Synaptic insulin resistance (IR) and metabolic syndrome (MetS)

Insulin resistance (IR) is defined as an imbalance of insulin-glucose homeostasis in which the ability of cells to respond to insulin is reduced, leading to an impairment in insulin-induced glucose uptake in peripheral tissues (e.g. skeletal muscle and adipose tissue) or in inhibition of hepatic gluconeogenesis (Wheatcroft et al., 2003). IR develops as a result of genetic factors combined with lifestyle and environmental factors, i.e. high caloric nutrition together with low physical exercise, all factors having a high prevalence in western countries (Lebovitz & Harnold 2006). IR is present in several severe metabolic diseases such as type-2 diabetes, obesity and the so-called metabolic syndrome (MetS). MetS was first described in 1988 by Reaven (Reaven, 1988) and can be defined as a "lifestyle disease" characterized by several factors comprising overweight, high blood pressure, lipid metabolism disorder with IR being at the core of the syndrome (DeFronzo, 2010).

1.2.1. Synaptic IR

IR and the MetS are direct consequences of the interruption of the normal insulin homeostasis, and this can also occur in the central nervous system. It is indeed known that IR and MetS severely affect regular brain activity with a particular impact on the hippocampus and prefrontal cortex (Crawley, 1999; Wiedenmann & Franke, 1985). These structures are the most important for learning and memory, but also the most metabolically active brain regions with the highest expression of protein members of the insulin cascade (De Felice & Benedict, 2015). Since its discovery decades ago, this suggests that insulin could play a role in synaptic plasticity mechanisms and memory formation. Furthermore, studies carried out on individuals with MetS, e.g. diabetic or obese patients, have found an association between MetS and significantly poorer cognitive performance, further followed by a decline in cognitive function (Lutski et al., 2017). The cognitive impairment is extensively correlated to the development of synaptic IR, a direct consequence of the reduced activity of the downstream insulin signaling in synapses (Zhao & Alkon, 2001). Thus, the synaptic IR is nowadays considered as an important risk factor for neurodegenerative diseases (Schubert et al., 2003). Moreover,

the effects of the MetS on synaptic activity are more prominent in elderly people, who seem to be more prone to develop dementia (Kuljiš & Salković-Petrišić, 2011). As a confirmation of the dual relationship between IR and cognition, it has been shown that high-intensity physical exercise ameliorates IR as well as cognitive deficits, affecting brain plasticity and positively influencing the wellbeing (Mandolesi et al., 2018). Therefore, people with MetS constitute a high-risk population for the development of diabetes and obesity, but also cognitive impairment and age-related cognitive decline (Frisardi et al., 2010). Additionally, it has been shown that IR and MetS show a functional interaction with amyloid-β deposition: this is believed to be a major risk factor for sporadic Alzheimer's disease (AD) (Frisardi et al., 2010; Pasinetti & Eberstein, 2008). Epidemiological reports have evidenced that MetS increases about 10 times the risk of contracting the diseases in subjects with amyloidosis (Biessels et al., 2006; Hämäläinen et al., 2007; Profenno et al., 2010) (Figure 2).

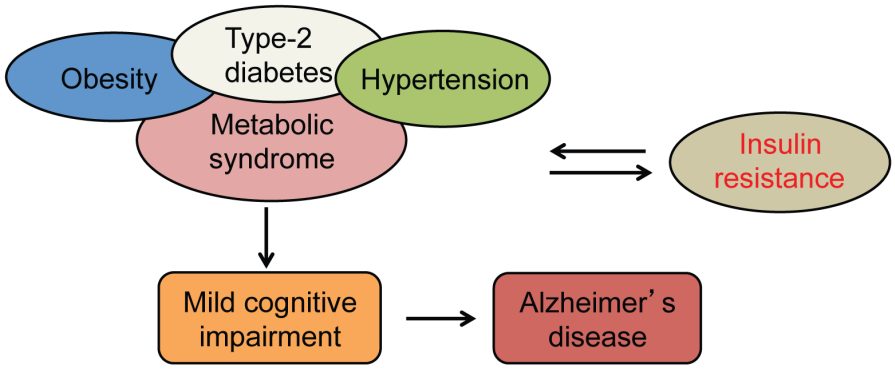

Figure 2: Metabolic syndrome, synaptic insulin resistance and cognitive impairment. MetS is a complex metabolic disorder characterized by overweight, high blood pressure, and lipid metabolism alterations. These conditions canonically are associated with pathologies such as obesity, hypertension and diabetes. MetS and related diseases have IR at the core of the pathology (De Fronzo et al., 2010). Moreover MetS is a risk factor for mild cognitive impairment and, in the interaction with amyloidosis, for sporadic Alzheimer's disease (Pasinetti & Eberstein, 2008).

In order to elucidate the consequences of synaptic IR on brain function, numerous animal models have been generated and fed with a high-fat/caloric diet (HFD) (Petrov et al., 2015). Nonetheless, the molecular mechanism, which can explain the onset of synaptic IR, is still far from being understood. It has been demonstrated that mice fed with an HFD develop cognitive deficits, decreased dendritic spine density and display a reduction

of the expression of some synaptic markers in prefrontal cortex and hippocampus already after 8 weeks of diet (Bocarsly et al., 2015). This is associated in cortical and hippocampal neurons with a reduced activity of proteins that are directly or indirectly under the control of the InsR such as IRS, AKT, S6K and GSK3β (Arnold et al., 2014).

1.2.2. Phosphorylation of IRS1

The phosphorylation of IRS proteins is a crucial regulatory step in the intracellular insulin pathway. E.g. IRS1 contains up to 20 potential tyrosine phosphosites. Those are mainly associated with a positive regulation of IRS1, which in turn activates the downstream effectors AKT, mTOR and GSK3β. However, IRS1 is also regulated via serine and threonine phosphorylation at numerous sites (Gual et al, 2005). Although serine phosphorylation at specific sites can enhance insulin signaling (Giraud et al., 2004; Luo et al., 2007; Paz et al., 1999), most studies support the hypothesis that hyper-serine/threonine phosphorylation of IRS1 results in reduced activity of the whole insulin cascade, triggering IR in many cell types: adipocytes (Sevillano et al., 2007), myocytes (Stuart et al., 2017) and neurons (Mayer & Belsham, 2010; Talbot et al., 2012). However, IRS1 serine phosphorylation is a normal adaptive feedback/feed-forward mechanism that finely regulates insulin signaling, limiting the action of insulin when it is not required. Nevertheless, over-activation of IRS mostly due to elevated food intake, might result in hyper serine phosphorylated IRS1.

At the molecular level, serine-phosphorylated IRS1 causes reduction of docking of IRS1 to PI3K, shutting-off of the insulin-induced activation of AKT. This is considered to be one of the main hallmarks of IR in both mouse and human (Hirosumi et al., 2002; Talbot et al., 2012; Yarchoan et al., 2014). Numerous kinases including mTOR have been linked to IRS1 regulation. For instance mTORC1 activation by rapamycin has been linked to phosphorylation of IRS1 at Ser632/635 (murine sequence) (Gual et al., 2005). IRS1 is also phosphorylated at Ser302 by S6K. Increased phosphorylation at this site along with Ser632, Ser635 and Ser302 has been observed in mouse models of obesity and IR (Harrington et al., 2004; Um et al., 2004; Werner et al, 2004). Additionally, insulin-independent kinases can phosphorylate IRS1 and IRS2 under basal conditions like GSK3β or the 5'-AMPK-activated protein kinase (AMPK) (Amato & Man, 2012).

AMPK is canonically activated by the presence of abundant ATP produced by the glucose metabolism, while GSK3β is regulated by direct phosphorylation/de-phosphorylation carried out by many phosphatases and kinases, including AKT (Doble & Woodgett, 2003) (Figure 3).

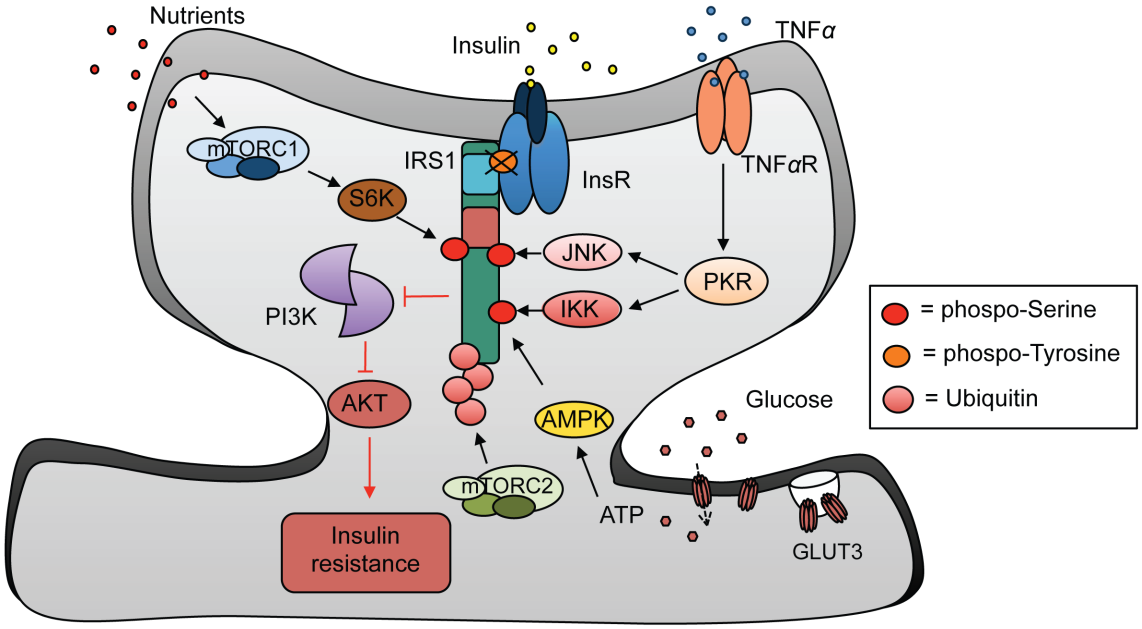

Figure 3: IRS1 phosphorylation and protein degradation. IRS1 is tyrosine phosphorylated upon insulin activation of InsR. TNFαR activates PKR and other stress-response kinases such as IKK and JNK, which phosphorylate IRS1 at serine residues. IRS1 can be serine-phosphorylated also by AMPK, which is active in presence of abundant ATP, and S6K, a protein kinase activated by mTORC1. Once phosphorylated by mTORC2, IRS1 is more prone to be ubiquitinated. Serine-phosphorylation of IRS1 as well as IRS1 degradation reduces the binding of InsR to IRS1, which can thus be de-phosphorylated at the tyrosine sites (marked with the black cross). Altogether, this results in the reduction of docking of PI3K to IRS1, de-phosphorylation of AKT and IR.

Pro-inflammatory cytokines such as tumor necrosis factor α (TNFα) can also regulate the insulin pathway. Following the activation of the TNFα receptor (TNFαR), stress-response kinases such as PKR, JNK and IKK induce serine-phosphorylation of IRS1 (Bomfim et al., 2012) and this has been strongly linked to IR and impaired insulin signal in neurons (De Felice, 2013). Protein kinase R (PKR) is a protein kinase activated by double-stranded RNA (dsRNA) typically generated by viral replication and is induced by pro-inflammatory cytokines such interferon-γ and TNFα. Active TNFα pathway leads to

phosphorylation of PKR, which has been linked to inhibition of IRS1 and IR via serine-phosphorylation of IRS1 (Lourenco et al., 2013).

1.2.3. IRS1 protein degradation

The phosphorylation of IRS is not the only regulatory mechanism controlling protein expression. It is known that an ubiquitin/proteasome-dependent degradation process also regulates protein levels of IRSs (Mayer & Belsham, 2010; Sun, Goldberg, Qiao, & Mitchell, 1999). Decreased cellular levels of IRS1 and IRS2 have been shown to be associated with IR in animal and human subjects (Tamemoto et al., 1994; Zhande et al., 2002). IRS1 down-regulation can by itself lead to IR and the development of diabetes (Hartley et al., 2006; Kerouz et al., 1997; Kido et al., 2000). At the molecular level, IRS1 protein degradation is tightly regulated by the activity of its own downstream effectors: the inhibition of PI3K or mTOR counteracts the down-regulation of IRS1 (Egawa et al., 2000; Scott et al., 1998). PI3K and mTORC2 regulate the ubiquitin ligase substrate-targeting subunit Fbxw8 leading to Fbxw8-dependent IRS1 turnover following insulin stimulation (Kim et al., 2012). In addition, serine-phosphorylation of IRS1 can eventually have a role in the regulation of IRS1 protein degradation, thereby promoting IR (Hotamisligil et al., 1996; Kim et al., 2012; Liu et al., 2004; Shah & Hunter, 2006; Tremblay et al., 2007). Intriguingly, it has been recently shown that mTORC1 and its main downstream target S6K phosphorylate IRS1 at specific serine residues (Ser422) making IRS1 more prone to be ubiquitinated and degraded (Yoneyama et al., 2018) (Figure 3). Collectively, published work has demonstrated that PI3K, mTORC1 and mTORC2 have a crucial role in IRS1 protein degradation.

1.3. Ubiquitin-dependent proteasomal protein degradation

Ubiquitin is a 76-long peptide that is conjugated to target proteins via a highly regulated enzymatic process called ubiquitination. The target proteins are generally poly-ubiquitinated and targeted to the 26 S proteasome, a multiprotein complex that recognizes the ubiquitin-bound proteins and induces proteolysis (Thrower et al., 2000). Ubiquitination is an essential process for degradation of certain proteins that are semi-

degraded or misfolded. Protein degradation regulates protein turnover and plays an important role in several cellular processes ranging from DNA replication, to glucose sensing and circadian rhythms (Varshavsky, 2017). It is well documented that not only novel protein synthesis (Byrne et al., 1991; Wang and Morris, 2010) but also proteasomal protein degradation is essential for synaptic plasticity, learning and memory consolidation (Artinian et al., 2008; Dong et al., 2014; Jarome et al., 2011; Karpova et al., 2006). It has been shown for instance that pharmacological inhibition of proteasome via injection of lactacystin in the CA1 region of the hippocampus impaired fear memory in mice (Karpova et al., 2006; Lopez-Salon et al., 2001). In addition, dysfunction in the ubiquitin-proteasome protein degradation leads to several neurodegenerative diseases, characterized by pathological aggregates of misfolded proteins (Chen et al., 2002; Tai & Schuman 2008).

1.3.1. NEDD8 and the neddylation pathway

Neural precursor cell-expressed developmentally down-regulated gene 8 (NEDD8) is an 82-amino acid long ubiquitin-like protein that shares 80% homology with the amino acid sequence of ubiquitin (Kamitani et al., 1997).

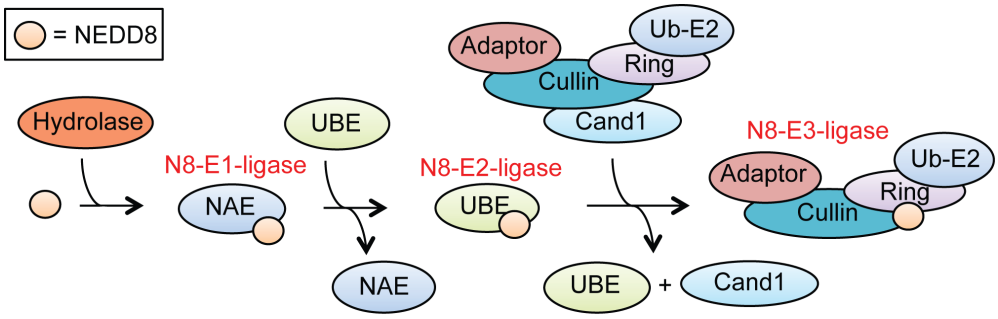

Figure 4: Schematic representation of the neddylation pathway. NEDD8 is conjugated to cullins through three enzymatic reactions that comprise NEDD8-E1 (NAE), NEDD8-E2 (UBE2F or UBE2M), and NEDD8-E3 (shown is only CAND1) ligases. In order to be loaded onto NEA enzyme, NEDD8 is first cleaved by C-terminus NEDD8-hydrolase. NAE activates NEDD8 by first adenylating its C-terminal glycine residue with ATP, thereafter linking this residue to the side chain of the catalytic cysteine, yielding a NEDD8-UBA3 thioester and free AMP. The exchange factor CAND1 regulates the transfer of NEDD8 to cullin–RING core complexes.

The process allowing conjugation of NEDD8 to target proteins is called neddylation. Neddylation, in a similar fashion to ubiquitination, consists of the covalent bound of NEDD8 to lysine residues of target proteins via three sequential enzymatic reactions, involving E1, E2 and E3 ubiquitin ligases (Pan et al., 2004) (Figure 4). The main substrates and most described targets of the neddylation pathway are proteins belonging to the family of cullins (Petroski & Deshaies, 2005). However, recent research revealed that neddylation may also occur on other substrates such as PSD95 regulating its protein function and the reorganization PSD (Vogl et al., 2015).

1.3.2. Cullin E3-ubiquitin ligases

Cullins are a family of proteins that provide support for ubiquitin ligases (E3). They combine with RING (really interesting new gene) proteins that appear to function as a docking site for ubiquitin-conjugating enzymes (E2s) to form cullin-RING ubiquitin ligases (CRL). CRLs are multi-subunit complexes that are composed of a RING protein Rbx1 or Rbx2, cullin protein, adaptor protein and a substrate recruitment factor (Kleiger et al., 2009).

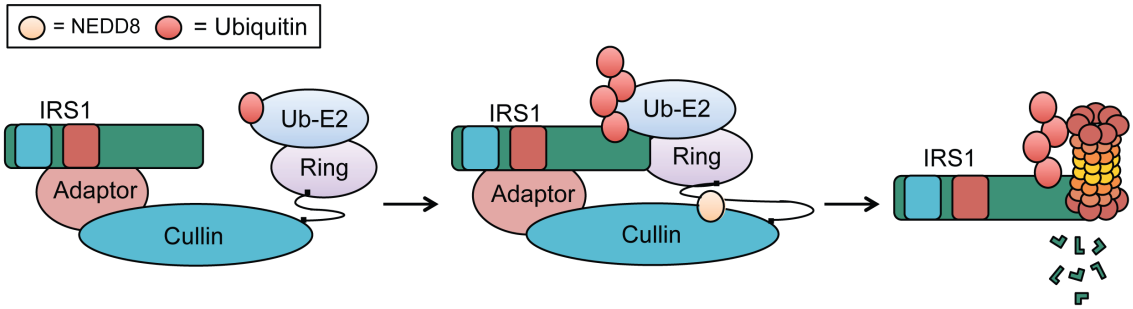

Figure 5: Neddylation triggers the ubiquitin-E3 ligase activity of cullins. The neddylation of cullin-RING complex induces a conformational change at the C-terminus of cullin that makes the substrate protein (in the figure is represented IRS1) in close proximity to the adaptor protein RING and the ubiquitin-E2 ligase (Ub-E2) that exchanges the ubiquitin to the substrate.

Each member of the cullin family is conjugated with NEDD8 in a highly regulated process (Figure 5) but the neddylation of cullins does not drive itself to the degradation of the protein. This post-translational modification instead modulates the activation of the corresponding CRL complex, probably through conformational regulation of the

interactions between cullin C-terminal tail and CRL's RING subunit (Sarikas et al., 2011). The activated cullins bind target proteins, ubiquitinate them and render them susceptible for proteosomal degradation.

In mammals, the cullin family consists 9 members: CUL1, CUL2, CUL3, CUL4A, CUL4B, CUL5, CUL7, CUL9 and the closely related p53-associated parkin-like cytoplasmic protein (Parc) (Figure 6). With the exclusion of CUL9, all the isoforms are expressed in the brain (Allen mouse and human Brain Atlas. http://portal.brain-map.org/). The cullin family proteins are involved in several processes among the different cell types and they seem to be widely expressed and to locate both in the nucleus and cytoplasm (Sarikas et al., 2011). Interestingly, it has been shown that Cullin 7 (CUL7) has an important role in the ubiquitin-dependent degradation of IRS1 in HEK cells (Xu et al., 2008). Fibroblasts from CUL7 -/- mice are prone to accumulate IRS1 in the cytoplasm and exhibit enhanced insulin responsiveness (Xu et al., 2008). How CUL7 functions at the molecular level is currently unknown (Ponyeam & Hagen, 2012). The molecular structure of this isoform differs from the rest of the family members by the absence of cullin repeat domains (Figure 6). However, CUL7 contains a Cullin Homology (CH) domain as encountered in the other cullins; therefore forming a CRL complex via the binding of CH domain to the RING protein Rbx1 (Arai et al., 2003; Dias et al., 2002), thus mediating poly-ubiquitination of specific substrates. The most studied interacting partner of CUL7 is the ubiquitin ligase substrate-targeting subunit Fbxw8 that binds to a CUL7 domain that is not conserved in other cullin proteins (DOC) (Dias et al., 2002; Ponyeam & Hagen, 2012). As discussed above, Fbxw8 is phosphorylated by the action of mTORC1/S6K. This suggests that together CUL7, Fbxw8 and mTOR may have an important role into IRS1 degradation and the regulation of the entire insulin pathway. Moreover, the conserved lysine residue for NEDD8 modification is also present in CUL7. However, it has not been clarified whether NEDD8 is covalently attached to CUL7 (Ponyeam & Hagen, 2012).

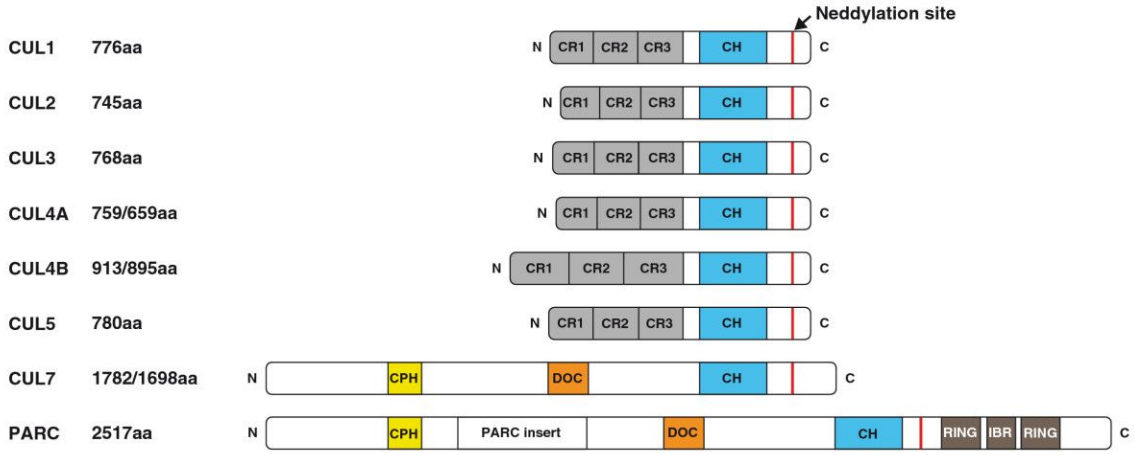

Figure 6: Structural organization of Cullin proteins. Cullin repeat (CR) anchors adaptor proteins of the CRL, and the cullin homology domain (CH) at the C-terminus is critical for binding of the RING-finger protein. The red line indicates the position of the neddylation site. CPH is a conserved domain in CUL7 and PARC; DOC is a domain similar to the domain of the anaphase-promoting complex/cyclosome but of unknown function; IBR is In Between RING while RING is the Really Interesting New Gene. Cartoon from Sarikas et al., 2011.

1.4. Alzheimer's disease (AD)

Alzheimer's disease (AD) is considered nowadays the most widespread cause of dementia in elderly (estimated about 60%-80% of all dementia cases) and it is estimated to be the 6th most frequent cause of death among the northern countries (Hebert et al., 2013). It is a debilitating disease characterized by neuronal cell loss, impairment of cognitive function and memory (Bronzuoli et al., 2016; Ferri et al., 2005; Selkoe, 2002; Shankar & Walsh, 2009; Viola & Klein, 2015). Patients with AD are unable to perform daily tasks and require constant care. Dr. Alois Alzheimer has described the disease for the first more than one century ago. Nowadays, despite the many years of investigation in the field, the etiology and pathogenesis of sporadic AD is still under debate and the disease remains incurable (Bronzuoli et al., 2016; Shankar & Walsh, 2009; Viola & Klein, 2015). Moreover, given the worldwide increase of life expectancy, the number of people at risk age to contract the disease increases constantly, rising up the costs for the national health care systems of these counties.

The hallmark that mainly characterizes AD is the accumulation of amyloid-β (Aβ) in the brain that leads to the formation of senile plaques. Aβ is formed by the cleavage of the

amyloid precursor protein (APP) by β- and γ-secretase. After cleavage, Aβ peptides often aggregate forming oligomers (Aβos), fibrils and plaques. Although some Aβos are believed to be essential for neuronal survival in picomolar concentrations (Abramov et al., 2009; Fogel et al., 2014; Pearson & Peers, 2006), several of these Aβ forms are found in the brain of AD patients. The two major isoforms of peptides produced by the activity of β- and γ-secretase are Aβ1-40 and Aβ1-42. These soluble Aβos are nowadays believed to be the major responsible agents for the onset of the disease (Klein, 2002; Lambert et al., 1998; Shankar & Walsh, 2009; Viola & Klein, 2015). It has been shown from several groups that Aβos induce LTP impairment (Cullen et al., 1997; Jo et al., 2011; Kamenetz et al., 2003; Lambert et al., 1998; Shankar & Walsh, 2009; Walsh et al., 2002), LTD (D'Amelio et al., 2011; Shankar et al., 2008), synapse loss (Heinonen et al., 1995; Selkoe, 2002; Shankar et al., 2007) and subsequent neuronal death (Ingelsson et al., 2004; Lacor et al., 2007; Viola & Klein, 2015).

1.4.1. Post-translational modification of Aβos

Besides Aβ1-40 and Aβ1-42, numerous Aβ species have been discovered in the brain of AD patients. These different isoforms of Aβos arise from post-translational modifications of Aβ1-40 and Aβ1-42 (Jawhar et al., 2011; Kummer & Heneka, 2014; Saido et al., 1996). Plenty of modifications have been identified, such as nitrosylation, racemization oxidation and many others. Many of these Aβ species are truncated at the N-terminus (Bayer & Wirths, 2014; Hosoda et al., 1998; Jawhar et al., 2011; Sergeant et al., 2003). Once truncated, glutamate residues at the N-terminus can be cyclized by the activity of the glutaminyl cyclase (QC), an enzyme that is known to be up regulated in the plasma of AD patients (Jawhar et al., 2011; Schilling et al., 2008). QC activity generates pyro-glutamylated-β amyloid peptide Aβ3(pE)-42. Some studies have indicated that Aβ3(pE)-42 is a major constituent of Aβ deposits in human AD brain (Harigaya et al., 2000; Portelius et al., 2010; Russo et al., 1997; Saido et al., 1996; Wirths et al., 2010). It has been shown that Aβ3(pE)-42 is prone to oligomerization and aggregation. Additionally the cyclic peptide is more resistant to degradation than the un-truncated Aβ1-40 and Aβ1-42 (D'Arrigo, Tabaton, & Perico, 2009; Mandler et al., 2014; Schilling et al., 2006; Schlenzig et al., 2009).

1.4.2. Neuroinflammation and AD

Unlike in familial AD (where defined genetic mutations cause overproduction of the Aβ peptide), in the sporadic form of the disease, amyloid-β deposition precedes of many years the onset of the first memory decline (Bateman et al., 2012; Jack et al., 2013; Petrella, 2013). Additionally, it has been shown that in many cases amyloid-β or neuro-deposition does not overlap with clinical disease manifestations (Davis & Chisholm, 1999; Matthews et al., 2009; Perez-Nievas et al., 2013; Price et al., 2009).

Pro-inflammatory cytokines have profound impact on the onset or exacerbation of many diseases including chronic inflammatory diseases and autoimmunity (Calsolaro & Edison, 2016; Sonar & Lal, 2017; Tiwari & Pal, 2017). For many years, the neuroinflammatory processes observed in AD patients' brains were attributed to side effects evoked by senile plaques and neurofibrillary tangles. Nevertheless, more recent studies have reported that prolonged neuroinflammation itself plays an important role in the onset and progression of the disease (Bronzuoli et al., 2016; Floden et al., 2005; Heneka et al., 2015; Johnston et al., 2011; Meraz-Ríos et al., 2013). Aβ internalization leads to microglia activation, which in turn produce pro-inflammatory chemokines and cytokines, including TNFα (He et al., 2007; Heneka et al., 2015; Heppner et al., 2015; Meraz-Ríos et al., 2013; Wang et al., 2004). Alteration of the astrocytic activation and uptake of Aβ can be observed during aging and correlates with clinical pathology of AD (Heneka et al., 2015; Meraz-Ríos et al., 2013; Nielsen et al., 2010; White et al., 2005). Recent work published from our group demonstrated that the post-translationally modified Aβ peptide Aβ3(pE)-42 has potent effects on the induction of glial release of TNFα after the uptake from astrocytes, contributing to synaptic dysfunction (Grochowska et al., 2017). In this context, Aβ3(pE)-42 is the initiator of a vicious cycle leading to release of pro-inflammatory cytokines that in turn contribute to the progression of AD.

1.4.3. Role of TNFα in synaptic IR and AD

In addition to this scenario, several authors reported that an abnormal neuroinflammatory mechanism has a major contribution to the onset of neuronal IR

(Borst, 2004). As described above, it is well established that TNFα release alone is able to induce serine-phosphorylation of IRS1, via the activation some stress-kinases such PKR, IKK and JNK (Aguirre et al., 2000; Lourenco et al., 2013; Motta et al., 2015; Zhang et al., 2016) as well as impact on AKT activation (da Costa et al., 2016; Fairaq et al., 2015; Kim et al., 2017; Plomgaard et al., 2005). Elevated serine-phosphorylated IRS1 have been found also in postmortem AD patients (Yarchoan et al., 2014). People with clinical AD, and/or Aβ biomarkers exhibit abnormal insulin levels and insulin metabolism (Correia et al., 2011; de la Monte, 2009). The presence of Aβ peptides and pro-inflammatory cytokines release has been associated to an altered phosphorylation of IRS1 and disrupted insulin pathway (Ma et al., 2009; Moloney et al., 2010; Talbot et al., 2012).

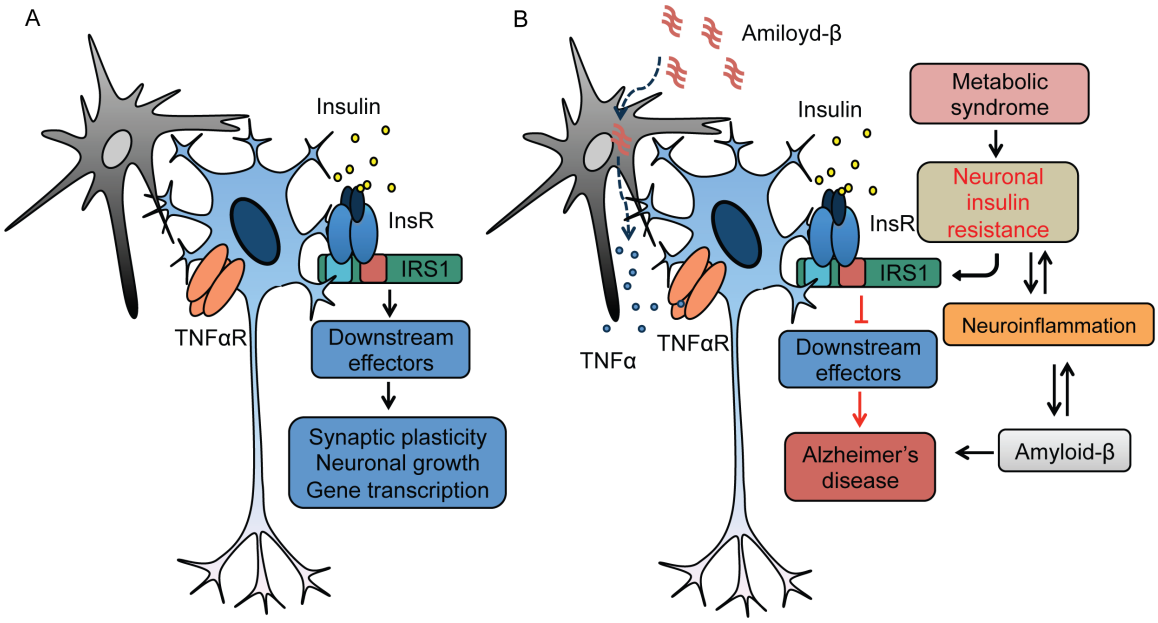

Figure 7: Panel summarizing schematically the relationship between IR, MetS and AD comparing the condition of healthy insulin signaling and pathological one. (A) Canonically, insulin activates the InsR and IRS1. Normal insulin activation results in the regulation of gene transcription of genes involved in cell survival, neuronal growth and synaptic plasticity. (B) MetS and the consequent neuronal IR interrupt the downstream effectors activation. Amyloid-β uptake by astroglia, followed by TNFα released, induces neuroinflammation. Neuroinflammation and amyloid-β exacerbate synaptic IR. Altogether amyloid-β, synaptic IR and neuroinflammation are significant contributors to AD onset. Picture modified from Kim et al., 2012

Moreover, it has been shown that Aβos are implicated in the removal of InsR from the neuronal plasma membrane (De Felice et al., 2009; Zhao et al., 2008) leading to IR. As a

confirmation of the tight relation between IR and AD, many authors have shown that administration of insulin or the insulin sensitizer-like metformin to patients with AD improve cognitive function and memory (Craft et al., 2012; Koenig et al., 2017).
Therefore, MetS and IR seem to interact with AD progression in a bidirectional manner, in which the neuroinflammation may act as a key link. A straightforward hypothesis deriving from this scenario is that pro-inflammatory signal is induced by amyloidosis, which in turn promotes synaptic IR via alteration of IRSs phosphorylation. Prolonged exposure to insulin causes IRSs degradation; this results in an increase of TNFα release, worsening AD pathology.

1.5. Aims of the project

"*Mens sana in corpore sano*" ("healthy brain in a healthy body"; cit. from D.I Iuvenalis, Satires, X, 356). The concept of the tight correlation of a healthy life style and the proper functionality of the brain is known since many centuries. However, the molecular mechanisms that can explain how the body health can positively affect cognitive performances are still far away from being understood.
In this PhD thesis we attempted to give new insights on the molecular mechanism behind the noxious effects of high-caloric diet that overexpose neurons to high concentrations of insulin. We wanted to elucidate, at the synaptic level, the effects of high-fat diet and its interplay with amyloidosis, in order to better understand how IR connects to neuronal dysfunction that results in age-related cognitive decline and AD. To this end, we have first generated an *in vitro* model of synaptic IR where we could investigate the molecular mechanism of IR at single molecule level. In particular we aimed to understand the role of neddylation-dependent IRS degradation in the onset of the disorder.
Little is known about NEDD8 in neurons and even less about a possible role of neddylation into AD's onset, therefore we aimed to find a nexus between synaptic IR and AD that can be explained by the action of NEDD8 on the insulin pathway. Our main purpose was to clarify the relationship between synaptic IR and neuroinflammation *in vivo* using TBA2.1 mice as a model for high-risk population with amyloidosis and HFD-induced synaptic IR. Last, we sought whether pharmacological blockade of neddylation could be a potential entry point for intervention against synaptic IR.

2. Materials and methods

2.1. Materials

2.1.1. Chemicals

The chemicals used in this study were obtained from Calbiochem, Clontech/Takara, Gibco Life Technologies, Invitrogen, Merck Millipore, Roche, Roth, Sigma-Aldrich, and Baxter Deutschland GmbH. Buffers and solutions for protein biochemistry and molecular biology were prepared using deionized water (SeralpurProCN®, Seral) and Milli-Q water (Milli-Q®, Millipore).

2.1.2. Enzymes and kits

Table 1. Enzymes and kits

Name	Supplier	Application
Restriction enzymes	New England Biolabs	Cloning
Nucleospin Gel and PCR clean-up	Macherey-Nagel	
Pfu/Pfu+ DNA polymerase	Roboklon	
Taq DNA polymerase	Invitrogen/Thermo Fisher Scientific	
T4 ligase	Invitrogen/Thermo Fisher Scientific	
dNTPs	Bio&SELL	
Primers/oligonucleotides	Invitrogen/Thermo Fisher Scientific	
pGemTeasy vector system	Promega	
Sensiscript Reverse Transcription	Qiagen	
Lipofectamine 2000	Invitrogen/Thermo Fisher Scientific	Transfection of neurons
Sensiscript Reverse Mouse TNFα Quantikine ELISA	Promega	Quantification of TNFα from tissues
Rat/Mouse Insulin ELISA kit	Merck Millipore	Quantification of Insulin from serum
PI3-Kinase Activity ELISA: Pico	Echelon Biosciences	Quantification of PI3Kγ activity

2.1.3. Buffers and solutions

Table 2. List of buffers and solutions

Name	Supplier	Application	
4X SDS-sample buffer (Laemmli buffer)	250 mM Tris-HCl, pH 6.8, 1% (w/v) SDS, 40% (v/v) Glycerol 20% (v/v) β-mercaptoethanol, 0.004 % Bromophenol Blue	Western blot and SDS-PAGE	Protein extraction and loanding buffer
Amido black solution	14.4 g amido-black in 1ml of 9:1 methanol-acetic acid solution		Protein concentration measurement
Electrophoresis buffer	192 mM glycine, 0.1 % (w/v) SDS, 25 mM Tris-base, pH 8.3		SDS-PAGE
Blotting buffer	192 mM Glycine, 0.2 % (w/v) SDS, 20% (v/v) Methanol, 25 mM Tris-base, pH 8.3		Western Blot
Ponceau red	0.5 % (w/v) Ponceau S in 3%(v/v) acetic acid		Verification of transferring
TRIS buffer saline (TBS)	25 mM Tris-HCl, 150 mM NaCl, pH 7.4		Washing buffer
TBS-T	TBS, 0.1% (v/v) Twien-20, pH 7.4		Washing buffer
TBS-A	TBS, 0.02% NaN3 pH 7.4		Primary antibody dilution
Blocking buffer	TBS-T, 5% either BSA or non-fat milk powder		Blocking membrane
Stacking polyacrylamide gel (5%) calculated for 5 gels	2.5 ml 0.5 M Tris-HCl pH 6.8, 1.6 ml 30% Acrylamide, 3.25 ml dH_2O, 100 µl 10% SDS, 100 µl 0.2 M EDTA, 50 µl Phenol red, 57 µl 10% APS, 7 µl TEMED		SDS-Page gel
Running polyacrylamide gel (20%) calculated for 5 gels	2.85 ml 1.5 M Tris-HCl pH 8.8, 6.75 ml 40% acrylamide, 0.58 ml dH_2O, 3 ml 87% Glycerol, 132 µl 10% SDS, 132 µl 0.2 M EDTA, 20 µl Bromophenol Blue, 57 µl 10% APS, 9 µl TEMED		SDS-Page gel

Running polyacrylamide gel (5%) calculated for 5 gels	2.85 ml 1.5 M Tris-HCl pH 8.8, 1.69 ml 40% Acrylamide, 7.89 ml dH_2O, 0.75 ml 87% Glycerol, 132 µl 10% SDS, 132 µl 0.2 M EDTA, 48 µl 10% APS, 9µl TEMED	Western blot and SDS-PAGE	SDS-Page gel
Permeabilization buffer	PBS, 0,25% Triton-X 100, pH 7.4	ICC	Cell permeabilization
ICC blocking buffer	2% glycine, 2% BSA, 0.2% gelatin and 50 mM NH_4Cl		Blocking buffer
IHC blocking buffer	10% goat serum, 0,3% Triton-X 100 in PBS	IHC	Blocking buffer
10xphospho buffer saline (PBS) 100 mM	1.4 M NaCl, 83 mM Na_2HPO_4, 17mM NaH_2PO_4, pH 7.4	ICC/IHC	Washing buffer
Mowiol	10% mowiol, 25% glycerol, 100 mM Tris-HCl, pH 8.5, 2.5% 1,4-Diazabicyclo[2.2.2]octane		Mounting reagent
DNA mini (B1)	50mM Tris-HCl, pH 8.0, 10mM EDTA	DNA extraction	DNA mini-prep
DNA mini (B2)	200mM NaOH, 1% (w/v) SDS		DNA mini-prep
DNA mini (B3)	3M CH_3CO_2K, pH 5.5		DNA mini-prep
50xTAE buffer	2 M Tris-acetate, 0.05 M EDTA		DNA electrophoresis
6x DNA loading dye	30% glycerol, 0.25 % bromophenol blue, 0.25 % xylene cyanol, 50 mM EDTA, pH 8.0		DNA electrophoresis
Solution A	500 mM $CaCl_2$	HEK393T	Transfection
Solution B	140 mM NaCl, 50 mM HEPES, 1.5 mM Na_2HPO_4, pH 7.05		Transfection
RIPA buffer	50 mM Tris-HCl, pH 8.0, 150 mM NaCl, 1% NP40, 0,5% Na-deoxycholate, 0,1%, SDS, protease and phosphatase inhibitor		Cell lysis
Buffer A	20 mM Tris-HCl, pH 7.4, 137 mM NaCl, 1 mM $CaCl_2$ 1 mM $MgCl_2$, 1 mM Na_3VO_4	PI3Kγ IP and ELISA	Cell harvest

Lysis buffer	Buffer A supplied with 1% NP-40 and 1 mM phenylmethylsulfonyl-fluorid	PI3Kγ IP and ELISA	Cell lysis
Wash buffer 1	Buffer A supplied with 1% NP-40		Beads wash
Wash buffer 2	0.1 M Tris-HCl, pH 7.4, 5 mM LiCl, 1 mM Na_3VO_4		Beads wash
TNE buffer	0.1 M Tris-HCl, pH 7.4, 5 mM LiCl, 1 mM Na_3VO_4		Beads wash
Reaction buffer	20 mM Tris-HCl; 4 mM MgCl2; 10 mM NaCl; ATP 150 μM		ELISA reaction
Kinase stop solution	Reaction buffer supplied with 4 mM EDTA		ELISA reaction
Buffer A	0.32 M sucrose, 5 mM HEPES, pH 7.4	Synaptosome preparation	Mouse brain homogenization
Buffer B	0.32 M sucrose, 5 mM Tris, pH 8.1		Samples preparation
0.85 M Sucrose	0.85 M Sucrose/5 mM Tris/HCl pH 8.1		Sucrose gradient
1 M Sucrose	1 M Sucrose/5 mM Tris/HCl pH 8.1		Sucrose gradient
1.2 M Sucrose	1.2 M Sucrose/5 mM Tris/HCl pH 8.1		Sucrose gradient
HEPES-buffered Krebs-like buffer (HBK)	308 mM NaCl, 308 mM KCl, 154 mM $MgSO_4$, 1 M $CaCl_2$, 100 mM Na_2HPO_4, 87 mM HEPES/Tris, pH 7.4, 0.48 g D(+)-glucose		*ex vivo* insulin stimulation

2.1.4. Common media

Table 3. Common media

Name	Supplier	Application	
LB-medium	20 g LB Broth Base (Invitrogen), 1000 ml H_2O	Bacterial cells	Bacteria culturing medium
LB-agar	15 g Select Agar (Invitrogen), 1000 ml LB-medium		Bacteria culturing medium

SOC-medium	20 g/l peptone 140 (Gibco); 5 g/l yeast extract (Gibco); 10 mM NaCl; 2.5 mM KCl; 10 mM $MgSO_4$; 10 mM $MgCl_2$; 20 mM glucose	Bacterial cells	Transformation
Dulbecco's Modified Eagle Medium (DMEM+)	1% (v/v) Penicillin/Streptomycin 100x, 10% (v/v) fatal calf serum, 0.8 mM L- Glutamine in DMEM (all from Gibco)	HEK293T cells culturing	
Complete Neurobasal medium (NB+)	2% B27 serum, 0.8 mM L-Glutamine, 1% Penicillin/Streptomycin 100x in serum-free NB (all from Gibco)	Primary neurons	Cell culturing
Neurobasal medium (NB-)	0.55 mM L-Glutamine in serum-free NB		Transfection
Neurobasal medium for insulin treatment	0.8 mM L-Glutamine, 1% Penicillin/Streptomycin 100x in serum-free NB		Insulin treatment
Artificial cerebrospinal fluid (aCSF)	110 mM NaCl, 2.5 mM KCl, 2.5 mM $CaCl_2$, 1.5 mM $MgSO_4$, 1.24 mM KH_2PO_4, 10 glucose, 27.4 mM $NaHCO_3$, pH 7.3	Acute slices electrophysiology	

2.1.5. Pharmacological reagents

Table 4. List of drugs and chemicals

Name	Biological activity	Concentration	Supplier
MLN-4924	NEDD8-activating enzyme (NAE) inhibitor	1 μM cell culture; 20 mg/kg intraperitoneal injection; 50 nM LTD	Active Biochem
MG-132	Proteasome inhibitor	20 μM	AG-Scientific
Bicuculline	$GABA_A$ receptor antagonist	50 μM	Tocris
4-AP	Kv1 type of voltage-activated potassium channels inhibitor	2.5 mM	Sigma-Aldrich Chemie
Bovine insulin	Insulin stimulation	100 nM neuronal culture; 500 nM LTD induction	Sigma-Aldrich Chemie

Name	Biological activity	Concentration	Supplier
Rat TNFα	Insulin resistance in culture	10 ng/ml	Preprotech
LY-341495	Group II metabotropic glutamate receptor antagonist	10 μM	Tocris
D-AP5	NMDA receptor antagonist	50 μM	Tocris
AS-605240	PI3Kγ inhibitor	100 mM	Selleckchem
SP-600125	JNK inhibitor	20 μM	Merck Millipore
SB-203580	p38 MAPK inhibitor	10 μM	Cell signaling
2-Hydroxy propyl-β-cyclodestrin	Non-toxic solubilizer for drugs in aqueous buffer	10 % w/v	Sigma Aldrich Chemie
Adenosin-5'-triphosphate (ATP)	Insulin stimulation for synaptosomes preparation	8 mM	Sigma Aldrich Chemie
4',6-diamidin-2-fenilindolo (DAPI)	ICC/IHC staining	1 μg/ml	Sigma Aldrich Chemie

2.1.6. DNA constructs

Constructs were cloned in the lab or purchased from Addgene (Boston, USA)

Table 5. List of plasmids, backbones and insert

Name	Vector backbone	Insert	Application
IRS1-GFP	peGFP N1	IRS1 Rat	Heterologous co-IP
IRS2-GFP	peGFP N1	IRS2 Mouse	Heterologous co-IP
Cullin1-Myc (Addgene)	pcDNA3	CUL1 Homo sapiens	Heterologous co-IP
Cullin2-Myc (Addgene)	pcDNA3	CUL2 Homo sapiens	Heterologous co-IP
Cullin3-Myc (Addgene)	pcDNA3	CUL3 Homo sapiens	Heterologous co-IP
Cullin4A-Myc (Addgene)	pcDNA3	CUL4A Homo sapiens	Heterologous co-IP
Cullin4B-Myc (Addgene)	pcDNA3	CUL4B Homo sapiens	Heterologous co-IP
Cullin5-Myc (Addgene)	pcDNA3	CUL5 Homo sapiens	Heterologous co-IP
Cullin7-Myc (Addgene)	pcDNA3	CUL7 Homo sapiens	Heterologous co-IP

Name	Vector backbone	Insert	Application
Active-Nedd8-HA (Addgene)	pcDNA3	Active-Nedd8 Homo sapiens	Heterologous co-IP
Active-Nedd8-HA	pAAV2-MCS	Active-Nedd8-HA Homo sapiens	AAV9 virus
pAAV2-HA	pAAV2-MCS	HA-tag	AAV9 virus

2.1.7. Antibodies used for immunoblots and immunostainings

Table 6. Primary antibodies used for WB, ICC, IHC and neutralization studies.

Name	Supplier	Specie	Dilution and application
Anti-AKT (pan)	Cell Signaling Technology	Mouse	1:2000 WB 1:500 ICC
Anti-Human Aβ (82E1)	IBL international	Mouse	1:200 IHC
Anti-Aβ3(pE)-42	Synaptic Systems	Rabbit	1:200 IHC
Anti-phospho AKT (Ser473)	Cell Signaling Technology	Rabbit	1:2000 WB 1:300 ICC
Anti-β-actin	Sigma-Aldrich Chemie	Mouse	1:3000 WB
Anti-CUL3	Sigma-Aldrich Chemie	Mouse	1:1000 WB
Anti-CUL7	Sigma-Aldrich Chemie	Rabbit	1:1000 WB
Anti-ERK 1/2	Enzo Life Sciences	Rabbit	1:2000 WB
Anti-phospho ERK 1/2 (Thr183/Tyr185)	Sigma-Aldrich Chemie	Mouse	1:2000 WB
Anti-GFAP	Sigma-Aldrich Chemie	Rabbit	1:500 IHC
Anti-GFP	Covance (Biolegend)	Mouse	1:2000 WB
Anti-HA High affinity tag	Roche Diagnostics	Rat	1:1000 WB
Anti-Homer1	Synaptic Systems	Mouse	1:500 ICC
Anti-Iba1	Synaptic Systems	Guinea pig	1:300 IHC
Anti-IGF-1R	Cell Signaling Technology	Rabbit	1:1000 WB
Anti-InsR (pan)	Cell Signaling Technology	Rabbit	1:1000 WB
Anti-phospho InsR (Tyr1150/1151), phospho IGF-1R (Tyr 1135/1136)	Cell Signaling Technology	Rabbit	1:1000 WB
Anti-IRS1 (pan)	Merck Millipore	Mouse	1:1000 WB
Anti-phospho IRS1 (Ser636/639)	Cell Signaling Technology	Rabbit	1:1000 WB
Anti-IRS2	Merck Millipore	Mouse	1:1000 WB
Anti-IRSp53	Merck Millipore	Rabbit	1:2000 WB

Name	Supplier	Specie	Dilution and application
Anti-MAP2	Sigma-Aldrich Chemie	Mouse	1:750 ICC
Anti-MAP2	Merck Millipore	Rabbit	1:750 ICC
Anti-MAP2 pre-labeled with Alexa Fluor 488	Merck Millipore	Mouse	1:1000 ICC
Anti-Myc-tag	Cell Signaling Technology	Mouse	1:1000 WB
Anti-active-NEDD8	Proteintech	Rabbit	1:1000 WB
Anti-NeuN	Merck Millipore	Mouse	1:500 ICC
Anti-PI3Kγ (#4252)	Cell Signaling Technology	Rabbit	1:1000 WB
Anti-PI3Kγ (#5405)	Cell Signaling Technology	Rabbit	1:200 endogenous IP
Anti-PSD95	NeuroMab	Mouse	1:1000 WB 1:500 ICC
Anti-PKR (pan)	Abcam	Rabbit	1:1000 WB
Anti-phospho PKR (Thr451)	Merck Millipore	Rabbit	1:1000 WB
Anti-Shank3	Synaptic Systems	Rabbit	1:1000 WB 1:500 ICC
Anti-Rat TNFα (Neutralization antibody)	R&D Systems,	Goat	1:5000 neutralization
Anti-mono and poly-Ubiquitin	Enzo Life Sciences	Mouse	1:1000 WB

Table 7. Secondary antibodies used for WB, ICC and IHC.

Name	Supplier	Specie	Dilution and application
Anti Rat-HRP	Dianova	Goat	1:5000 WB
Anti Mouse-HRP	Dianova	Goat	1:20000 WB
Anti Rabbit-HRP	Dianova	Goat	1:20000 WB
Name	**Supplier**	**Specie**	**Dilution and application**
Anti Guinea pig-Alexa Fluor 488	Invitrogen/Thermo Fisher Scientific	Goat or donkey	1:1000 ICC 1:500 IHC
Anti Mouse-Alexa Fluor 488	Invitrogen/Thermo Fisher Scientific	Goat or donkey	1:1000 ICC 1:500 IHC
Anti Rabbit-Alexa Fluor 488	Invitrogen/Thermo Fisher Scientific	Goat or donkey	1:1000 ICC 1:500 IHC
Anti Guinea pig-Alexa Fluor 568	Invitrogen/Thermo Fisher Scientific	Goat or donkey	1:1000 ICC 1:500 IHC

Anti Mouse-Alexa Fluor 568	Invitrogen/Thermo Fisher Scientific	Goat or donkey	1:1000 ICC 1:500 IHC
Anti Rabbit-Alexa Fluor 568	Invitrogen/Thermo Fisher Scientific	Goat or donkey	1:1000 ICC 1:500 IHC
Anti Guinea pig-Alexa Fluor 647	Invitrogen/Thermo Fisher Scientific	Goat or donkey	1:1000 ICC 1:500 IHC
Anti Mouse-Alexa Fluor 647	Invitrogen/Thermo Fisher Scientific	Goat or donkey	1:1000 ICC 1:500 IHC
Anti Rabbit-Alexa Fluor 647	Invitrogen/Thermo Fisher Scientific	Goat or donkey	1:1000 ICC 1:500 IHC

2.1.8. Animals

TBA2.1 mice (C57BL/6 background) (Alexandru et al., 2011) were a kind gift of ProBiodrug (Halle, Germany).

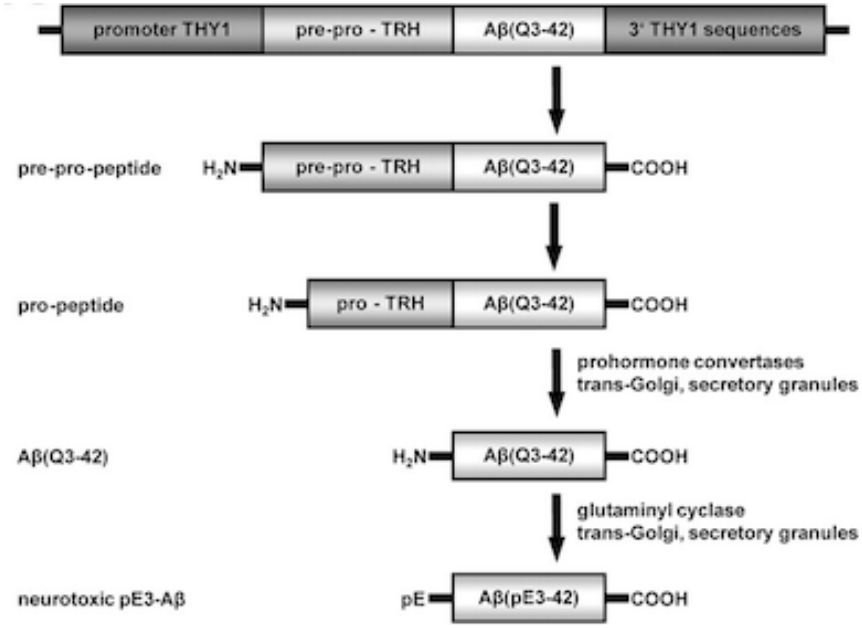

Figure 8: TBA2.1 gene structure and the targeting construct. Transgenic TBA2.1 were generated by chromosomal integration of an expression cassette, which directs human Aβ polypeptide Aβ(Q3–42) expression into neuronal tissue and is based on murine Cluster of differentiation Thy1 regulatory sequence (Lüthi et al., 1997). The regulatory elements flank the coding sequence for a fusion protein consisting of the pre-pro-peptide of murine thyrotropin-releasing hormone (TRH, Thyroliberin), fused to the N terminus of the modified Aβ(Q3–42). Prohormone convertase (PC) cleavage within the *trans*-Golgi and secretory vesicles release the N-truncated Aβ species preferentially within the secretory pathway, in which they are modified by QC activity (Cynis et al., 2006; Friedman et al., 1995) Picture from Alexandru et al., 2011.

These mice over-express the Aβ3(pE)-42 peptide driven by Thy1 promoter. The upstream sequence coding for pre-pro-peptide of murine thyrotropin releasing hormone leads to cleavage within the trans-Golgi and vesicular secretion of Aβ3(pE)-42. The mice used in experiments were heterozygous (+/Tg TBA2.1). All the animals used were male. The animal experiments were conducted according to the German and European law under the license AZ 42502-2-1264LIN from the Land Sachsen-Anhalt.

2.1.9. Bacterial strains and cell lines

- *E. Coli* XL10-Gold for cloning and plasmid DNA amplification
- HEK293T cell line for heterologous co-immunoprecipitation studies

2.2. Methods

2.2.1. DNA cloning and plasmids purification

The constructs used throughout the study were purchased from different companies (paragraph 2.1.6, Table 4) and the gene of interest sub-cloned into varying vectors carrying a tag-protein by following standard polymerase chain reaction (PCR) protocols. Alternatively rat cDNA was used as a template to amplify the gene of interest with gene-specific primers using Pfu-plus polymerase. The PCR reactions were carried out in a TC-300 thermocycler (Techne, Invitrogen/Thermo Fisher Scientific, Braunschweig, Germany) using the following reaction mixture and cycling conditions:

PCR mix:

- Pfu-plus polymerase 1 µl
- 10x Pfu-plus polymerase buffer 3 µl (final concentration 1x)
- dNTPs 1.5 (final concentration 0.75 mM)
- Forward primer 1 µl (final 0.2 mM)
- Reverse primer 1 µl (final 0.2 mM)
- DNA template 50 ng
- dH_2O up to a final volume of 30 µl

PCR reaction:

- Initial denaturation 95 °C, 2 min, 1 cycle
- Denaturation 95 °C, 45 sec
- Annealing 45-60 °C, 45 sec
- Extension 72 °C, 1kb/60sec

} 30 cycles

- Final extension 72 °C, 2 min, 1 cycle

Agarose gel electrophoresis was used to confirm the amplified PCR products. Obtained products were purified from the gel using PCR cleanup and gel extraction kit (Macherey-Nagel, Düren, Germany) according to manufacturer's instructions. Purified insert and vector backbone were double-digested with specific restriction enzymes and purified again with PCR cleanup kit after run in agarose gel electrophoresis. The digested insert and vector were ligated using T4 ligase overnight at 16 °C. Products of ligation were transformed into chemically competent *E. coli* XL10-Gold incubating the ligation mixture with the bacteria on ice for 20 min, then followed by a 45 s heat shock at 42 °C. The mixture was immediately placed on ice for 2 min and incubated in SOC medium for 1 h at 37 °C under constant shaking. The bacterial suspension was plated onto antibiotic containing LB-agar plates and cultured up to 16 h at 37°C. Single colonies were picked to isolate plasmid DNA. DNA sequences of the inserts were confirmed by restriction digestion and sequencing. Colonies carrying the positive clones were inoculated into LB media for 13-16 h at 37 °C for small or large-scale DNA purification.

The plasmids were purified from o/n LB bacterial culture by an alkaline-based lysis method. For small scale plasmid DNA purification, the bacteria were pellet at 500 g for 5 min and after medium removal, resuspended in 300 µl of ice-cold buffer containing 50 mM Tris-HCl pH 8.0, 10 mM EDTA, 100 ug/ml of RNAase A and then lysed in 20 mM NaOH containing 1% (w/v) SDS. Chromosomal DNA was precipitated with 3 M potassium acetate buffer pH 5.5 and centrifuged for 10 min. Plasmid DNA was precipitated in isopropanol and then pelleted from the supernatant by centrifugation at 12000 rpm. The samples were washed with 70% (v/v) ethanol, air-dried and resuspended in dH_2O. For large scale DNA purification suitable for neuronal cells transfection,

endotoxin-free DNA purification kit (paragraph 2.1.2, Table 1) was used according to manufacturer's instructions.

2.2.2. HEK293T cells cultures

2.2.2.1. Calcium phosphate transfection

Human embryonic kidney-293T (HEK293T) cells were cultured in Dulbecco's Modified Eagle Medium (DMEM), supplemented by L-Glutamine and serum (DMEM+) in a Heraeus incubator at 37°C, 5% CO_2 and 95% humidity. Cells were plated in T-75 flasks, and transfected at the confluence of 50-60% using calcium phosphate ($Ca_3(PO_4)_2$) method. Briefly, the DNA was mixed with Solution A and then Solution B (paragraph 2.1.3, Table 2). The mixture was incubated for 1 min at RT, and immediately added to the cells. The medium was changed to fresh DMEM+ after 3 h of incubation.

2.2.2.2. Heterologous co-immunoprecipitation assay

For heterologous co-immunoprecipitation (co-IP) experiments, HEK293T cells grown in T-75 or T-175 flasks were transfected with different proteins of interest, tagged with GFP, Myc or HA-tag using $Ca_3(PO_4)_2$ method as described above. Cells were harvested in ice-cold Tris-buffered saline (TBS) supplied with EDTA-free Protease inhibitors (Complete, GE Healthcare, Germany) cocktail. Cells were pelleted at 500 g for 5 min and supernatant was discarded. Pellet was next re-suspended in 1 ml of RIPA buffer and lysed for 1 h while rotating at 4°C. After centrifugation at 14000 g for 20 min, 20 to 50 µl of supernatants were mixed to 4X SDS-sample buffer and kept as inputs. Remaining supernatants were incubated with 30 µl of µMACS Anti-GFP or Anti-Myc or Anti-HA MicroBeads (Miltenyi Biotec GmbH, Teterow, Germany) according to the experimental design, for 1 h in 4°C, rotating. Beads were collected using µMACS magnetic column and washed 4 times with RIPA buffer and 1 time with 20 mM Tris-HCl (pH 7.5). Protein complexes were eluted with 40 µl of hot 2X SDS-sample buffer. 20 µl of inputs and eluates were loaded onto SDS-PAGE gradient gels.

2.2.3. Rat primary cell culture

Rat cortices and hippocampi were dissected from embryonic day 18 rats (Sprague Dawley). Primary neuronal cultures were prepared by technical assistants according to previous described protocols (Karpova et al., 2013). For immunocytochemical studies the cells were seeded in 12-well plates on 18 mm glass coverslips coated with poly-D-lysine at a density of 30,000 cells per coverslip. For western blot analysis or synaptosomes preparation, neurons were plated directly on a 6-wells plate (600.000 cells per well) or in T-75 flasks (10 million per flasks). Neurons were plated in 1 ml of DMEM medium supplemented with 10% FBS, 2 mM glutamine and 1% of penicillin/streptomycin. After the first day in culture, medium was changed to complete Neurobasal medium (NB+). Cultures were kept in incubator at 37°C, 5% CO_2 and 95% humidity.

2.2.3.1. Neuronal transfection

For knockdown experiments, neurons were transfected at DIV11-12 with endotoxin-free plasmids carrying either shRNA or Scrambled control. 0,4 to 1,8 µg of DNA was transfected using Lipofectamine-2000 (Life Technologies) in ratio of 1:2 to the DNA. Briefly, DNA and Lipofectamine-2000 were separately added to 50 µl of Neurobasal medium supplemented with 0.55 mM L-Glutamine (NB-) and then mixed with each other. The mix was incubated 20 min at room temperature and applied onto the coverslips after replacement of the medium with fresh NB- medium. Conditioned NB+ medium was previously collected from the 12-well plates and stored at 37°C. After 1 h incubation, the NB- medium was again replaced with conditioned NB+ medium previously collected. Neurons were fixed with 4% paraformaldehyde (PFA) and 4% sucrose for 10 min after 3-4 days of transfection. After several washes with PBS buffer, coverslips were processed for immunocytochemistry (ICC) staining.

2.2.3.2. AAV9 virus infection

The DIV10 cortical neurons cultured in T-75 flasks were infected with 10000 vg/cells of AAV9 adeno-associated viral particles carrying either NEDD8-HA or empty

HA-tag vector for 14 days. Afterwards neurons were harvested and processed for synaptosomes preparation (paragraph 2.2.10.1).

2.2.3.3. Insulin/TNFα stimulation of cultured neurons

In order to investigate the effects of IR in *in vitro*, DIV21 cortical neurons were treated with insulin (100 mM), rat TNFα (10 ng/ml) or a combination of the two drugs. Prior to apply the drugs, half of the medium of each plate was replaced with fresh and pre-warmed serum-free NB medium in order to decrease as much as possible the concentration of the insulin coming from the serum (B27) without affecting neuronal environment in culture. TNFα was directly applied into the medium, while insulin was pre-incubated in the serum-free NB and incubated in the Heraeus incubator prior applying to the neurons. This was done in order to buffer the acidity of insulin that solubilized in 1% acetic acid. Treated cells were incubated for 24 h. After a washing step with fresh serum-free medium, cells were stimulated for 15 min with insulin or vehicle to test the responsiveness after the insulin resistance induction. The medium was fully removed and cells were harvested in 300 µl of ice-cold TBS buffer with Protease inhibitors (Complete, GE Healthcare, Germany) and Phosphatase inhibitors (PhospoSTOP, Roche Diagnostics GmbH, Germany) cocktails.

2.2.3.4. MLN-4924, Aβ3(pE)-42 oligomers and TNFα-neutralizing antibody treatments

Aβ3(pE)-42 oligomers were prepared according to previously established protocol (Nussbaum et al., 2012). The lyophilized peptide was disaggregated in 1,1,1,3,3,3-hexafluoro-2-propanol (HFIP) to 0.5 mg/ml and the aliquots were stored at - 80°C. HFIP was evaporated for 24 h at room temperature. The peptide was dissolved in 0.1 M NaOH, vortexed, diluted in 0.1 M HCl to buffer pH. Mixture was next diluted in NB medium to a final concentration of 5 µM. Oligomers were formed during incubation for 24 h. For every experiment the fresh preparation of oligomers was used. NB medium containing the oligomers was added directly onto DIV 21 neuronal culture at the final concentration of 500 nM together with insulin/TNFα or vehicle. In the TNFα neutralizing experiments,

a TNFα neutralization antibody (1:5000) was co-applied with Aβ3(pE)-42 oligomers and cells were incubated for 24 h. The neddylation inhibitor MLN-4924 solubilized in DMSO applied in the culture at the final concentration of 1 μM. Insulin/TNFα were co-applied according to the experimental design.

2.2.4. Protein sample preparation and quantification

Total protein homogenates were prepared from DIV21 cultured cortical neurons or dissected mice hippocampi and cortices. Tissues were mechanically homogenized using a pellet pestle motor (Kimble Kontes, Vineland, USA) in ice-cold TBS buffer in a proportion of 10 ml per 1 g of tissue, in the presence of protease and phosphatase inhibitor cocktails (Roche Diagnostics, Mannheim, Germany). The homogenates were mixed in an equi-volume of 4X SDS-sample buffer and denatured for 5 min at 95°C. Protein concentration was measured colorimetrically using Amido Black assay. Bovine Serum Albumin (BSA) was used to obtained standard curve ranging between 1 and 20 ug and processed together with samples. Protein samples were incubated with amidoblack solution at room temperature for 20 min. After 3 rounds of washing in methanol-acetic acid solution and centrifugations, pellets were air-dried and dissolved in 300 μl of 100 mM NaOH solution. After 30 min of shaking at room temperature the optic density was measured at 620 nm with Fluoro Star Optima Fluorimeter (BMG Lab technologies, Offenburg, Germany).

2.2.5. SDS-PAGE and immunoblot

For protein detection standard western blot protocols were applied (Seidenbecher et al., 2004). The protein samples, already solubilized in 2X SDS-sample buffer, were denatured for 5 minutes at 95°C and loaded onto a 5-20% gradient polyacrylamide gel. A constant electric field of 12 mA per gel was applied to samples and protein standard, and run for c.a. 1.5 h. The amount of protein loaded ranged between 10 μg and 30 μg depending on the experiment. The samples were transferred from the gel to a nitrocellulose membrane using a blotting chamber (Hofer Scientific Instruments) at a constant current of 200 mA for 1.5 h with a voltage between 90 and 60 mV. Membranes were blocked for 45 min at room temperature with 5% non-fat milk or BSA in TBS-T

according to the manufacturer's instruction of the antibody. Primary antibodies diluted in TBS-A were incubated o/n at 4°C on shaker. Membranes were therefore washed 4 times with TBS and TBS-T buffers and incubated for 1.5 h at room temperature with secondary antibody diluted in 5% non-fat milk or BSA prepared in TBS-T. Following again 4 washes with TBS and TBS-T buffers, the bands are revealed using ECL solution (Luminata^{TM}, Merck Millipore, Darmstadt, Germany). The images were acquired with Intas ECL Chemocam imager (Licor, Cambridge, UK).

Protein bands on the membranes were quantified using the Image-J software (NIH, http://rsb.info.nih.gov/ij/). Size and intensity of bands were measured and divided by those of the loading control protein of the same lane (i.e. β-actin or β-tubulin). In the case of quantitative immunoblot analysis of phospho-antibodies (i.e. phospho-AKT, phospho-InsR and phospho-IRS1), the size and intensity values of the phospho-antibody, already divided by the loading control, were furthermore divided by the size and intensity of the respective pan-antibody, also normalized by loading control. Ratios were normalized within blots and normalized values from different blots plotted together according to the treatment.

2.2.6. *In vivo* IR in TBA2.1 mice

Male +/+ and +/Tg TBA2.1 mice (described in paragraph 2.1.9.) were fed with normal chow until the age of 8-9 weeks. After this period and for the rest of their life, mice were fed with either a normal chow (Regular diet, RD) or an high fat/high calories chow (High fat diet, HFD) (ssnff® EF R/M with 30% fat: Dry matter 96.6 %, Crude protein (N x 6.25) 20.7%, Crude fat 30.0%, Crude fiber 5.0% Crude ash 5.6% N free extracts 34.3% Starch 17.2% Sugar 16.3%). Animals were kept in the diet between 14 to 26 weeks. In order to be sure to efficiently induce IR, mice were selected for further experiments only when they reach the 70% of body weight increase compared to begin of the diet. Contrary the RD mice were excluded from experiment if their body weight exceeded the 40% of body weight increase compared to begin of the diet.

2.2.6.1. Glucose tolerance test

The glucose tolerance test is a medical test in which a dose of glucose is injected intraperitoneally in animals and the concentration is measured from the blood at different time points. Through the assay is possible to determine how quickly the sugar is cleared from the blood by the insulin-dependent glucose uptake from the cells. Prior to start the experiment, +/+ and +/Tg TBA2.1, both on RD or HFD mice were put to fast for 6 h. A small drop of blood (<5 µl) was taken from the tail of the animals and placed on the test strip of the blood glucose meter Contour Next (Bayer, Munich, Germany). This is the baseline glucose level (t=0). Straight after the first measurement, a D(+)glucose solution of 0.25 g/ml was intraperitoneally injected into the animals to a final concentration of 1 g/kg. The blood glucose levels were measured at 15, 30, 60 and 120 minutes (t=15, t=30, t=60 and t=120) after glucose injection.

2.2.6.2. Serum insulin ELISA assay

Animals were first narcotized with a mix of 100 mg/kg Ketamine and 10 mg/kg Xylazine injected intraperitoneally. The blood was collected with the use of a syringe directly from the heart ventricle. After coagulating at room temperature for 45 min with the open tube, blood samples were centrifuged 10 min at room temperature at 1500 g. The serum was collected and stored at -20°C. Prior starting ELISA assay, the samples were let thawed slowly in ice and the assay was performed according to manufacturer's instruction.

2.2.7. Behavioral experiments

Behavioral experiments were performed with Dr. Guilherme Monteiro Gomes on male +/+ and +/Tg TBA2.1, both RD and HFD mice, as well as the MLN-4924 injected animals, to assess hippocampal-dependent learning and memory performances. Object location and novel object recognition experiments were done in a square apparatus (50 × 50 × 50 cm) under mild light conditions, according to Heyward and colleagues (Heyward et al., 2012). In the first day, the animals were habituated to the apparatus for 20 min. The training session took place 24 h later where the mice were free to explore for 20 min a

pair of similar objects (made of plastic mounting bricks), positioned in the arena. On the next day, in order to test object location recognition memory, one of the objects was displaced to a new position, and the animals were returned to the apparatus for another 20 minutes of free exploration. Twenty-four hours later, novel object recognition test was performed, where a new one replaced one of the familiar objects, and again the animals were returned to the apparatus for a 20 minutes exploration period. All four sessions were video recorded, and behavior was analyzed offline using the ANY-maze software (ANY-MazeTM Video Tracking System, version 4.50, Stoelting Co., Wood Dale, Il, USA). Exploration was considered only when the animal touched or reached the object with the nose at a distance of less than 2 cm. The time mice spent exploring the objects was recorded, and the discrimination index was calculated, taking into account the difference of time spent exploring the new and familiar object ($(T_{new}-T_{familiar})/(T_{new}+T_{familiar})x100$). The first 5 minutes of each test session were used to calculate the discrimination index. Chambers and objects were cleaned with 10% ethanol before and after each animal was tested.

2.2.8. Acute hippocampal slices, long term depression (LTD) and potentiation (LTP)

Long-term depression (LTD) and long-term potentiation (LTP) recordings were performed with Dr. PingAn Yuanxiang. Hippocampal slices from male +/+ and +/Tg TBA2.1, on RD or HFD were prepared according to a previously described protocol (Behnisch et al., 2011; Yuanxiang et al., 2014). Briefly, mouse brains were sliced using a Vibratome (Leica VT1000ST, Nussloch, Germany) into 350 μm thick slices. Slices were incubated in carbogenated (CO_2 5%, O_2 95%) aCSF solution at room temperature for 2 h. The slices were then transferred into recording chamber (at 31±1°C). Field excitatory postsynaptic potentials (fEPSPs) were evoked by stimulation of CA1 Schaffer-collateral fibers with metal electrodes. fESPSs were recorded with aCSF filled glass capillary microelectrodes (3-5 MΩ) and amplified by an Extracellular Amplifier (EXT-02B, NPI electronic, Germany) and digitized at a sampling frequency of 5 kHz by Digidata 1401plus AD/DA converter (CED, England). Stimulation strength was adjusted to 20% ~ 30% (LTP) or to 40% ~ 50% (LTD) of the maximum fEPSP-slope values. A single

stimulus with 0.1 ms width was applied every 30 s (at 0.0333 Hz) and was averaged every 3 min. Following a 30 min stable baseline recording, 3 trains of high frequency stimulus with 10 min inter-train interval were using for LTP-induction, each train was lasting for 1s at 100Hz. For LTD induction, a low frequency stimulus (900 stimuli at 1 Hz frequency) was applied.

In case of bath application of MLN-4924 on acute hippocampal slices, the drug was solubilized in DMSO and diluted in aCSF at 1 μM final concentration. Following a 10 min stable baseline recording, the MLN-4924 or DMSO was applied in bath 20 min before the LTD induction and kept for the entire duration of the recording. Long-term depression was induced as described above. Data are represented as mean ± s.e.m. The Mann-Whitney U-test was used to compare the averaged field potentials (210-240 min) between two groups of differentially treated slices.

2.2.9. MLN-4924 intraperitoneal injection in TBA2.1 mice

Male +/+ and +/Tg TBA2.1 were kept on HFD until they reached the threshold of 70% of body weight increase as described above. Animals were injected intraperitoneally with MLN-4924 once a day for 14 days with the collaboration of Dr. Guilherme Monteiro Gomes and Monika Marunde. MLN-4924 powder was previously solubilized in DMSO at the concentration of 10 mg/ml. In order to increase the solubility of MLN-4924 in aqueous buffer, the drug was mixed with a solution of 10% of the non-toxic hydrophilic solubilizer 2-Hydroxypropyl-β-cyclodestrin to a final concentration of 5 mg/ml. A dose of 20 mg/kg of MLN-4924 or vehicle was given to each animal. One day after the end of the injection period, animals were tested for behavioral tasks or glucose tolerance test.

2.2.10. Synaptosome preparation

Synaptosomes were prepared from either mouse tissues (cortices or hippocampi) or primary rat neuronal culture according to previously published protocols (Smalla et al., 2003; Wyneken et al., 2001).

2.2.10.1. Synaptosome preparation from primary cortical culture

21 DIV rat primary cortical cells were harvested in ice-cold TBS buffer with protease and phosphatase inhibitor cocktail (Roche Diagnostics, Mannheim, Germany). Cells were homogenized using the manual homogenizer Potter S (Sartorius AG, Göttingen, Germany) and centrifuged at 12000 g for 20 min. This process was repeated twice. Pellet was than resuspended in 300 µl of Buffer B and loaded onto a 1 M/1.2 M sucrose steps gradient (Figure 9 A). The columns were centrifuged at 33000 rpm for 1 h 30 min in ultracentrifuge Optima MAX-XP Ultracentrifuge (Beckman coulter, Pasadena, USA). The synaptosomes were collected at the interphase between the 1 and 1.2 M sucrose steps. The samples were mixed in Buffer B and centrifuged at 45000 rpm to remove the excess of sucrose. The pelleted synaptosomes were used for further experiments.

2.2.10.2. Synaptosome preparation from TBA2.1 mice cortices

Mice cortices were homogenized in ice-cold TBS buffer (10 ml of buffer per 1 g of material) in the presence of protease and phosphatase inhibitor cocktails (Roche Diagnostics, Mannheim, Germany) with the help of manual homogenizer Potter S (Sartorius AG, Göttingen, Germany) and centrifuged at 1000 g for 10 min. The supernatant was furthermore centrifuged at 12000 g for 20 min and the pellet was kept. After resuspending the pellet containing the crude membranous (P2-fraction) in 1.5 ml of Buffer B per each gram of tissue, samples were loaded onto a 0.85 M/1 M/1.2 M sucrose steps gradient (Figure 9B) and ultra-centrifuged at 85000 g for 2 h (Optima XPN-80 Ultracentrifuge, Beckman coulter, Pasadena, USA). From this step on, the protocol continues as for the primary cortical culture. Finally, and in order to assess synaptic responsiveness to insulin, isolated synaptosomes from +/+ and +/Tg TBA2.1 on RD or HFD mice were stimulated with 100 nM of insulin or vehicle for 10 min at 37°C. Reaction was performed in HEPES-buffered Krebs-like buffer (HBK) supplied with 8 mM of ATP (Franklin & Taglialatela, 2016). Synaptosomes were centrifuged at 10000 g, washed 2 times with fresh HBZ buffer and finally lysed in 2X SDS-sample buffer. Synaptosomes and P2-fractions were loaded onto SDS-gradient gel for western blot analysis.

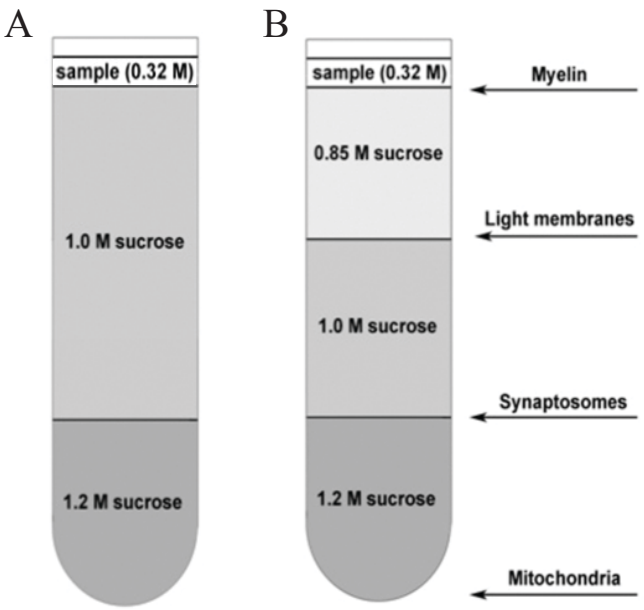

Figure 9: Sucrose gradient for synaptosomes preparation. (A) 2 steps sucrose gradient (1,2 M/1 M) was used to purify synaptosomes out of cultivated primary cortical neurons while (B) 3 steps sucrose gradient (1,2 M/1 M/0,85 M) was used for tissues. Third step in the column allows a better separation of the synaptosomes-containing fraction from myelin and light membranes.

2.2.11. Immunoprecipitation of endogenous PI3Kγ and ELISA

For endogenous PI3Kγ co-IP experiments, cultured primary cortical neurons or TBA2.1 hippocampi were used. The cultured cells were collected in buffer A and pelleted at 500 g. In the case of experiment with TBA2.1 mice, the hippocampi were dissected, snap-frozen in liquid nitrogen and stored at -80°C. Hippocampi were mechanically homogenized using a pellet pestle motor (Kimble Kontes, Vineland, USA) in Buffer A. Both cell pellet and the hippocampal total homogenates were used to perform endogenous PI3Kγ co-IP after lysis in 200 µl ice-cold lysis buffer. Samples were then centrifuged at 14000 g to sediment the insoluble material. 25 µl of each supernatant were collected, mixed with 10 µl of 4X SDS-sample buffer and run as input in the western blot. The rest of the aqueous fraction was incubated with 2 ug of rabbit polyclonal anti-PI3Kγ antibody (#5405) with gentle rotation for 1 h in cold room. 40 µl of dynabeeds protein G (Thermo Fisher Scientific Germany, Braunschweig, Germany) were incubated with the antibody-bound-PI3Kγ rocking for 1 h at 4°C. Beads were collected with the use of DYNAL magnet for Eppendorf (Invitrogen, Braunschweig,

Germany) and washed with a sequence of Wash buffer 1 and 2, TNE buffer and ELISA-reaction buffer. While still anchored at the beads, PI3Kγ's reaction was set up adding 60 µl of reaction buffer supplied with 10 µM of $PI(3,4)P_2$ and incubated at 37°C for 2 h. 10 nM of AS-605240 were added onto the negative control samples to inhibit PI3Kγ's activity. The kinase reaction was stopped with 90 µl of Kinase Stop Solution. Reaction buffer containing the product of the enzymatic reaction $PI(3,4,5)P_3$ was entirely collected and used for competitive ELISA assay according to manufacturer's instruction. PI3Kγ proteins were extracted from the beads using 20 µl of hot 2X SDS-sample buffer and used for western blot to check the presence of the enzyme during the assay.

2.2.12. Mouse TNFα ELISA assay

For the mouse TNFα Enzyme-linked Immunosorbent Assay (ELISA) assay, frozen cortices from +/+ and +/Tg TBA2.1 mice, both RD and HFD were homogenized in ice-cold PBS with the use of manual homogenizer Potter S (Sartorius AG, Göttingen, Germany). After two freeze-thaw cycles performed to break the cell membranes, the homogenates were centrifuged for 5 minutes at 5000 g at 4°C. The supernatant was removed and assayed immediately. The ELISA is a typical quantitative sandwich enzyme immunoassay assay with a monoclonal antibody specific for mouse TNFα pre-coated onto a microplate. The assay was performed according to manufacturer's instruction.

2.2.13. Immunocytochemistry (ICC)

Following the specific treatment varying upon the experiment, the neurons were fixated in 4% PFA and 4% sucrose for 10 min at room temperature. After three washes in PBS, cells were permeabilized using 0,2% Triton-X in PBS for 10 min, washed again with PBS and blocked for 45 min at room temperature in blocking buffer. Primary antibodies were diluted in blocking buffer and incubated o/n at 4°C. Coverslips were extensively washed with PBS and incubated for 1 h 30 min at room temperature with fluorescent, secondary antibodies diluted 1:1000 in blocking buffer. Optionally, cells were counterstained with the neuron specific marker pre-labeled AF488 anti-MAP2 primary antibody diluted 1:1000 in blocking buffer and/or 1ug/ml of 4′,6-diamidino-2-

phenylindole (DAPI) (Sigma-Aldrich Chemie GmbH, Steinheim, Germany) as nuclear marker diluted 1:1000 in PBS. Coverslips were mounted in Mowiol (Polysciences Inc., Warrington, USA) and stored in dark at 4°C.

2.2.14. Immunohistochemistry (IHC)

Male +/+ and +/Tg TBA2.1 mice, RD and HFD were anaesthetized with Isofluran (Baxter Deutschland GmbH), and then perfused with 0.9% NaCl, followed by fixation with 4% PFA in PBS. Brains were isolated, and post-fixed in 4% PFA, then transferred to 0.5 M sucrose and, subsequently, to 1 M sucrose (each step for 1 day). Fixed brains were cut in 40 µm thick sections using cryostat (Leica CM3050S, Leica Microsystems, Wetzlar, Germany). Slices were incubated in IHC-blocking buffer for 30 min at room temperature, washed once with PBS and then incubated with primary antibody o/n at 4°C rocking. The sections were washed for 2 h in PBS and incubated with secondary antibody diluted 1:500 in blocking buffer. Following washing, 1 µg/ml DAPI (Sigma-Aldrich Chemie GmbH, Steinheim, Germany) was applied in PBS to stain nuclei slices were mounted in Mowiol (Polysciences Inc., Warrington, USA).

2.2.15. Image acquisition

2.2.15.1. Confocal laser scan microscopy

Confocal images of mouse brain sections were acquired on a TCS-SP5 Confocal Laser Scanning system, attached to an upright DM6000 CFS microscope (Leica microsystem, Mannheim, Germany). Images of immunostained 40 µm thick brain slices from TBA2.1 mice were acquired and analyzed in collaboration with Dr. Guilherme Monteiro Gomes. Hippocampi of both hemispheres were imaged on a SP5 CLSM system (Leica Mycro system, Mannheim, Germany) using laser lines for excitation 405 nm (Diode), 488 nm Argon-Ion), 561 nm (Diode Pumped Solid State (DPSS) and 633 nm (HeNe). Coronal sections were scanned using a 20X water-immersion objective, 400 Hz scanning speed and 1024 px x 1024 px image size. Maximum projection of the scans, comprised of 5 z-stacks (0.39 µm z-step), was made using Image-J software (NIH, http://rsb.info.nih.gov/ij/) for subsequent analysis. The region of interest (ROI) for

quantification of neuronal loss (NeuN+ cells), astrogliosis (GFAP+ cells) and microgliosis (Iba1+ cells), as well as for amyloid-β deposition (Aβ3(pE)-42 and Aβ (82E1)) was defined by positioning a rectangular counting frame of 220 x 300 μm onto the pyramidal cell layer of CA1 adjacent to the fasciola cinereum at low-power magnification (20X). Three to four brain sections from each animal were used for quantification, and the number of positive cells for each marker was counted and directly plotted for statistical analysis.

2.2.15.2. Fluorescent microscopy

Studies of synaptic IR on hippocampal primary neurons were carried out using Zeiss Axio Imager A2 fluorescent microscope (Zeiss, Jena, Germany) with Cool Snap EZ camera (Visitron System) and MetaMorph Imaging software (MDS Analytical technologies). Up to 3 coverslips were treated individually and processed per group. For each coverslip the same exposure time and intensity were taken among the different groups. Upon background substraction using Image-J software (NIH, http://rsb.info.nih.gov/ij/), images of fluorescent positive puncta were measured along primary dendrites, right after the brunching point. The synaptic immunofluorescence intensities were assessed in a region of 400 nm x 400 nm square set by the mask in the channel for Shank3, used as synaptic marker. The mask was created semi-automatically using OpenView software (Lazarevic et al., 2017; Tsuriel et al., 2006). The intensities of the proteins of interest (i.e. pan-AKT or phospho-AKT) were measured at the co-localization spots with Shank3. Normalized to control mean values were plotted and statistical analysis were performed.

2.2.16. Statistics

Statistical analyses were carried out with GraphPad Prism software (GraphPad software, Inc., La Jolla, USA). Data were represented as mean ± s.e.m. Student's t-test (two experimental groups) or one-way ANOVA followed by Tukey's Multiple Comparison Test (more than two groups) were used for comparison as denoted in figure legend. For all the other western blot, ICC, IHC, and behavior analysis two-way ANOVA

was used to compare variances, followed by Bonferroni's Multiple Comparison Test. For LTD and LTP experiments averages from 210-240 min after LTD or LTP induction were compared by two-way ANOVA followed by Bonferroni's Multiple Comparison Test. For the glucose tolerance test two-way ANOVA of repeat measures followed by Bonferroni post hoc test was used.

3. Results

3.1. Induction of IR in primary neuronal cultures

Insulin binding to InsR leads to activation of a phosphorylation cascade resulting in the activation of several proteins, including the RAC-alpha serine/threonine kinase AKT. It is widely established in the field that a long exposure to high concentrations of insulin as well as treatment with TNFα induces IR in many cell types, including neurons (De Felice, 2013; Kim et al., 2017). One of the most important hallmarks of IR in many cell types is the diminished phosphorylation of AKT (Ser473) with a subsequently reduced activation of several proteins involved in cell homeostasis. However, IR does not affect only AKT but also the InsR itself. Generally speaking, InsR regulation involves protein degradation or modification of the tyrosine-kinase activity of individual InsR (Youngren, 2007).

An *in vitro* model of high-risk aging with the presence of MetS and high amyloid load would be advantageous to study synaptic IR. Therefore, the first goal of this thesis was to assess whether cultivated mature hippocampal or cortical primary neurons undergo a reduced insulin-induced activation of AKT and InsR after a prolonged treatment with insulin and TNFα. The combination of these two treatments attempted to resemble the condition of diet-induced prolonged exposure to insulin and amyloid-β derived neuroinflammation. Both molecules were applied in fresh and warm serum-free NB medium and incubated for 24 h. Cells were afterwards washed for 1 h with fresh serum-free NB medium and, followed by an acute stimulation with insulin for 15 min (Figure 10 A). Quantitative immunoblots of the total extracted proteins were performed using specific antibodies detecting the total level of AKT or the phosphorylated-AKT as well as InsR or phosphorylated-InsR (Figure 10 B). The insulin/TNFα treatment resulted in an apparent reduction of the insulin-stimulated AKT and InsR phosphorylation compared to the non-treated samples, meaning that the activation of the phosphorylation cascade is now impaired (Figure 10 C-D). Additionally, while AKT total protein levels are not regulated, IR causes a clear reduction of the total InsR (Figure 10 E-F).

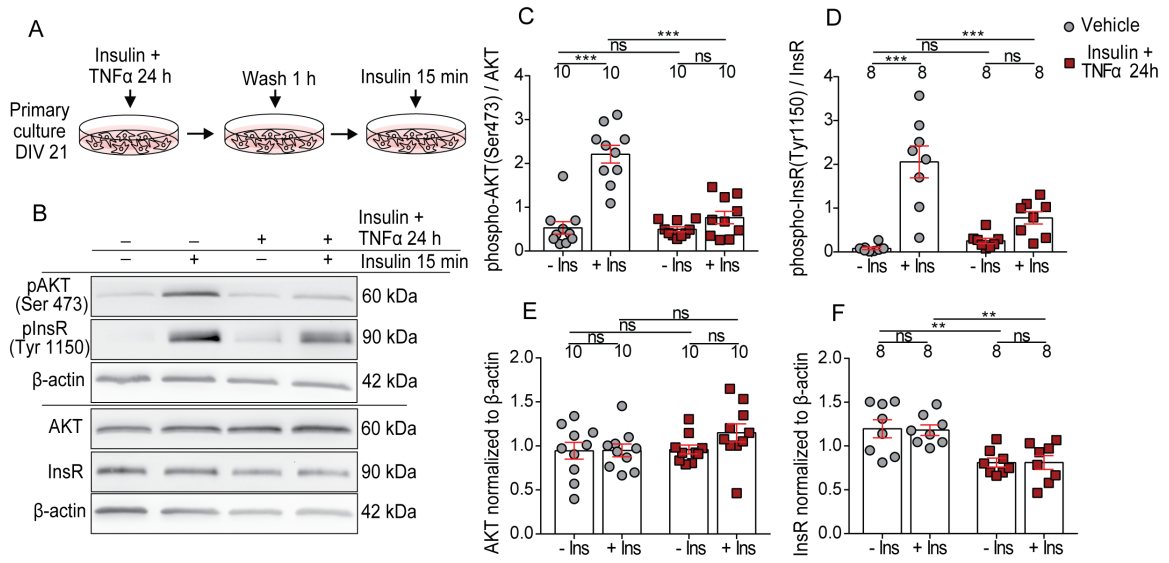

Figure 10: IR in 21 DIV cortical neuronal cultures reduces phospho-AKT and phospho-InsR. (A) Scheme representing the protocol used to induce IR and test the responsiveness of cells to insulin. 100 nM insulin and 10 ng/ml TNFα (or the respective vehicles) were co-applied on primary cortical neurons for 24 h, which was followed by washing for 1 h and an acute stimulation with insulin or vehicle for 15 min. (B) Representative pictures of immunoblots of total cell extracts probed with antibodies detecting phospho-AKT (Ser473), phospho-InsR (Tyr1150), AKT and InsR. Each blot was probed in addition with a β-actin antibody. (C-D) Scatter dot plots depict the quantification of the phosphorylated AKT and InsR, which were carried out by means of normalization to the respective non-phosphorylated protein. Each value was previously normalized to the respective β-actin, used as an internal control. Acute stimulation with insulin had a reduced effect in the phosphorylation and activation of AKT and InsR in the Insulin/TNFα treatment cells compared to the non-treated. (E-F) Quantification of AKT and InsR normalized to β-actin depicts that 24 h treatment reduces the total level of the InsR, independently of the acute insulin stimulation. Differently, the total level of AKT is not regulated. The numbers above each bar indicate the loading of samples obtained from independent experiments. ***p<0.001, **p<0.01 versus control, by two-way ANOVA followed by Bonferroni's post hoc test. ns = non-significant. Data are presented as the mean ± s.e.m.

It is known that insulin stimulation of the InsR activates IRS1 proteins by means of phosphorylation at specific tyrosine residues. This results in activation of IRS1, which in turn regulates downstream effectors such as PI3K and AKT. On the other hand hyper-serine/threonine phosphorylation of IRS1 is generally associated with reduced activity of the substrate protein and the entire insulin cascade (Gual et al., 2005; Mayer & Belsham, 2010; Yarchoan et al., 2014). Additionally, ubiquitin/proteasome-dependent degradation of IRS1 was described in IR (Tamemoto et al., 1994; Zhande et al., 2002). We therefore examined whether our protocol for induction of IR results in any regulation of the activity of this essential protein of the neuronal insulin pathway (Figure 11 A). The total levels of

IRS1 were first checked and a significant reduction of the protein content was observed in primary cortical culture upon the treatment with insulin and TNFα for 24h (Figure 11 B). Protein degradation concerned also the other main neuronal isoform of the insulin receptor substrate, IRS2 (Figure 11 C). Together with this, IRS1 showed increased phosphorylation at regulatory serine residues (Ser636/639) as evidenced by the normalized phospho-IRS1 to total IRS1 (Figure 11 D-E). This occurred in IR-treated cells, both at basal level and after acute stimulation with insulin. These results suggested that neuronal IR develops as a consequence of an altered phosphorylation as well as an active protein degradation of IRS1.

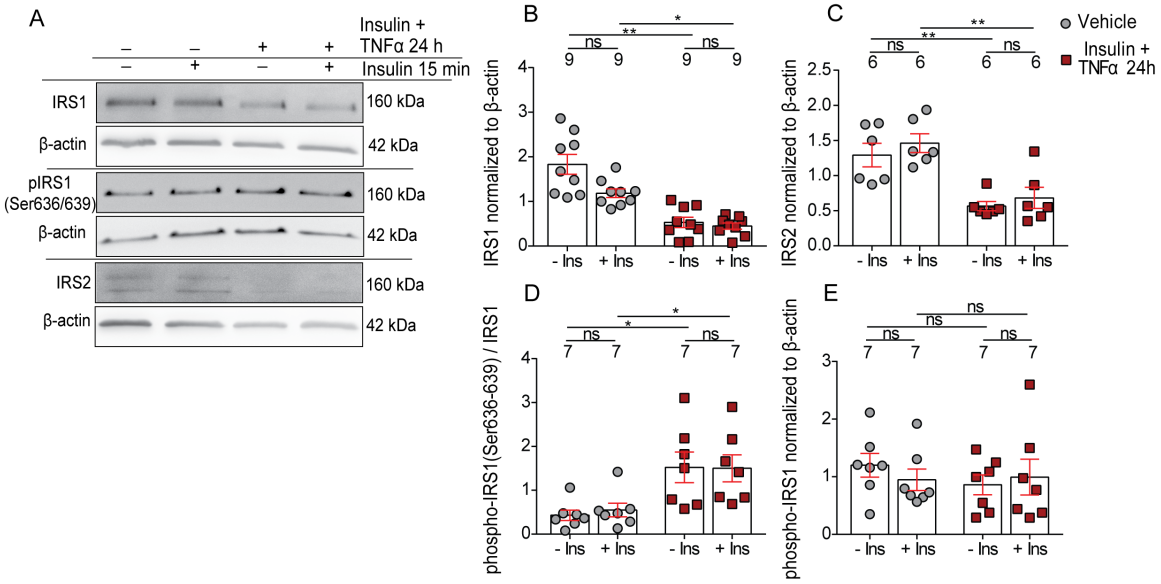

Figure 11: IR in cortical neuronal culture caused IRS1 and IRS2 protein degradation, as well as hyper-serine phosphorylated IRS1. (A) Representative immunoblots of total neuronal cell extracts are shown. Membranes were probed with antibodies detecting phospho-IRS1 (Ser636/639), IRS1 and IRS2. β-actin was used as an internal control for the normalization of the quantitative immunoblot. (B-C) Values normalized to β-actin levels of IRS1 and IRS2 blots are plotted, showing that IR treatment for 24 induces protein down-regulation of both scaffold IRS1 and IRS2. (D-E) Scattered dot plots show the quantified phopsho-IRS1 normalized to the respective non-phosphorylated IRS1 (D) or to β-actin (E). Quantification displayed a clear increased phospho-IRS1 only when this is normalized to the pan-IRS1, which is sensibly down-regulated by the same treatment. The numbers above each bar indicate the loading of samples obtained from independent experiments. **p<0.01, *p<0.5 versus control, by two-way ANOVA followed by Bonferroni's post hoc test. ns = non-significant. Data are presented as the mean ± s.e.m.

3.1.1. Immunocytochemical and biochemical evaluation of synaptic IR

Having established that cultured neurons undergo de-regulation of the insulin pathway at different levels after a prolonged exposure to insulin and TNFα, we next checked whether such changes occur directly at synapses. For this purpose, we employed two different approaches and performed immunostaining of hippocampal neurons and sub-cellular fractionation followed by purification of synaptosomes.

Immunocytochemistry was carried on 21DIV hippocampal neurons stained with AKT or phospho-AKT and their quantification at primary dendrites was performed. Neurons were co-stained with Shank3 antibody, which was used as mask to quantify the intensity of phospho-AKT (Figure 12 A-B) or AKT (Figure 12 C-D) at the co-localization spots.

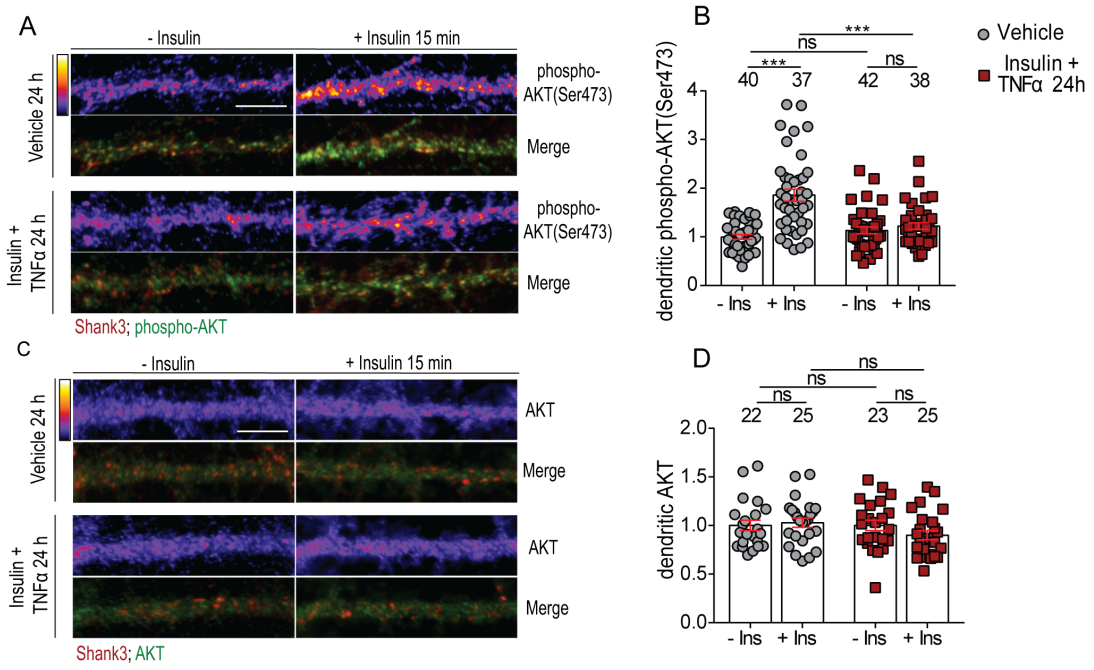

Figure 12: A chronic treatment with insulin and TNFα caused reduced phospho-AKT in hippocampal primary dendrites. (A and C) Representative pictures of primary dendrites of hippocampal neurons immunostained using antibodies anti-phospho-AKT (A) or pan-AKT (C). Coverslips were co-stained with Shank3, used as synaptic marker. Original pixel intensities from 0 to 255 are represented as a gradient lookup table. Scale bar is 10 µm. (B and D) Scatter dot plot representing mean of phospho-AKT or pan AKT at the co-localization sites with the post-synaptic marker Shank3, normalized to control mean values. The Shank3 mask was created semi-automatically using Openview software (Lazarevic et al., 2017; Tsuriel et al., 2006). The numbers above bar correspond to the number of dendrites from different neurons analyzed from at least 3 independent coverslips and at least 2 independent cell cultures. ***p<0.001 versus control, by two-way ANOVA followed by Bonferroni's post hoc test. ns = non-significant. Data are presented as the mean ± s.e.m.

While the total level of AKT were not changed among the groups, immunostaining with an antibody directed against phospho-AKT revealed a reduced activation of AKT along the dendrites and at the post-synaptic sites in IR cells as compared to control groups.

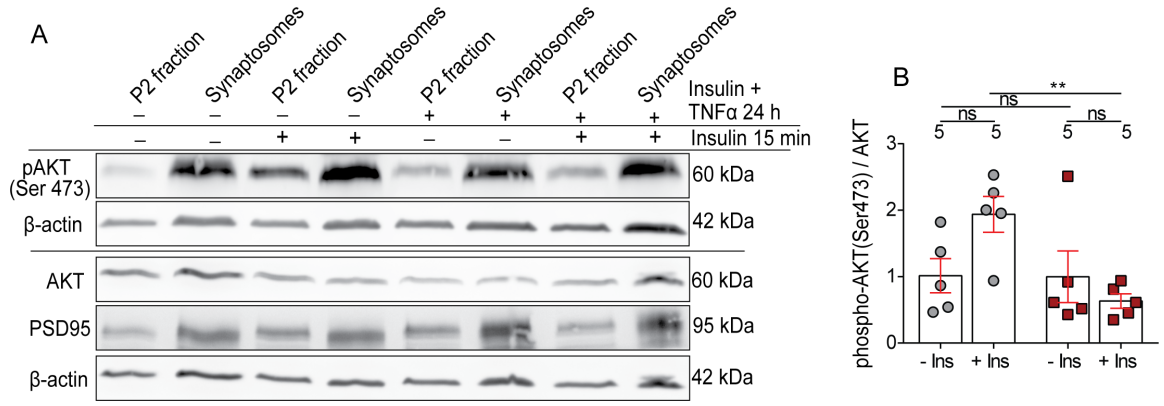

Figure 13: Synaptosomes isolated from IR-treated mature cortical neurons manifested reduced phosphorylated-AKT. (A) Representative picture of immunoblots of synaptosome preparations and their respective P2-fraction loaded as input. Membranes were probed with antibodies against phospho-AKT (Ser473), AKT followed by β-Actin. (B) IR treatment caused in synaptosomes a reduced activation of insulin pathway as depicted by the reduced levels of phospho-AKT as compared to cells treated with vehicle. Quantification was carried out only from the synaptosomes samples (line 2, 4, 6 and 8). The numbers above each bar indicate the number of quantified synaptosomal preparations obtained from independent experiments. **p<0.01 versus control, by two-way ANOVA followed by Bonferroni's post hoc test. ns = non-significant. Data are presented as the mean ± s.e.m.

Synaptosomes were isolated from 21 DIV cortical primary cultures using ultra-centrifugation in a 1M/1.2M sucrose gradient. Total neuronal homogenate were previously centrifuged in order to get a crude membrane preparation (P2-fraction), which was then loaded onto the sucrose gradient column. The ultracentrifugation of the column allows the deposition of synaptosomes at the interphase between the two sucrose steps, where the density of the gradient equates the density of the synaptosomes. Synaptosomes were collected and proteins extracted using SDS-containing buffer. Proteins from both synaptosomes and P2-fractions were separated through SDS-PAGE gradient gel and quantitative immunoblot was performed (Figure 13 A). The western blot revealed a reduced responsiveness to acute insulin stimulation in synaptosomes upon cell treatment with insulin and TNFα as outlined by the reduced phosphorylated AKT (Figure 13 B).

Taken together, these results indicated that cultivated neurons undergo synaptic IR induced by long exposure to insulin and TNFα and characterized by disruption of the insulin-signaling pathway at the synapse.

3.1.2. Synaptic IR inhibits activity of PI3Kγ

The production of $PI(3,4,5)P_3$ from $PI(4,5)P_2$ by PI3K family proteins is important in numerous aspects of cell signaling, including the insulin pathway. $PI(3,4,5)P_3$ is a second messenger recognized by PDK1 proteins, which then phosphorylates and thus activates AKT. PI3K are ubiquitously expressed and play diverse roles such as regulation of cell growth, migration, differentiation and survival (Gross & Bassell, 2014). In neurons, PI3K have been implicated in synaptic plasticity, cell survival and other key physiological functions (Borrie et al., 2017; Kim et al., 2011). Interestingly, it has been recently found that the isoform PI3Kγ has a crucial role in NMDA receptor-mediated synaptic plasticity at mouse Schaffer collateral-CA1 synapses (Kim et al., 2011). PI3Kγ belongs to the Class IB of PI3K family. While the Class IA PI3Ks are usually activated by a receptor tyrosine kinase, including InsR, the Class IB PI3Ks are usually activated by the βγ subunit of G protein–coupled receptors (GPCRs) (Hawkins, et al., 2006; Oudit et al., 2004; Pomel et al., 2006; Wymann & Pirola, 1998). In contrast to the major Class IA PI3Ks, PI3Kγ are expressed only in immune system, cardiovascular system and brain (Pomel et al., 2006; Stoyanov et al., 1995). Apparently, PI3Kγ have important role in inflammatory processes. E.g. reduced recruitment of PI3Kγ was observable in *in vivo* models of inflammation (Hirsch et al., 2000) and mice lacking the catalytic subunit of class IB PI3K are remarkably resistant to the development of several inflammatory pathologies in mouse models of human inflammatory disease (Andrews et al., 2007).

In order to specifically address the role of synaptic IR in the activity of PI3Kγ *in vitro*, a competitive colorimetric ELISA was performed. To this end, PI3Kγ was immunoprecipitated from a total cell extract of primary cortical neurons using specific antibodies. The substrate $PI(4,5)P_2$ was then added to the reaction and the amount of $PI(3,4,5)P_3$ converted by immunoprecipitated PI3Kγ was quantified using $PI(3,4,5)P_3$-coated detection plate for competitive binding (Figure 14 A). The ELISA revealed a prominent reduction in the activity of the PI3Kγ in neurons in which IR was induced by

means of the treatment with insulin and TNFα for 24 h (Figure 14 B). AS-605240 (5-quinoxalin-6-ylmethylene-thiazolidine-2,4-dione) is a selective inhibitor of PI3Kγ (Barber et al., 2005; Kim et al., 2011) and it was added to the control group during the enzymatic reaction and was used as negative control. Western blot of the eluted PI3Kγ revealed that the difference observed in the ELISA is not due to the amount of immunoprecipitated PI3Kγ but relies on the activity of the enzymes as such (Figure 14 C-D).

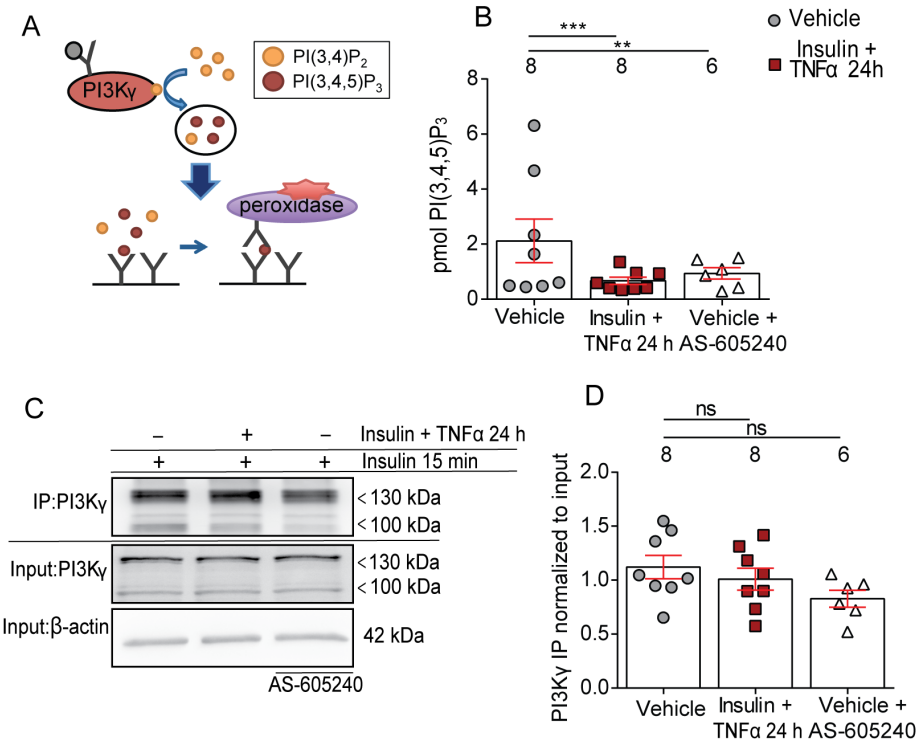

Figure 14: IR induced by insulin and TNFα reduced PI3Kγ activity. (A) Schematic representation of endogenous PI3Kγ immunoprecipitation and conversion of $PI(4,5)P_2$ in $PI(3,4,5)P_3$. The product of the reaction is measured by colorimetric reaction in $PI(3,4,5)P_3$-coated detection plate for competitive binding. (B) ELISA competitive assay shows reduced activity of the immunoprecipitated PI3Kγ in insulin/TNFα treated cells as compared to control cells treated with vehicle. AS-605240 added to the control group in a separate IP was used as negative control. (C) After the enzymatic reaction was completed and $PI(3,4,5)P_3$ collected, PI3Kγ enzyme was eluted from the beads and the amount of immunoprecipitated protein was evaluated by quantitative immunoblot. (D) Quantification of the IP PI3Kγ, normalized to the respective input PI3Kγ, is plotted and shows no significant differences of immunoprecipitated PI3Kγ among the groups. ***p<0.001, **p<0.01 versus control, by two-tailed Student's t-test. ns = non-significant. Data are presented as the mean ± s.e.m.

3.1.3. Insulin and TNFα elicit neuronal IR by different mechanisms and their combination exacerbates IR

The experiments carried out in cultivated neurons so far indicated a potent effect of insulin and TNFα to induce IR *in vitro*. As mentioned above, the co-application of the two drugs together tried to take into the account the two major events in brains affected by MetS and amyloidosis that might result in AD pathology.

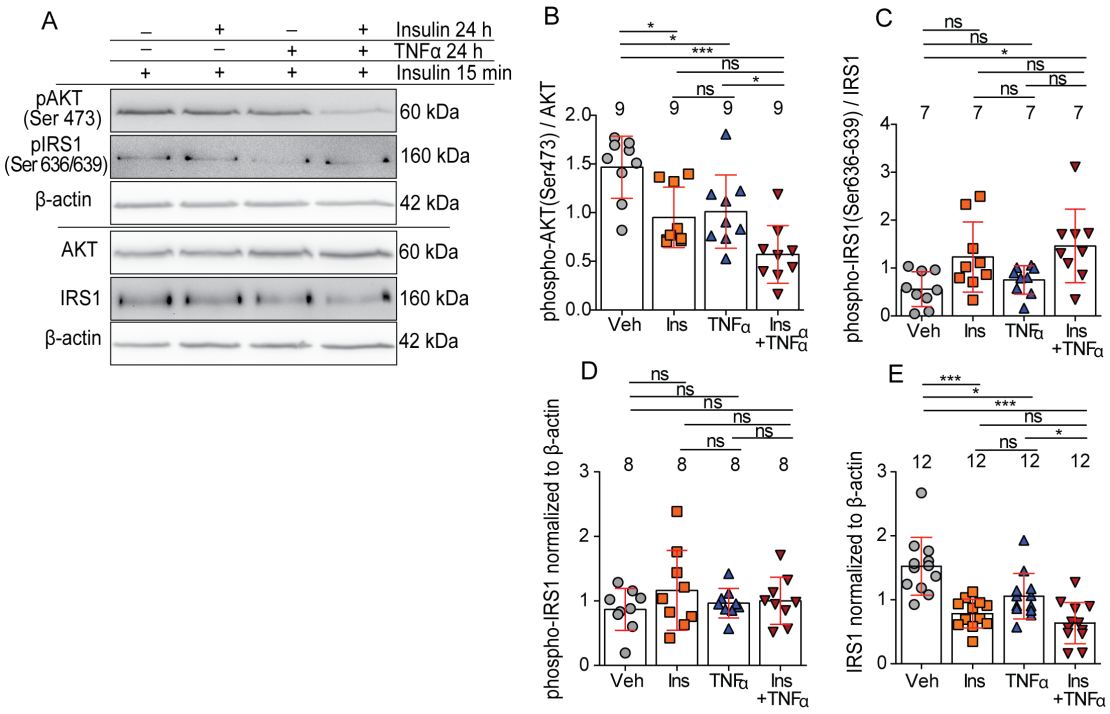

Figure 15: Long exposure to insulin induced IRS1 protein degradation, while TNFα increased serine-phosphorylation of IRS1. Together, insulin and TNFα cooperated to elicit neuronal IR. (A) Representative immunoblots of total cortical cell extracts probed with antibody anti-AKT, -phospho-AKT (Ser473), -IRS1 and -phospho-IRS1 (Ser636/639). β-actin was used as an internal control for the normalization of the quantitative immunoblot. (B) Quantification of phospho-AKT normalized to AKT shows reduced activation when cells are treated with either insulin (100 nM) or TNFα (10 ng/ml) as compared to vehicle-treated control. Reduction of the phosphorylated AKT is significantly more pronounced in neurons that received co-application of insulin and TNFα together. (C-D) Quantification of serine-phosphorylated IRS1 normalized to total IRS1 (C) or β-actin (D). Quantification displayed an increased phospho-IRS1 only when this is normalized to the pan-IRS1, which is sensibly down-regulated by the same treatment. (E) Quantification of total IRS1 protein levels highlights the prominent effect of the chronic application of insulin to induce IRS1 degradation. Much less prominent is instead the effect of TNFα on this regard. The numbers above each bar indicate the loading of samples obtained from independent experiments. **p<0.01, *p<0.05 versus control, by one-way ANOVA followed by Tukey's post hoc test. ns = non-significant. Data are presented as the mean ± s.e.m.

We next investigated what are the effects elicited by IR and neuroinflammation, respectively, and whether they work in concert to disrupt the insulin pathway. To this end, 21DIV cortical neurons were treated with either insulin or TNFα for 24 h and compared to cells treated with both. Quantitative immunoblot revealed that both bath applications of insulin or TNFα reduced AKT activation. However, interestingly the co-application of both drugs results in an exacerbated phenotype (Figure 15 B). In a similar fashion, the serine-phosphorylation of IRS1 was also incremented by insulin and TNFα together as compared to single application (Figure 15 C-D). Notably, TNFα elicited a limited effect on IRS1 protein degradation, which is instead observed sensibly higher in cells treated with insulin (Figure 15 E). This can be interpreted with a potential limited role of TNFα in the protein degradation of IRS1 that instead relies on the prolonged insulin action. TNFα and neuroinflammation on the other hand contribute to IR activation of stress-response kinases (e.g. PKR, JNK or IKK) phosphorylating IRS1 at inhibitory serine residues.

To follow-up on the hypothesis that insulin and TNFα induce IR acting respectively on the IRS1 protein degradation and serine-phosphorylation, we next tested whether Aβ3(pE)-42-induced astroglial TNFα release is counteracted by a specific TNFα neutralizing antibody applied to the culture. Pyro-glutamylated-β amyloid peptide Aβ3(pE)-42 is known to have seeding properties for other Amyloid-β species (Schilling et al., 2006; D'Arrigo et al., 2009; Schlenzig et al., 2009) and a potent effect in the induction of glial release of TNFα after the uptake from astrocytes (Grochowska et al., 2017). Interestingly, co-application of Aβ3(pE)-42 and insulin to glia-containing neuronal culture induced neuronal IR in a similar manner to insulin/TNFα treated cells, evoking similar effects in terms of phosphorylated-AKT (Figure 16 B), IRS1 (Figure 16 C) and phospho-IRS1 (Figure 16 D-E). Co-application of a TNFα neutralizing antibody rescued Aβ3(pE)-42-induced hyper-phosphorylation of IRS1 at inhibitory serine residues, whereas no rescue of the total IRS1 levels was observed. IRS1 protein degradation is sufficient to keep the insulin pathway inactive, as highlighted by the phosphorylated AKT (Figure 16 B). A straightforward hypothesis deriving from this scenario is that over-activation of the insulin pathway by insulin causes the activation of a pathway that results in the degradation of IRS1. Under neuroinflammatory conditions, the efficiency of the

insulin signaling is worsened by the inhibition of the leftover pool of IRS1 protein.

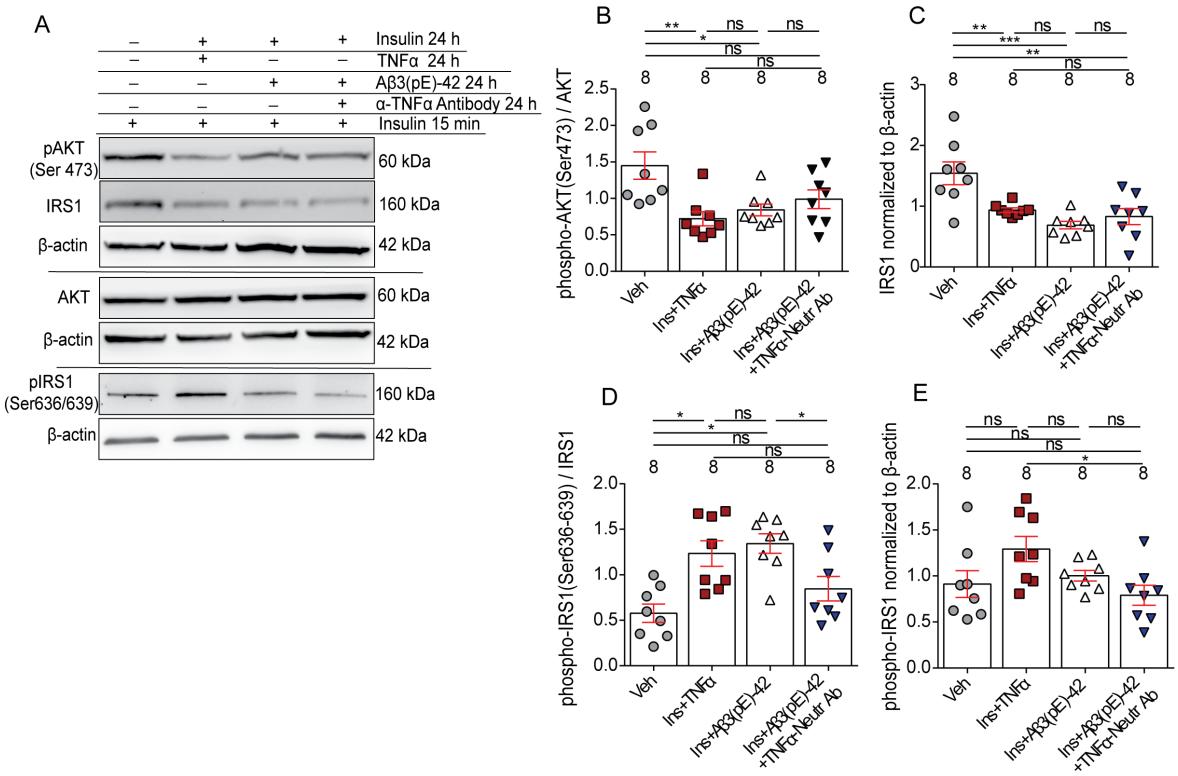

Figure 16: Aβ3(pE)-42 application to glia-containing neuronal culture induced TNFα release and the co-application of anti-TNFα antibody prevented Aβ3(pE)-42-caused hype-phosphorylated IRS1, but not IRS1 protein degradation. (A) Representative immunoblots of total cortical cell extracts probed with antibodies directed against anti-AKT, -phospho-AKT (Ser473), -IRS1 and -phospho-IRS1 (Ser636/639). Each blot was probed in addition with a β-actin antibody, used for normalization (B-C) Quantification of phospho-AKT normalized to AKT and IRS1 total levels shows reduced insulin pathway activation when cells are treated with insulin and Aβ3(pE)-42 as in the insulin and TNFα group. Anti-TNFα does not prevent IR-dependent reduced AKT phosphorylation and IRS1 down-regulation. (D-E) Quantification of serine phosphorylated-IRS1 normalized to total IRS1 (C) or β-actin (D). Insulin and Aβ3(pE)-42 increase serine-phosphorylated IRS1 as in the insulin and TNFα group. Anti-TNFα fully prevents it. The numbers above the bars indicate the loading of the samples obtained from independent experiments. ***p<0.001, **p<0.01, *p<0.5 versus control, by one-way ANOVA followed by Tukey's post hoc test. ns = non-significant. Data are presented as the mean ± s.e.m.

3.2. Neddylation-dependent regulation of insulin signaling

3.2.1. IRS1 and InsR protein degradation is neddylation dependent and is rescued by the selective neddylation inhibitor MLN-4924

Like many other cells, neurons employ the ubiquitin-proteasome protein degradation to regulate crucial processes. Neddylation is a post-translation modification

of proteins, which mainly belong to the family of cullins, and consists of the attachment of the small ubiquitin-like protein NEDD8 to cullins. Neddylation/de-neddylation of cullins regulates their ubiquitin E3-ligase activity. Once neddylated, cullins ubiquitinate target proteins leading to proteasomal degradation of those. The experiments performed hitherto have evidenced that a chronic treatment of neurons with high concentration of insulin causes a massive protein down-regulation of IRS1, IRS2 and InsR in neurons. Consequently, we hypothesized that these proteins might be actively degraded by the proteasome system in a NEDD8-dependent manner. To test this hypothesis, we took advantages of the usage of the NEDD8-activating enzyme (NAE) inhibitor MLN-4924. NAE is an E1-like enzyme that recognizes cleaved NEDD8 and catalyzes the first reaction of the neddylation cascade. MLN-4924 forms a NEDD8-AMP mimetic and thereby prevents the initial loading of NEDD8 to NAE (Soucy et al., 2009).

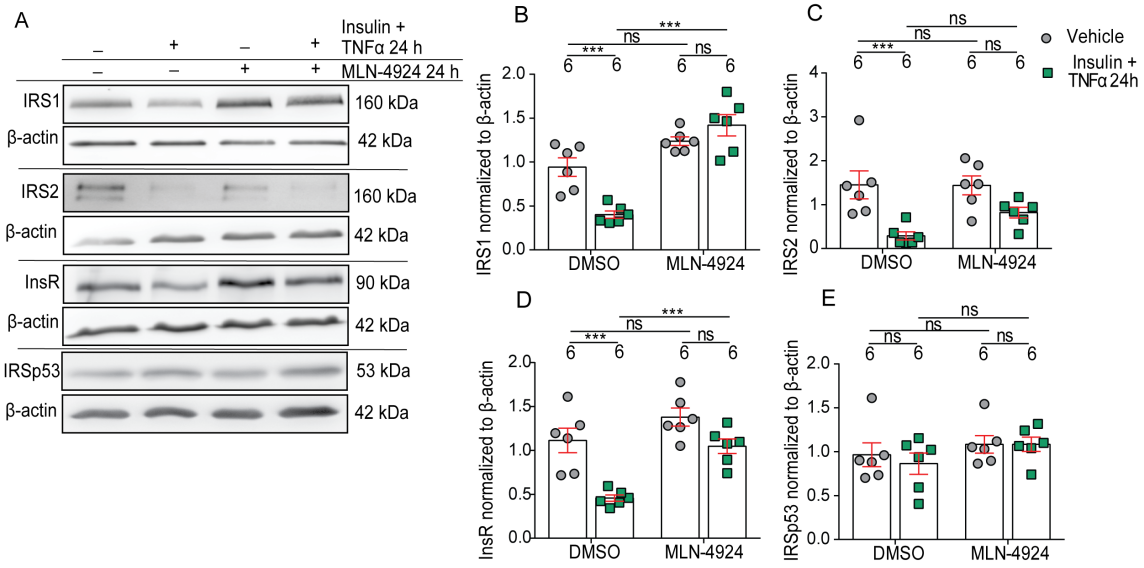

Figure 17: MLN-4924 prevented IR by means of blocking the protein degradation of IRS1 and InsR. (A) Representative pictures of immunoblot of total cell extracts from cortical neurons in which IR was induced and MLN-4924 or DMSO were co-applied for 24 h. Neurons were harvested directly after the treatment. Membranes were probed with antibodies directed against anti-IRS1, -IRS2, -InsR and -IRSp53. All blots were probed with β-actin antibody for normalization. (B-E) Scatter dot plot with the quantification of the total levels of normalized proteins show that MLN-4924 abolishes the protein degradation of IRS1 and InsR. Although IRS2 is degraded under IR condition, the treatment with MLN-4924 shows only a partial rescue. Differently from the other IRS proteins, IRSp53 seems not to be regulated at all by the IR. The numbers above the bars indicate the loading of the samples obtained from independent experiments. ***p<0.001, **p<0.01 versus control, by two-way ANOVA followed by Bonferroni's post hoc test. ns = non-significant. Data are presented as the mean ± s.e.m.

In order to address whether the degradation of InsR, IRS1 and IRS2 that we observed after neuronal IR induction is neddylation-dependent, 1 μM MLN-4924 was co-applied with insulin and TNFα to primary cortical neurons. DMSO was used as control. 24 h later cells were harvested and quantitative immunoblot of the total cellular extract was performed. Membranes were probed with anti-IRS1, -IRS2, -InsR and -IRSp53 antibodies (Figure 17 A). Notably, MLN-4924 was able to fully counteract the IR-induced degradation of IRS1 and InsR as compared to control group (Figure 17 B and D), while only a partial rescue of IRS2 levels was observed (Figure 17 C). Differently from the other proteins investigated, IRSp53 was not regulated by insulin and TNFα and consequently, MLN-4924 had no effect (Figure 17 E).

3.2.2. MLN-4924 rescues insulin-dependent AKT phosphorylation in IR neurons

Given the positive effect of MLN-4924 on rescuing the total level of those proteins that are key regulators of the insulin pathway, we next investigated whether MLN-4924 might restore also the responsiveness to insulin in IR neurons. As in the previous experiment, DIV21 primary cortical neurons where treated with insulin and TNFα or vehicle and MLN-4924 or DMSO were co-applied. Cells were harvested 24 h later after washing and acute insulin stimulation. Western blot was executed from the total neuronal homogenate and membranes were probed with phospho-AKT and AKT as well as phospho-InsR and InsR antibodies. Consistent with the previous data, prolonged treatment with insulin and TNFα caused a de-phosphorylation of AKT and InsR in the acute insulin-stimulated group. Interestingly, MLN-4924 application prevented de-phosphorylation of AKT and the InsR in IR neurons as compared to DMSO application (Figure 18 A-C).

In parallel, immunocytochemical analysis of hippocampal primary neurons stained with phospho-AKT and pan-AKT was performed. As described above, DIV21 neurons received the co-application of insulin/TNFα and MLN-4924 for 24 h followed by acute insulin stimulation for 15 min. The mean intensity of phospho-AKT and pan-AKT was evaluated at the Shank3 co-localizing spots. As expected, immunostaining with antibody

against phospho-AKT depicted a reduced phosphorylation in dendrites of IR cells. The co-application of MLN-4924 rescued the phosphorylation of AKT (Figure 19 A-B), while it had no effect on the total level of AKT (Figure 19 C-D). Taken together, these results show that inhibition of neddylation via MLN-4924 prevents IR inhibiting the neddylation-dependent proteasomal degradation of IRS1 and InsR and therefore counteracting de-phosphorylation of AKT.

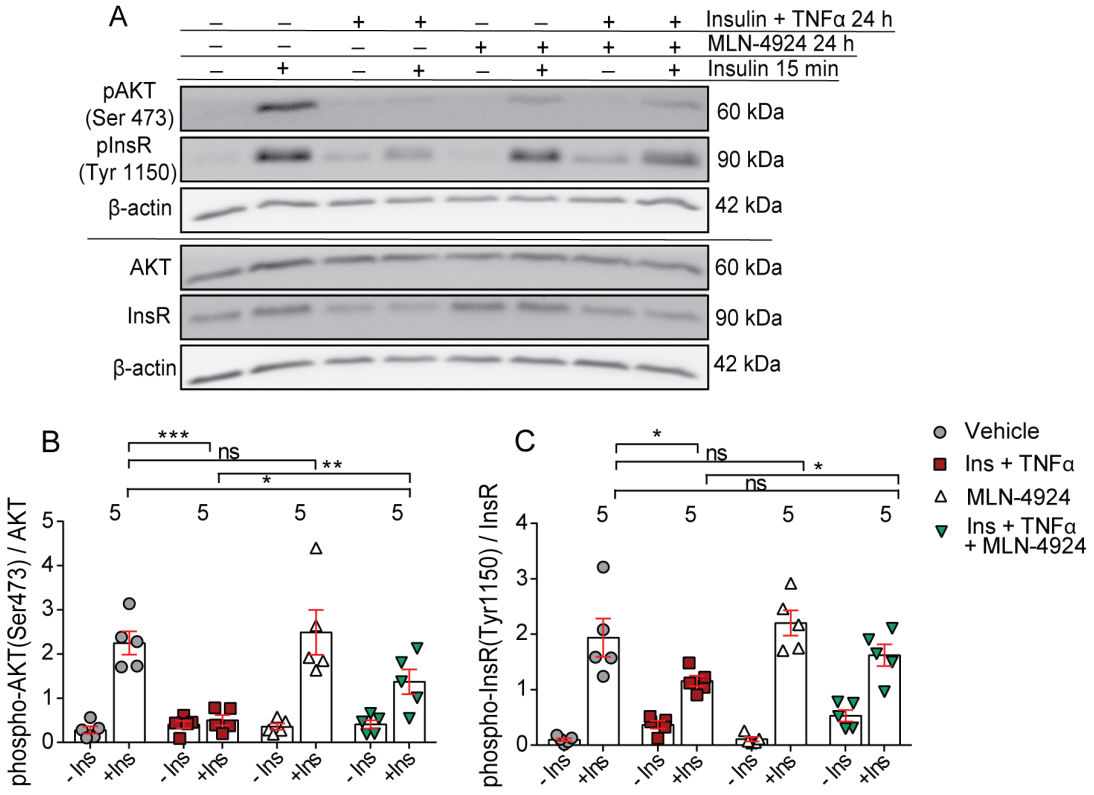

Figure 18: MLN-4924 prevented IR and de-phosphorylation of AKT and InsR in cortical primary neurons. (A) Primary cortical neurons were treated with insulin and TNFα or vehicle for 24 h. MLN-4924 or DMSO was co-applied. Treatment was followed by a wash for 1 h and an acute stimulation with insulin or vehicle for 15 min. Representative pictures of immunoblots are shown. Membranes were probed with antibodies detecting phospho-AKT (Ser473), phospho-InsR (Tyr1150), AKT, InsR and β-actin. (B-C) Quantification of blots was carried out as in the above described experiments and the normalized values were plotted. Statistical analysis refers to the groups that have received the insulin acute simulation only. The numbers above the bars indicate the replicates obtained from independent experiments. ***p<0.001, **p<0.01, *p<0.05 versus control, by two-way ANOVA followed by Bonferroni's post hoc test. ns = non-significant. Data are presented as the mean ± s.e.m.

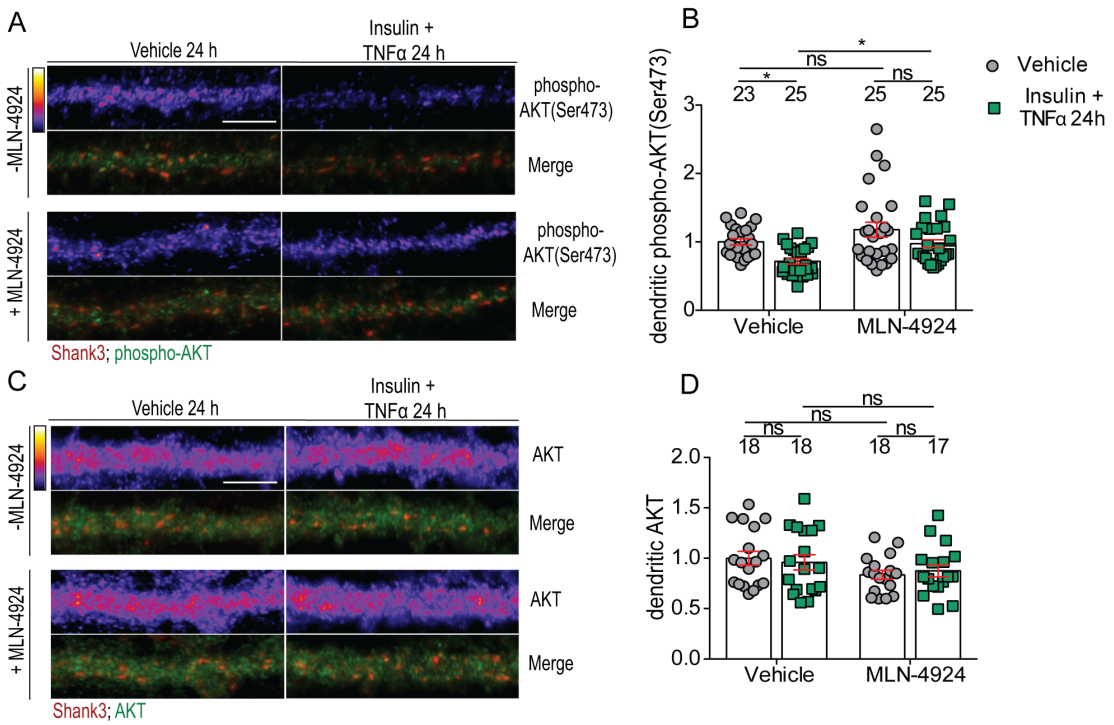

Figure 19: MLN-4924 prevented IR and de-phosphorylation of AKT in hippocampal dendrites. (A and C) Representative picture of primary dendrites of hippocampal neurons immunostained using antibodies anti-phospho-AKT or pan-AKT. Coverslips were co-stained with Shank3, used as synaptic marker. Original pixel intensities from 0 to 255 are represented as a gradient lookup table. Scale bar is 10 µm. (B and C) Quantification was carried out using Shank3 as mask, which was generated semi-automatically by Openview software (Lazarevic et al., 2017; Tsuriel et al., 2006). Numbers above the bars correspond to the number of dendrites from different neurons analyzed from at least 2 independent coverslips and at least 2 independent cell cultures. *p<0.05 versus control, by two-way ANOVA followed by Bonferroni's post hoc test. ns = non-significant. Data are presented as the mean ± s.e.m.

3.3. NEDD8-dependent IRS1 degradation involves specific cullins

Potential mediators of IRS1 degradation are members of the cullin family of E3-ubiquitin ligases. As already mentioned above, cullins are substrates of neddylation. They are generally neddylated by the covalent bound to NEDD8, which occurs through three enzymatic reactions. Thus, cullins combine with RING proteins to form Cullin-RING ubiquitin E3 ligases (Petroski & Deshaies, 2005), which generally ubiquitinate specific target proteins and render them susceptible to proteosomal degradation. Seven different cullins are expressed in the brain: CUL1, CUL2, CUL3, CUL4A, CUL4B, CUL5, CUL7 (Allen mouse and human Brain Atlas. http://portal.brain-map.org/). It was reported that, among the various isoforms, CUL7 could have a specific role in the degradation of IRS1

in non-neuronal cells (Xu et al., 2008). Nevertheless, it is not excluded that other isoforms could also be in complex with IRS1 and have a possible role in its degradation.

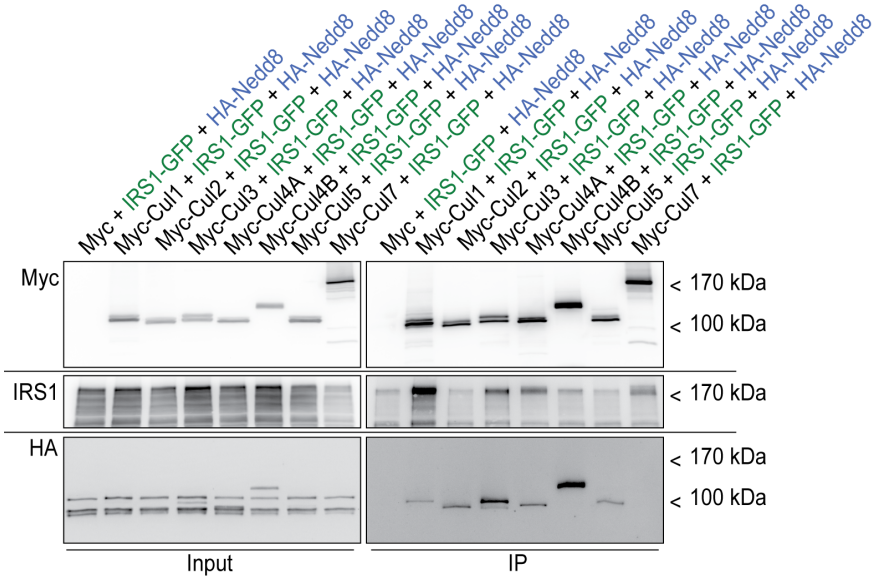

Figure 20: IRS1 co-immunoprecipitated with certain cullins: CUL1, CUL3, CUL4A and CUL7. HEK293T cells were transfected with expression vectors for GFP-IRS1, HA-NEDD8 and Myc-vector containing one of the family members of cullins known to be expressed in neurons (CUL1, CUL2, CUL3, CUL4A, CUL4B, CUL5, and CUL7). Transfection with empty Myc-vector was used as control. Total protein extracts were immunoprecipitated using anti-Myc microbeads. Inputs and co-IP were loaded in separated gels. IRS1 was detected along with immunoprecipitated CUL1, CUL3, CUL4A and CUL7. The experiment was repeated twice.

To follow-up on this hypothesis, we performed an initial experiment to test whether IRS1 immunoprecipitates with one or more cullins. Heterologous co-IP experiments revealed that IRS1 indeed co-immunoprecipitated with CUL7, but also with CUL1, CUL3 and CUL4A from HEK293T cell lysate following heterologous expression together with NEDD8 labeled with the HA-tag (Figure 20). Interestingly, this experiment highlighted another important point: co-expression of CUL7 with IRS1 caused IRS1 degradation in a specific manner as depicted in the input. This suggests that, consistently with what published by Xu and colleagues (Xu et al., 2008), CUL7 plays a role in the degradation of IRS1. Additionally, despite the presence of a neddylation site along CUL7, NEDD8 did not co-immunoprecipitate with CUL7. A possible explanation coming from this scenario is that CUL7-dependent IRS1 ubiquitination degradation depends from other

mechanisms different from neddylation. Alternatively, the activation of CUL7 by neddylation relies on the formation of a more complex interaction with other proteins.

Moreover, to confirm the contribution of cullins to IRS1 degradation, we next performed co-IP from HEK293T cells using GFP microbeads and checked for the ubiquitination levels of IRS1 (Figure 21).

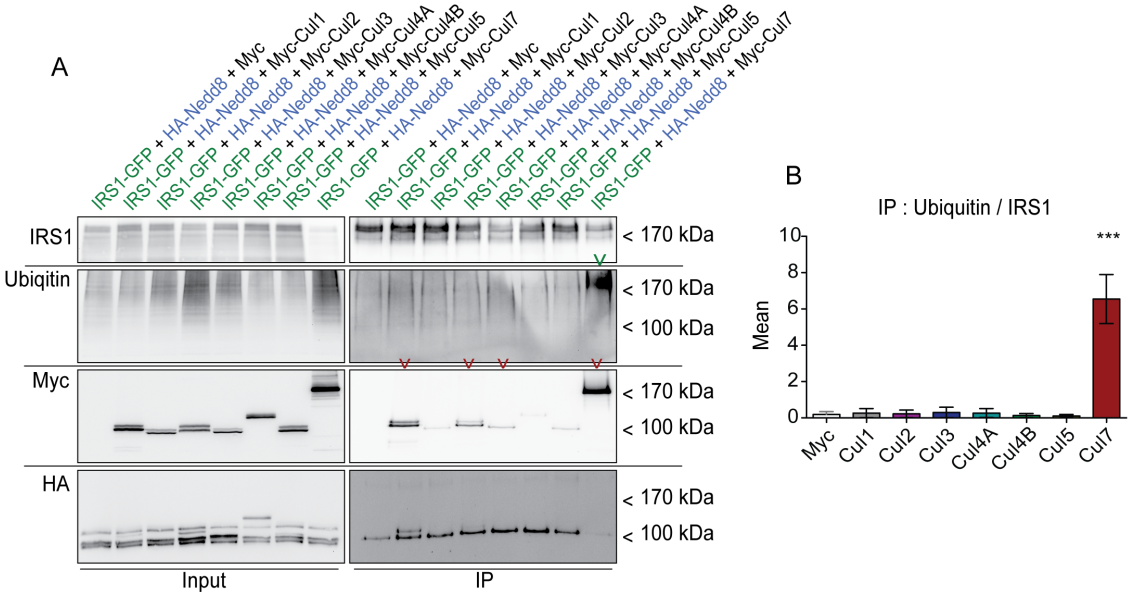

Figure 21: The interaction between CUL7 and IRS1 enhanced IRS1 ubiquitination. HEK293T cells were transfected with expression vectors for GFP-IRS1, HA-NEDD8 and Myc-vector containing one of the family members of cullins (CUL1, CUL2, CUL3, CUL4A, CUL4B, CUL5, and CUL7) or empty Myc-vector. Total protein extracts were immunoprecipitated using anti-GFP microbeads. (A) Western blot of inputs and co-IP probed with mono- and poly-ubiquitin detecting antibody revealed massive ubiquitination at the molecular weight corresponding of the size of IRS1 (green arrow). (B) Ubiquitination of IRS1 is quantified by mean of the ratio between immunoprecipitated ubiquitin band and IRS1. The results of two independent experiments are displayed. ***p<0,001 versus control, by one-way ANOVA followed by Tukey's post hoc test. Data are presented as the mean ± s.e.m.

Interestingly, although IRS1 co-immunoprecipitated with CUL1, CUL3, CUL4A and CUL7 (red arrows), it turned out that only co-expression of IRS1 with CUL7, but no other cullins, specifically enhanced IRS1 ubiquitination (green arrow) (Figure 21 A-B).

Since the interaction between IRS1 and CUL7 affected IRS1 poly-ubiquitination, we next investigated whether IRS1 ubiquitination is regulated by neddylation. To this end, HEK293T cells were transfected with expression vectors for GFP-IRS1, HA-NEDD8 and Myc-CUL7. Cells were treated for 24h with the neddylation inhibitor MLN-4923 or the

selective proteasome inhibitor MG-132. Bath application of MG-132 showed pronounced increase in the ubiquitination of IRS1, indicating that IRS1 degradation is proteasome-dependent. Albeit it is not significant, less ubiquitination was instead observed when MLN-4924 was applied.

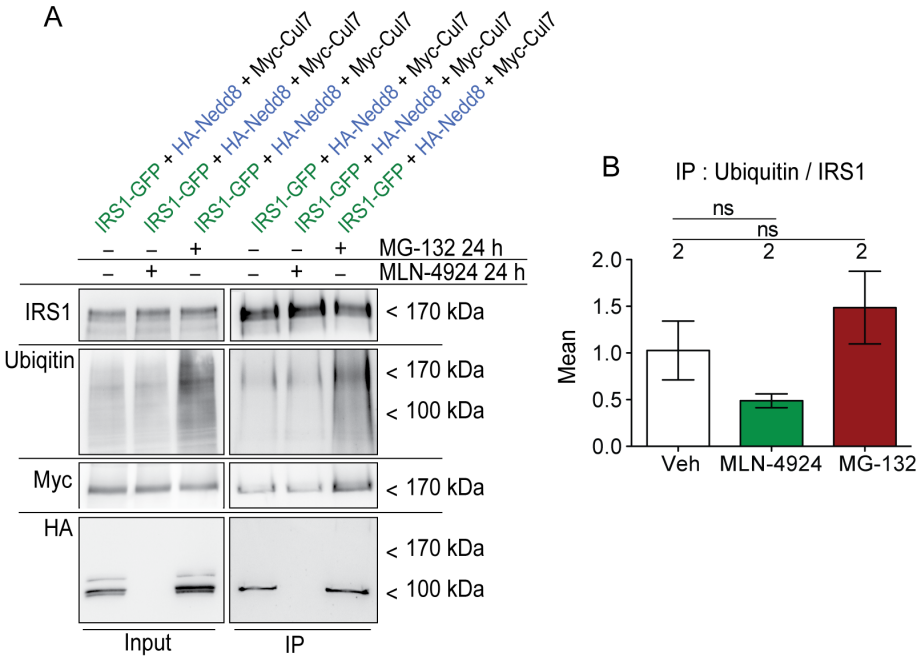

Figure 22: Neddylation inhibition reduces IRS1 ubiquitination. (A) HEK293T cells were transfected with expression vectors for GFP-IRS1, HA-NEDD8 and Myc-CUL7. Total protein extracts were immunoprecipitated using anti-GFP microbeads. Less ubiquitination was observed when NAE inhibitor MLN-4924 (1 μM) was applied for 24 h. Proteasomal inhibitor MG-132 (20 nM) was applied also for 24 h and shows increased ubiquitination of IRS1, meaning that IRS1 degradation is proteosomal-dependent. NEDD8 was detected with an anti-HA antibody showing complete abolishment of neddylation. (B) Ubiquitination of IRS1 is quantified by mean of the ratio between immunoprecipitated ubiquitin band and IRS1. The results of two independent experiments are displayed. ns = non-significant versus control, by one-way ANOVA followed by Tukey's post hoc test. Data are presented as the mean ± s.e.m.

This finding supported the idea that IRS1 ubiquitination depends on the neddylation of CUL7. As confirmation that MLN-4924 efficiently blocked neddylation we proved that co-immunoprecipitation of NEDD8, detected by anti-HA antibody, is abolished in treated cells with MLN-4924. However, and in accordance with the previous data, NEDD8 band was detected at approximately 100 kDa, while the molecular weight of CUL7 is around 170 kDa. These findings raised the hypothesis that NEDD8 is not directly conjugated to

CUL7, but rather to some other cullin(s), which successively activates CUL7 as ubiquitin E3-ligase specific for IRS1.

3.3.1. CUL7 and CUL3 co-immunoprecipitate with NEDD8 in neurons

In order to better study the role of neddylation in neurons and to clarify the molecular mechanism of IRS1 degradation at the synapses, adeno-associated viruses AAV9 carrying HA-tagged active-NEDD8 were employed. Primary cortical neuronal cultures were infected at DIV11 and NEDD8-HA was expressed for 11 more days. AAV9-NEDD8-HA infection efficiency in neurons and over-expression of NEDD8-HA was first assessed by western blot (Figure 23 A). Furthermore, we performed co-IP assays in AAV9-NEDD8-HA infected neurons using anti-HA microbeads and checked for the co-immunoprecipitated cullins. Nuclei were previously removed to avoid contamination with the nuclear cullins and the rest of the cellular extracts were used as input. Although in low amounts, CUL7 and CUL3 co-immunoprecipitated with NEDD8 in the post-nuclear fraction following NEDD8-HA expression (Figure 23 B).

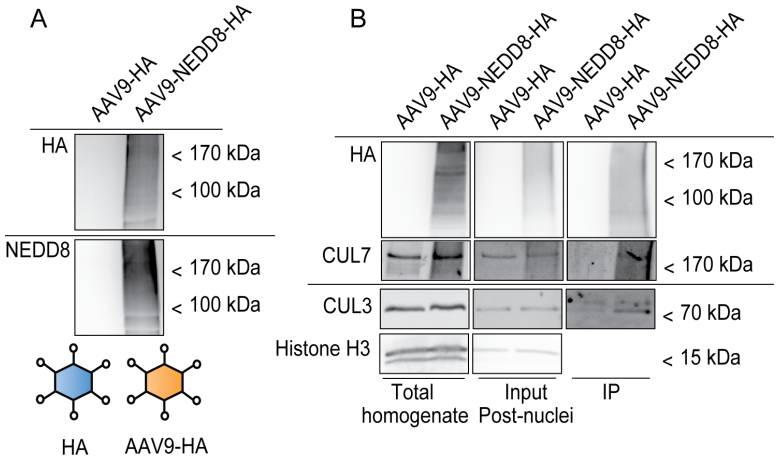

Figure 23: CUL7 and CUL3 co-immunoprecipitated with NEDD8 in NEDD8-HA AAV9 infected neurons. (A) Primary cortical neurons were cultured until DIV11 and then infected with either AAV9-NEDD8-HA or AAV9-empty HA-tag. Cells were harvested at the DIV 21. Western blot of total protein extracts showed massive expression of the construct NEDD8-HA as underlined by both HA and NEDD8 antibodies detection. (B) Post-nuclear fraction was prepared from 10 days long infected neurons and immunoprecipitated using anti-HA microbeads. Western blot of inputs and co-IP probed with CUL3 or CUL7 antibody shows co-immunoprecipitation of CUL3 and CUL7 in NEDD8-HA infected neurons. Histone H3 was used to prove purity of the nuclear preparation. The result of one experiment is displayed.

3.4. TBA2.1 mice can be used as an *in vivo* model for synaptic IR and amyloidosis

The *in vitro* experimental batteries showed that cultivated neurons chronically treated with insulin and TNFα undergo synaptic IR. Although insulin overexposure and neuroinflammation seem to be in tight relation with each other in the elicitation of IR, they apparently have different roles into the pathological process of neuronal IR.
In order to validate these hypotheses *in vivo*, TBA2.1 mice were employed. +/Tg TBA2.1 mice express human pyro-glutamylated-β amyloid peptide Aβ3(pE)-42 in the brain (Paragraph 2.1.9.). Precursor human Aβ peptide is translated under Thy-1 promoter as fusion protein with the murine TRH hormone. Peptides are cleaved within the trans-Golgi and released via the secretory pathway, where they are converted by QC to the final product Aβ3(pE)-42 (Alexandru et al., 2011). The TBA2.1 mice were therefore used as a model for elevated amyloidosis. Additionally, MetS and IR were induced in +/+ or +/Tg TBA2.1 mice by feeding them with an high fat diet (HFD) in order to study the interplay between Aβ3(pE)-42-iduced neuroinflammation and IR *in vivo*.

3.4.1. HFD induces peripheral IR in mice

Male +/+ or +/Tg TBA2.1 mice were fed with high fat/high calories chow for up to 22 weeks until they reached the threshold of 70% of body weight increase as compared to the beginning of the diet. Animals fed with a regular chow (Regular diet, RD) were employed from both genotypes as control. Control animals were used at the same age of HFD animals. However, they were used only if their body weight did not exceed the threshold of 40% increase (Figure 24 A).

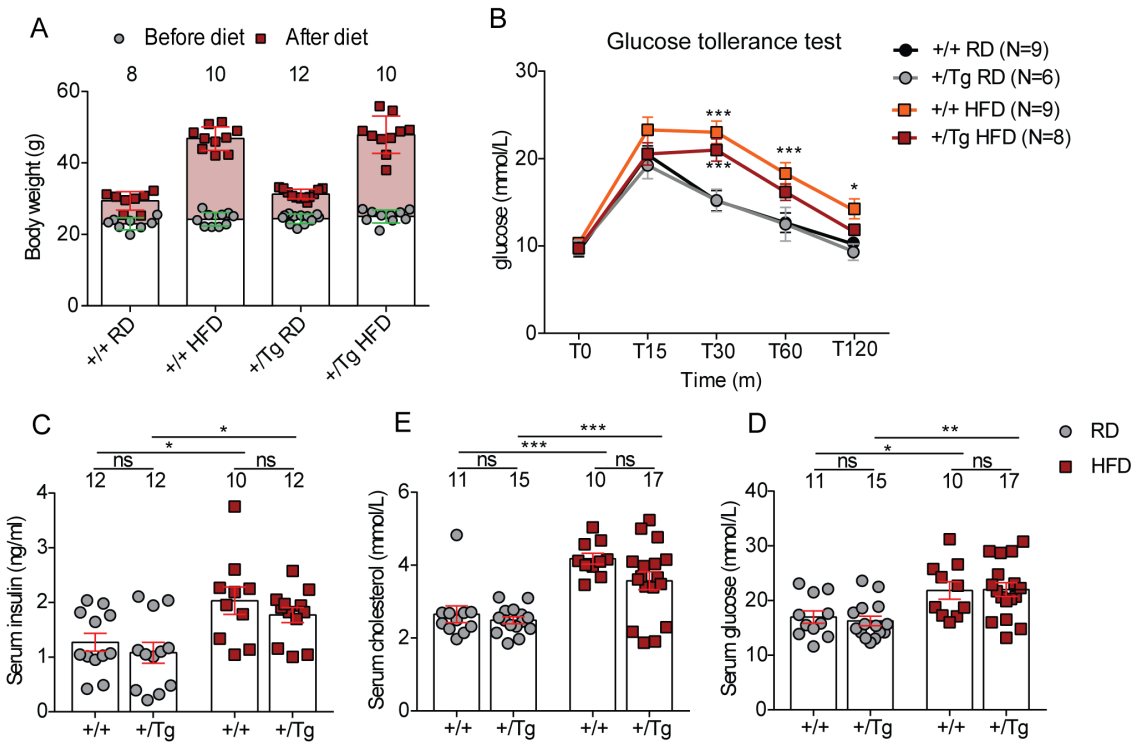

Figure 24: 14 to 26 weeks of high fat/caloric diet induced peripheral IR in TBA2.1 mice. (A) Scatter dot plot of the body weight of +/+ and +/Tg TBA2.1 mice both RD and HFD measured at the beginning of the diet (8-9 weeks old) and before starting every experiment (23-35 weeks old). (B) A dose of 1 g/kg glucose was injected intraperitoneally in mice previously fasted for 6 h to perform glucose tolerance test. Blood glucose concentrations were measured before the injection (t=0) and then repeated at different time points (t=15, t=30, t=60 and t=120). Each time a fresh drop of blood was taken by making a small incision in the tail of the mouse. A blood glucose-meter was used to measure the glucose concentration and the values were plotted. Graph shows that HFD +/+ and +/Tg TBA2.1 mice require much longer time to clear up glucose from the blood as compared to RD. Only after 2 h the glucose concentration comes back to resting point in HFD animals. ***p<0.001, *p<0.05 versus control, by two-way ANOVA of repeated measures followed by Bonferroni's post hoc test. (C-E) Scatter dot plots show quantification of insulin (C), cholesterol (D) and glucose (E) from serum of mice. Blood was collected and coagulated 45 min. Serum was separated from blood cells via centrifugation. Insulin concentration was measured using quantitative mouse/rat insulin ELISA kit (paragraph 2.2.6.2), whereas the concentration of cholesterol and glucose were measured from the Institute for clinical chemistry and pathobiochemistry of the University Otto-von-Guericke of Magdeburg. Mice fed with HFD have high concentration of all peripheral marker of IR. No difference was spotted between genotypes. The numbers above each bar indicate the sera obtained from as many animals. ***p<0.001, **p<0.01, *p<0.05 versus control, by two-way ANOVA followed by Bonferroni's post hoc test. ns = non-significant. Data are presented as the mean ± s.e.m.

The glucose tolerance test is an assay commonly used to evaluate how fast the body clears up a given dose of glucose from the blood and was performed as a diagnostic test for IR. One of the main actions of insulin in the body is to induce glucose uptake into adipocytes, fibroblasts, hepatocytes or myocytes via translocation at the plasma membrane of vesicles containing the glucose transporter GLUT4 (Brewer et al., 2014; Karnieli et al., 1981).

The mice on HFD, both +/+ and +/Tg showed significantly reduced sensitivity of cells to insulin as depicted from the slower clearance of the circulating glucose (Figure 22 B). This is an indication that these mice developed peripheral IR. In addition, the blood from narcotized mice was collected from the heart ventricles and the concentrations of insulin, cholesterol and glucose were measured. Blood was first left to coagulate and the serum was separated from the solid fraction by centrifugation. As expected, the animals on HFD showed increased levels of these peripheral markers of IR as compared to RD mice (Figure 24 C-E).

3.4.2. HFD causes synaptic IR in cortex and hippocampus in mice

We next investigated whether HFD induces synaptic IR. To this end, hippocampi and cortices from +/+ and +/Tg TBA2.1 mice kept on RD or HFD were dissected and levels of phosphorylated AKT as well as the total protein levels of IRS1 and IRS2 were examined. Proteins were extracted from the tissues and quantitative immunoblots were performed (Figure 25 A-B). Consistent with the *in vitro* experiments, quantitative analysis of total protein extracts from hippocampal samples depicted a substantial reduction of the basal phosphorylation of AKT (Figure 25 C). Moreover, AKT dephosphorylation was accompanied by reduced IRS1 and IRS2 levels (Figure 25 D-E). A similar outcome was observed in the cortex (Figure 25 F-H).

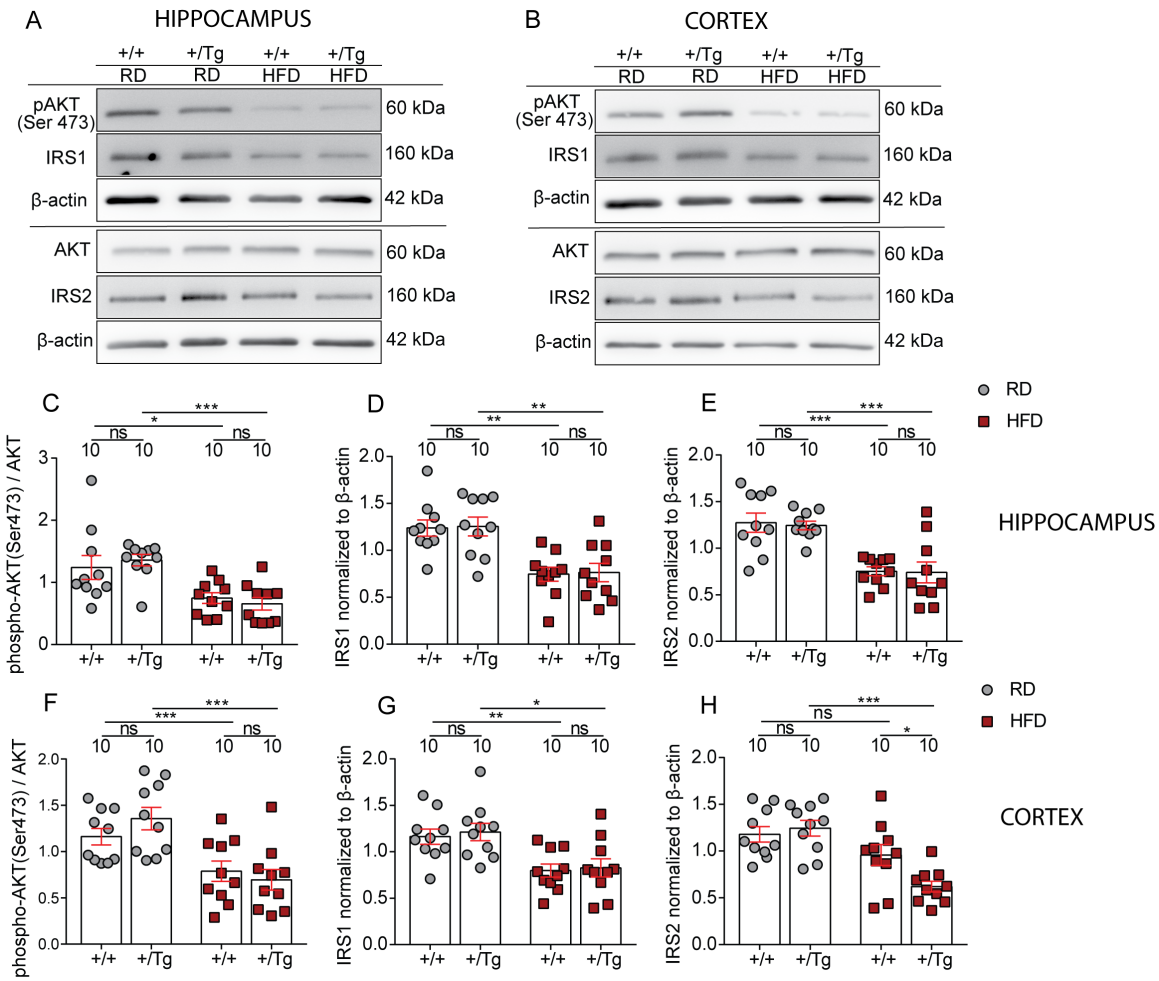

Figure 25: HFD induces synaptic IR in +/+ and +/Tg TBA2.1 mice. (A-B) Representative pictures of immunoblot of total protein extracts from hippocampus (A) and cortex (B) of TBA2.1 mice that reached the threshold of 70% body weight increment at the moment of sacrifice. Membranes were probed with antibodies detecting phospho-AKT (Ser473), AKT, IRS1 and IRS2 followed by β-actin detection in each blot. Scatter dot plots of the quantified phospho-AKT, IRS1 and IRS2 show the alterations in the insulin cascade in hippocampus (C-E) and cortex (F-H) of HFD TBA2.1 animals as evidenced by reduced IRS1 and IRS2 protein levels and de-phosphorylation of AKT. Blots were normalized as previously described. The numbers above the bars indicate the loading of the samples obtained from independent experiments. ***p<0.001, **p<0.01, *p<0.05 versus control, by two-way ANOVA followed by Bonferroni's post hoc test. ns = non-significant. Data are presented as the mean ± s.e.m.

Furthermore, in order to address the effects of neuronal IR specifically at the synapses, sub-cellular fractionation was performed and functional synaptosomes were isolated from cortices of TBA2.1 mice. Insulin responsiveness of the isolated synaptosomes was tested upon stimulation with 100 nM insulin for 10 min in the presence of ATP (Figure 26 A).

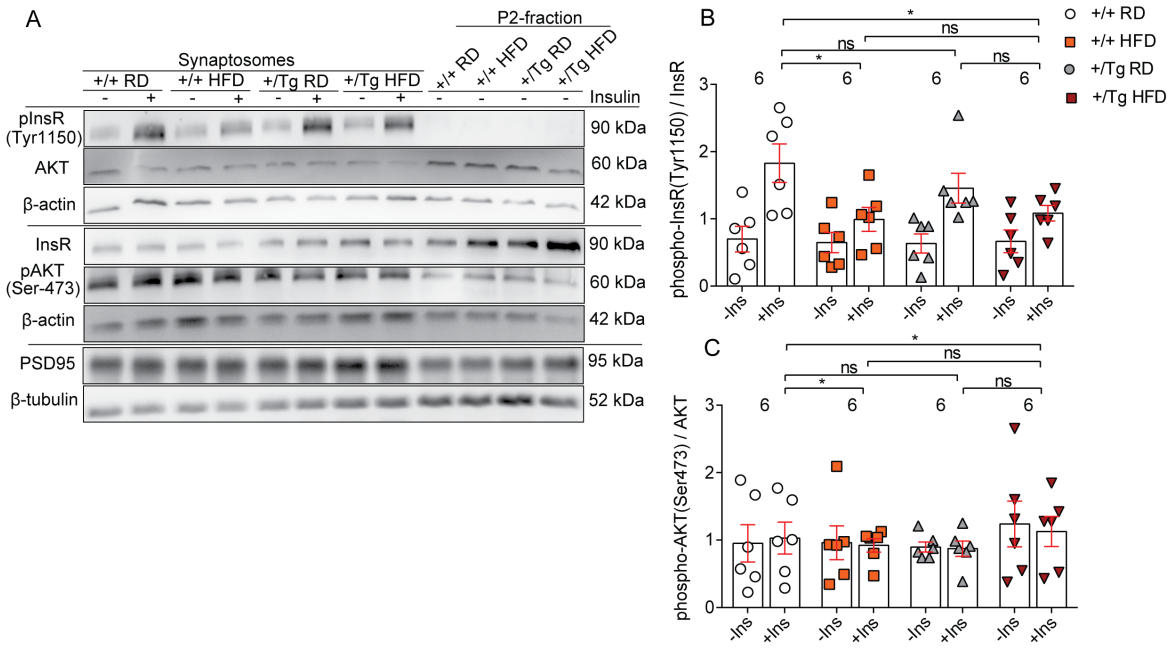

Figure 26: HFD impaired insulin responsiveness in functional isolated synaptosomes. (A) Representative pictures of immunoblot of synaptosomes isolated from cortices of TBA2.1 mice followed by insulin stimulation in the presence of ATP. Stimulated and non-stimulated synaptosomes were loaded onto SDS-PAGE gel as well as the crude membrane fraction (P2-fraction) used as input in the sucrose gradient column. Membranes were probed with antibodies detecting phospho-AKT (Ser473), AKT, phospho-InsR (Tyr1150), InsR and PSD95. Each blot was furthermore probed with β-actin antibody used as loading control. The post-synaptic marker PSD95 was used to show the purity of the synaptosomal fraction as compared to the crude membrane fraction. (B-C) Scatter dot plots show the quantification of phospho-AKT, and phospho-InsR evidence reduced responsiveness to insulin in the +/+ TBA2.1 HFD animals as compared to RD. Each blot was normalized to the respective non-phosphorylated antibody and β-actin band. Statistics refer to the synaptosomes samples bands stimulated with insulin. The numbers above the bars indicate the loading of the samples obtained from independent experiments. *p<0.05 versus control, by two-way ANOVA followed by Bonferroni's post hoc test. ns = non-significant. Data are presented as the mean ± s.e.m.

Insulin stimulation apparently failed to phosphorylate AKT in any group. We attributed the outcome to the fact that the protocol for *ex vivo* stimulation of synaptosomes from Franklin and colleagues used in this experiment has not been optimized for the activation of downstream proteins of the insulin pathway but rather for the InsR (Franklin & Taglialatela, 2016). Synaptosomes preparation can unavoidably generate breakage of membranous structure resulting in the loss of the some cytosolic elements such as AKT (Figure 26 C). Therefore, immunoblots were probed with anti –InsR and –phopho InsR antibodies showing efficient phosphorylation of the receptor upon insulin stimulation. Interestingly we observed reduced phosphorylation of the InsR in the insulin-stimulated

synaptosomes from +/+ and +/Tg TBA2.1 on HFD mice as compared to +/+ on RD (Figure 26 B).

3.4.3. HFD and Aβ3(pE)-42 impair synaptic plasticity in TBA2.1 mice

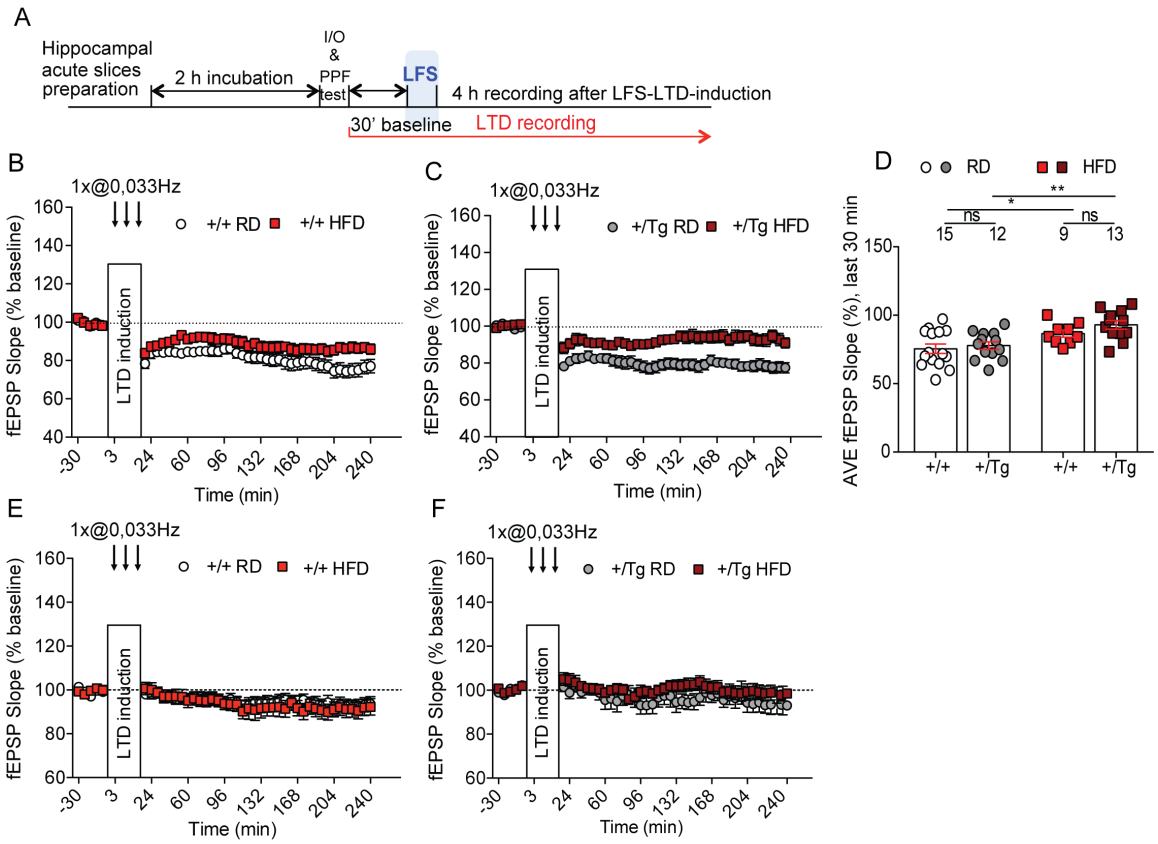

Figure 27: High fat diet caused impairment of LTD with a prominent effect in transgenic TBA2.1 mice. (A) Schematic representation of LTD induction by low-frequency stimulation (LFS) in acute CA1 hippocampal mice slices and experimental design. LFS was applied by a single stimulus with 0.1 ms width every 30 s at 0.0333 Hz, averaged every 3 min. LFS trains were applied after 2 h incubation and 30 min baseline recording. HFD induced impairment of LTD as compared to RD slices in +/+ (B) and in +/Tg (C) TBA2.1 mice. (D) Averaged fEPSP slopes values measured 210-240 min after LTD induction showed significant reduced LTD in the HFD groups, with a greater effect in +/Tg TBA2.1 mice. (E-F) Baseline was recorded by second input on the same slice which was induced LTD by the first input. The numbers above the bar graphs refer to the slices used from at least 3 different mice. Dr. Yuanxiang performed the LTD recordings. **p<0.01, *p<0.05 versus control, by two-way ANOVA followed by Bonferroni's post hoc test. ns = non-significant. Data are presented as the mean ± s.e.m.

Collectively the results of the experiments carried out in TBA2.1 mice showed that prolonged HFD causes peripheral IR, which provokes neuronal IR and impacts the functionality of insulin pathway of both +/+ and +/Tg mice. Insulin action in the brain has been extensively correlated to the LTD triggering (Labouèbe et al., 2013). Thus, the next step was to determine whether HFD-induced synaptic IR results in synaptic plasticity impairments and whether the expression of Aβ3(pE)-42 in +/Tg TBA2.1 mice plays any further role in it. To this end, NMDAR-dependent LTD with low-frequency stimulation (Figure 27 A) or LTP with high-frequency stimulation (Figure 28 A) of Schaffer-collaterals were induced in CA1 region of acute hippocampal slices (Malenka, 1994) from +/+ and +/Tg TBA2.1 mice, both RD and HFD groups. As expected, the fEPSP slope was negatively impaired in slices from HFD animals after LTD induction; interestingly the effect was stronger in +/Tg TBA2.1 mice which predominantly express and accumulate Aβ3(pE)-42 (Figure 27 B-D), whereas no effect was observed in RD +/Tg compared to +/+ mice. The diet and the genotype did not affect baseline fEPSP slope (Figure 27 E-F).

It is well established in the field of AD that Aβos induce LTP impairment (Cullen et al., 1997; Jo et al., 2011; Kamenetz et al., 2003; Lambert et al., 1998; Shankar et al., 2007; Walsh et al., 2002). Therefore LTP with high-frequency stimulation of Schaffer-collaterals was performed in TBA2.1 mice. Consistently with that, here we found that +/Tg TBA2.1 expressing Aβ3(pE)-42 have severe impaired LTP compared to +/+ mice (Figure 28 B and D). No further reduction was observed in HFD animals compared to RD of the same genotype. However, although no significant, +/+ TBA2.1 show a tendency of reduction in fEPSP slope when fed with HFD as compared to RD (Figure 28 B and D). The diet and the genotype did not affect baseline fEPSP (Figure 28 E-F).

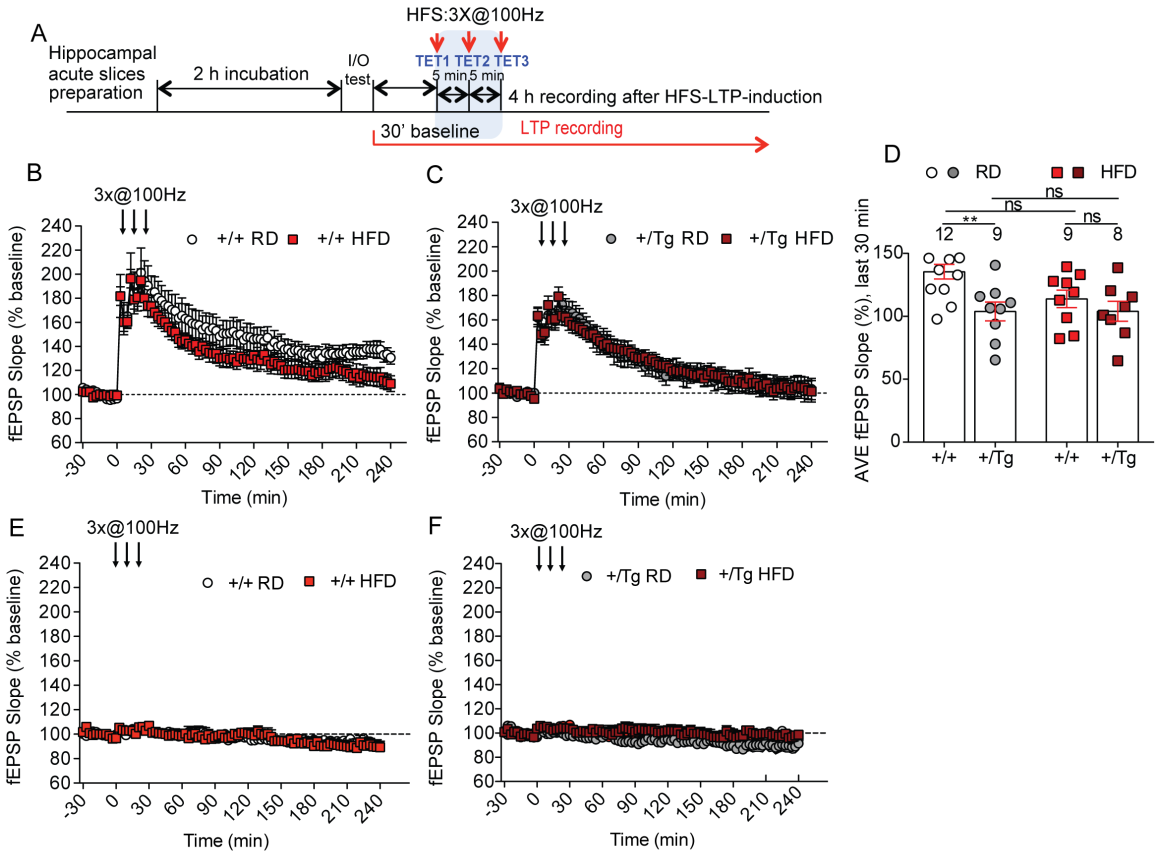

Figure 28: Transgenic TBA2.1 mice have impaired LTP, regardless of the diet. HFD worsened LTP in wild-type mice. (A) Schematic representation of LTP induction by high-frequency stimulation (HFS) in acute CA1 hippocampal mice slices and experimental design. HFS trains lasting 1s at 100 Hz followed by 30 min resting period were applied after 2 h incubation and 30 min baseline recording. HFD induced impairment of LTP as compared to RD slices in +/+ (B) and in +/Tg TBA2.1 (C) mice. (D) Averaged fEPSP slopes values measured 210-240 min after LTD induction showed a drastic reduction of the LTP in the +/Tg TBA2.1 compared to +/+ mice. (E-F) Baseline was recorded by second input on the same slice which was induced LTP by the first input. The numbers above the bar graphs refer to the slices used from at least 3 mice. Dr. Yuanxiang performed the LTP recordings. **p<0.01 versus control, by two-way ANOVA followed by Bonferroni's post hoc test. ns = non-significant. Data are presented as the mean ± s.e.m.

3.4.4. MetS and Aβ3(pE)-42 cause novel object location/recognition memory impairments in TBA2.1 mice

Altogether the electrophysiology data showed that TBA2.1 mice exhibit impairment in CA1 synaptic plasticity. Aβ3(pE)-42 alone induces LTP impairment whereas HFD impacts more specifically the LTD. Building memory for the spatial

localization and recognition of objects in an open field requires synaptic plasticity of CA1 neurons (Assini et al., 2009; Haettig et al., 2013). We therefore next tested TBA2.1 mice for novel location discrimination and novel object recognition. The mice were first tested in an open field arena to assess the locomotor activity revealing no significantly different among the groups, despite the striking differences of body weight of the animals (Figure 29 B). Following a 20 min training session novel, object recognition memory was checked 24 h later (Figure 29 A). Interestingly, animals on HFD, both +/+ and +/Tg TBA2.1 exhibited lower discrimination of the new located or replaced object as compared to the familiar one (Figure 29 C-D). Notably, the discrimination of the new located object was significantly worse in +/Tg TBA2.1 HFD than in +/+ HFD mice (Figure 29 C).

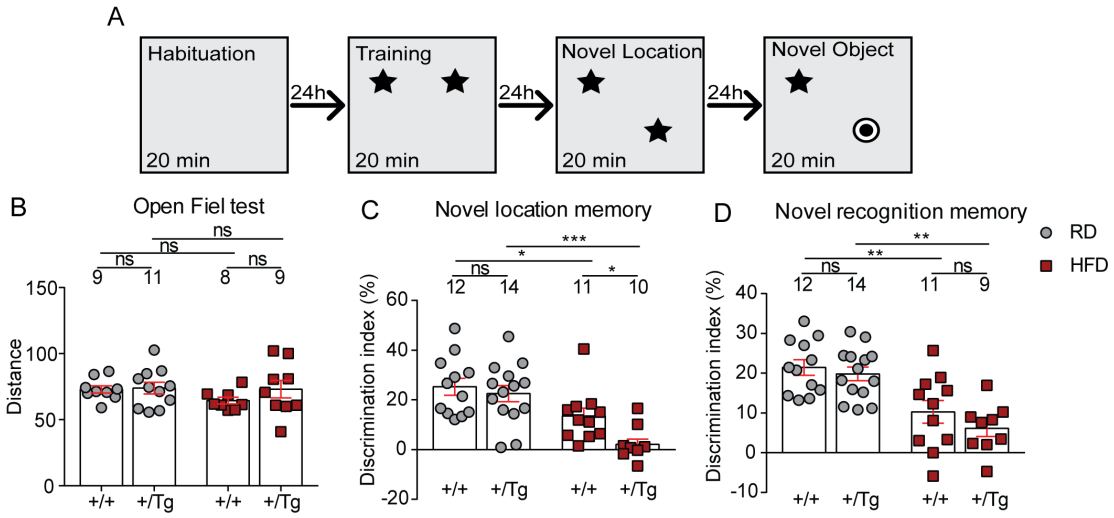

Figure 29: HFD induced impairment in the novel object location and recognition task. (A) Schematic representation of the object location and recognition memory experimental protocol. Mice were habituated for 20 min in the open field during which the walked distance was measured. They were tested for novel object location memory 24 h after and again for novel object recognition 24 h later. Each session lasted 20 min. (B-C-D) Scatter dot plot shows the total distance walked during the habituation phase (B), the discrimination index of the new located (C) or replaced object (D) as compared to the old one. The discrimination index shows that mice in HFD have difficulties to discriminate, and consequentially to remember the new position or the substitution of one of the two objects. Aβ3(pE)-42 apparently worsens memory impairment in +/Tg TBA2.1 mice, at least as depicted in the new location task. Dr. Gomes performed the behavioral experiments. The numbers above the bars indicate the number of mice tested. ***p<0.001, **p<0.01, *p<0.05 versus control, by two-way ANOVA followed by Bonferroni's post hoc test. ns = non-significant. Data are presented as the mean ± s.e.m.

3.4.5. *PI3Kγ activity is reduced in HFD TBA2.1 mice*

The experiments performed *in vitro* in cultivated neurons showed that PI3Kγ activity is reduced by long-term treatment with insulin and TNFα. To further investigate the role of neuronal IR on synaptic plasticity at Schaffer collateral-CA1 synapses in our mouse model, we next evaluated whether PI3Kγ activity is reduced also in TBA2.1 upon diet-induced IR. For this purpose, endogenous PI3Kγ was immunoprecipitated from total homogenate of hippocampi from TBA2.1 mice and $PI(3,4,5)P_3$ produced by the enzyme was measured by means of competitive colorimetric ELISA assay as described in paragraph 3.1.2. The reduced amount of $PI(3,4,5)P_3$ produced correlates to a reduced enzymatic activity of PI3Kγ in TBA2.1, which is evident in animals fed with HFD, both +/+ and +/Tg (Figure 30 A). Total immunoprecipitated PI3Kγ proteins were furthermore extracted from the beads and measured by western blot, showing no differences among the groups (Figure 30 B-C). This is an indication that the differences of $PI(3,4,5)P_3$ detected are not due to discrepancy in the amount of immunoprecipitated enzyme but rather to its activity.

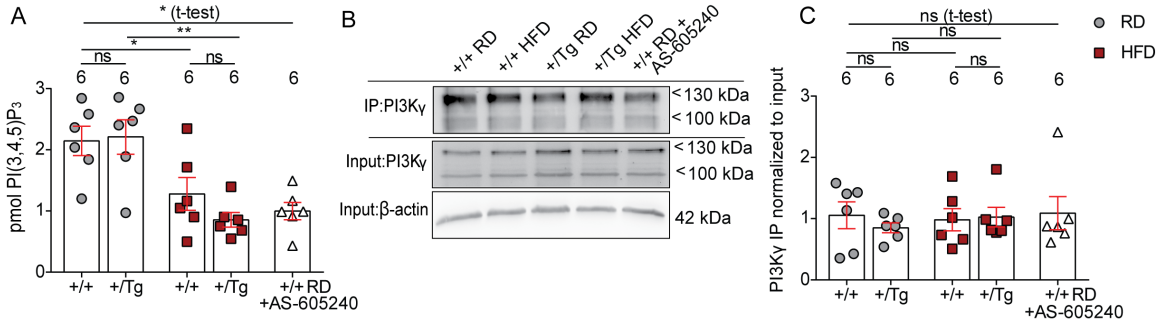

Figure 30: High fat diet reduced PI3Kγ activity in TBA2.1 mice. (A) Endogenous PI3Kγ was immunoprecipitated from hippocampi of +/+ and +/Tg TBA2.1 mice using specific antibody. The $PI(3,4,5)P_3$ produced by the enzyme coupled to the beads was measured by $PI(3,4,5)P_3$-coated detection plate for competitive binding. The assay showed reduced PI3Kγ activity in HFD fed TBA2.1 +/+ and +/Tg mice as compared to control animals fed with a RD. AS-605240 was added to the control group +/+ RD in a separate IP group and used as negative control. (B) After the enzymatic reaction was completed and $PI(4,5)P_3$ collected, PI3Kγ enzyme was extracted from the beads and the amount of immunoprecipitated protein evaluated by western bot. (C) Quantification of the IP PI3Kγ, normalized to the respective PI3Kγ, is plotted in the dot plot graph and shows no significant differences of immunoprecipitated PI3Kγ among the groups. **p<0.01, *p<0.05 versus control by two-way ANOVA followed by Bonferroni's post hoc test. ns = non-significant. Statistic analysis of +/+ RD versus +/+ RD + AS-605240 negative control was done by two-tailed Student's t-test. Data are presented as the mean ± s.e.m.

3.4.6. HFD activates microglia and astrocytes in Aβ3(pE)-42-expressing mice and induces neuronal cell loss in hippocampal CA1

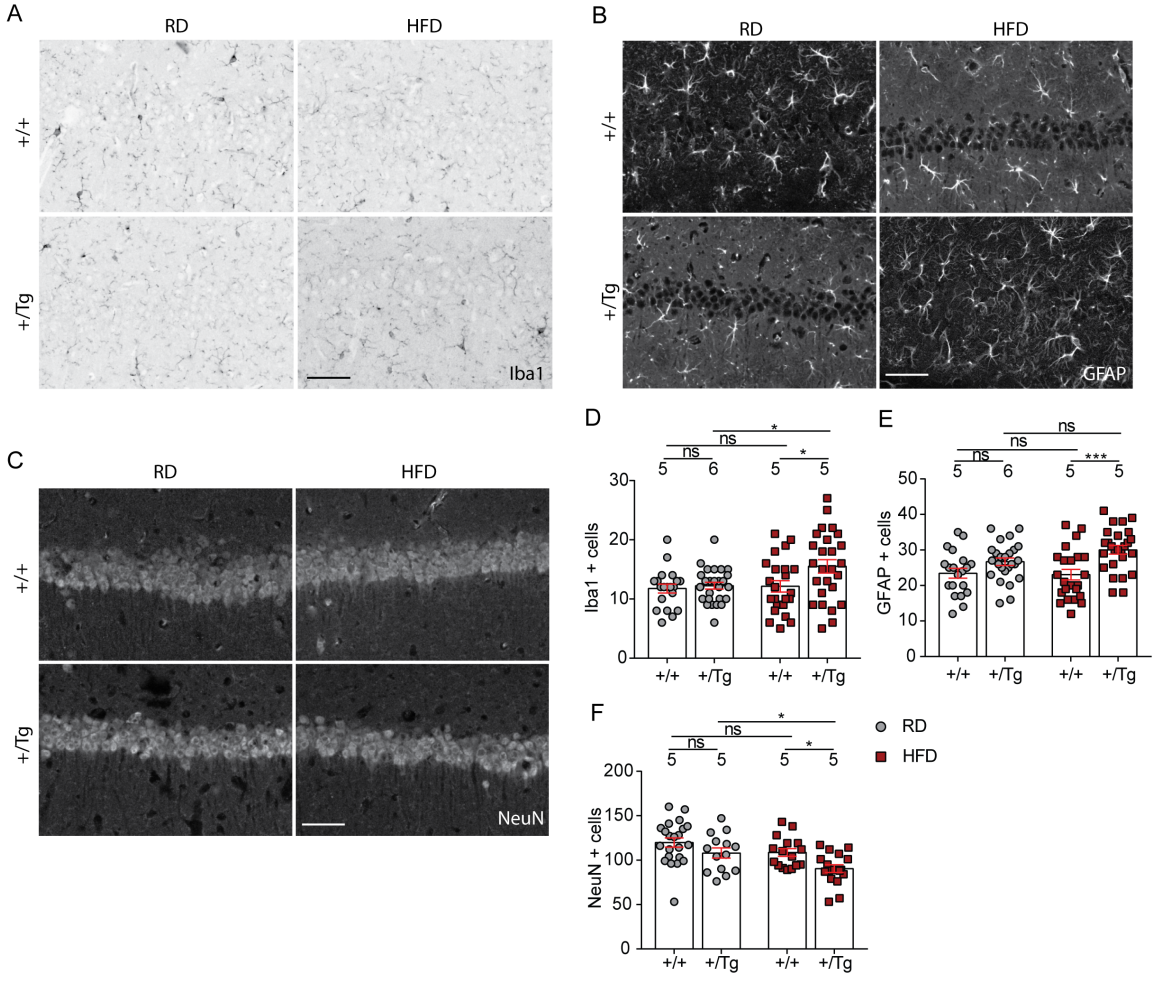

Figure 31: HFD caused prominent microglia and astroglia activation, as well as cell loss in hippocampal CA1 of TBA2.1 mice expressing Aβ3(pE)-42. Acute slices were cut in the coronal plane of mouse brain. Confocal images of slices stained for (A) Iba1 or (B) GFAP indicate that there is an increased activation of microglia and astrocytes in the CA1 region. (C) NeuN staining shows the loss in neuronal cells in the same region. Scale bar is 100 µm. Scatter dot plot graphs show quantification of Iba1 (D), GFAP (E) and NeuN (F) positive cells. The numbers above the bars indicate the number of animals used per group. From each animal up to 2 slices were cut and stained. The 2 hippocampi of each slice were quantified and averages were plotted. ***p<0.001 and *p<0.05 versus control, by two-way ANOVA followed by Bonferroni's post hoc test. ns = non-significant. Data are presented as the mean ± s.e.m.

Astroglia activation is a vital part of the neuroinflammatory response in AD (Heneka et al., 2015; Simpson et al., 2011; Tuppo & Arias, 2005) and the neuronal cell loss in the CA1 hippocampal region is one of the most established hallmarks of early

stage AD (Casas et al., 2004). To further investigate this aspect we used acute hippocampal slice of the brain of mice and immunostained for astroglia activation markers. Immunohistochemical analysis of slices stained for activated microglia (Iba1) revealed that HFD induces microglia activation in the combination with Aβ3(pE)-42 expression in TBA2.1 mice (Figure 31 A and D). Aβ3(pE)-42 caused also astrocytic cells proliferation and increased GFAP expression, as outlined by the increase of GFAP immunoreactivity, in the animals fed with HFD (Figure 31 B and E). Probably as a consequence of the elevated level of activated astroglia, a significant reduction of neuronal cells in the hippocampal CA1 molecular layer of +/Tg TBA2.1 HFD mice was spotted (Figure 31 C and F). Neuronal cells were counted by mean of immunostaining with the neuronal specific marker NeuN.

In parallel, the total levels of the pro-inflammatory cytokine TNFα were evaluated in the cortex of TBA2.1 mice by means of quantitative sandwich ELISA. The assay depicted an overall higher production of TNFα in +/Tg TBA2.1 mice, expressing Aβ3(pE)-42 while no further effect of the diet was detected (Figure 32).

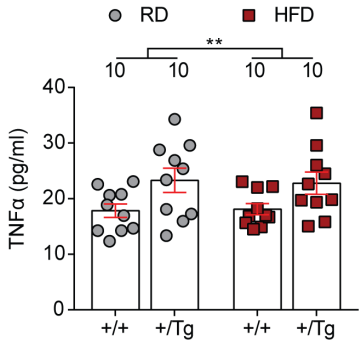

Figure 32: TNFα level was augmented in Aβ3(pE)-42-expressing TBA2.1 mice. Cortices from +/+ and +/Tg both RD and HFD mice were manually homogenized and centrifuged to remove organelles, membrane structures and insoluble particles. TNFα levels were evaluated from supernatants using monoclonal mouse anti-TNFα antibody pre-coated ELISA microplate. Quantitative ELISA detected overall an increase of the TNFα in the +/Tg TBA2.1 mice with no effect of the diet. **p<0.01 versus control, by two-way ANOVA followed by Bonferroni's post hoc test. ns = non-significant. Data are presented as the mean ± s.e.m.

3.5. MLN-4924 injection in TBA2.1 mice ameliorates synaptic IR *in vivo*

The experiments that have been carried out in TBA2.1 mice highlighted, under different angles, that animals fed with a high caloric diet develop synaptic IR. This causes the disruption of insulin pathway in hippocampus and cortex as well as impairment in synaptic plasticity and CA1-dependent memory. The consequences of the HFD are evident already in +/+ TBA2.1 as compared to RD animals. However, the effects of the HFD are exacerbated in +/Tg TBA2.1 mice that express Aβ3(pE)-42 and increased release of TNFα from astroglia. Additionally, the bath application of the neddylation-specific inhibitor MLN-4924 in cultivated neurons is protective against IRS1 protein degradation induced by prolonged exposure to insulin and TNFα. We believed that the effects of the HFD in both +/+ TBA2.1 and +/Tg TBA2.1 mice develop as a direct or indirect consequence of the neddylation-dependent degradation of IRS proteins in the synapses. In order to validate this hypothesis, TBA2.1 animals were injected with MLN-4924 and test whether neddylation inhibition counteracts neuronal IRS1 degradation *in vivo*. Furthermore, improvement in the cognitive performances and synaptic plasticity were also evaluated.

3.5.1. Intraperitoneal MLN-4924 injection in mice has minor effect in the peripheral IR

Male TBA2.1 +/+ and +/Tg were fed with HFD until they reach the above-mentioned threshold of 70% body weight increase and afterward a dose of 20 mg/kg MLN-4924 was intraperitoneally injected one time per day for 14 days. MLN-4924 was prepared in DMSO and furthermore diluted in the lipophilic drug solubilizer 2-Hydroxypropyl-β-cyclodestrin. Both +/+ and +/Tg animals used for these experiments were all fed with the HFD and used always at the same age. Control animals were injected with an equi-volume of vehicle.

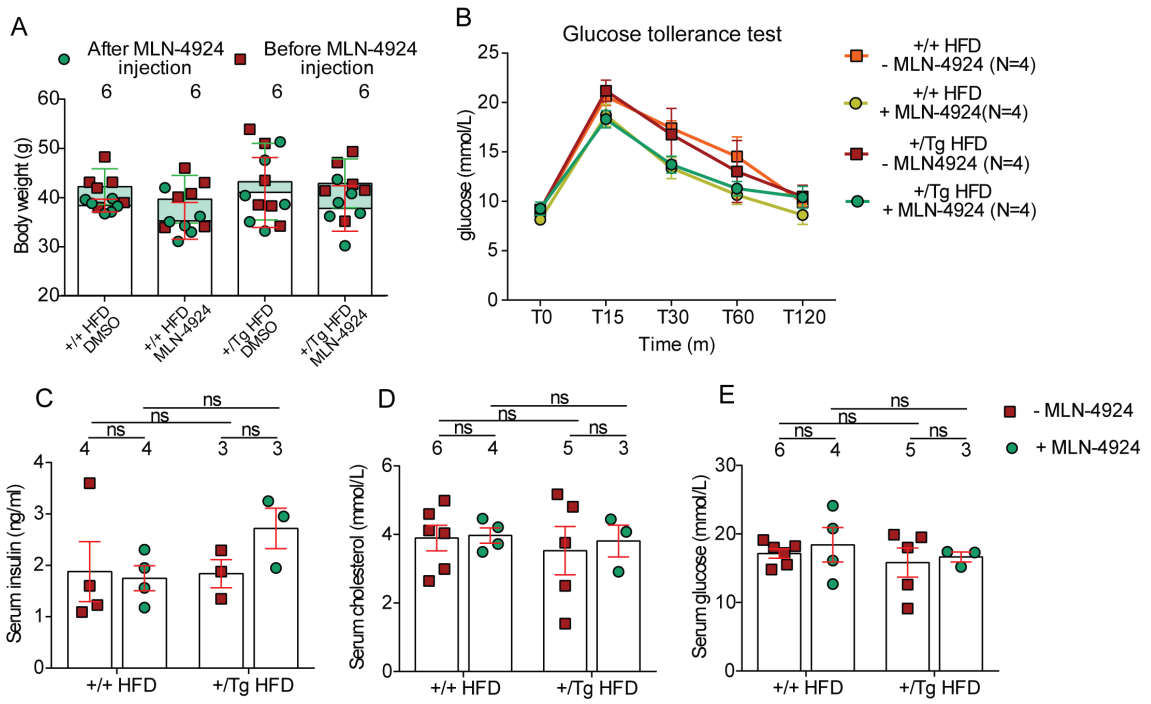

Figure 33: MLN-4924 intraperitoneal injection in TBA2.1 mice ameliorated glucose sensitivity but did not affect other peripheral marker of insulin resistance. (A) Body weight of HFD TBA2.1 +/+ and +/Tg mice injected either with vehicle or MLN-4924 was measured before and after the injection period of 14 days and the body weight mass (g) is plotted in the scattered dot plot. (B) Glucose concentration was first measured after 6 h fasting one day after the last injection with vehicle/MLN-4924. Furthermore, 1 g/kg glucose was IP injected and glucose measurements repeated after 15, 30, 60 and 120 min. TBA2.1 mice, both +/+ and +/Tg, injected with MLN-4924 have a tendency to faster metabolize the injected glucose as compared to the animals that received the vehicle. ns = non-significant versus control, by two-way ANOVA of repeated measures followed by Bonferroni's post hoc test. (C-D-E) Scatter dot plot of the measured serum concentration of insulin (C), cholesterol (D) and glucose show no significant differences between genotypes or drug injection. Serum was separated from blood cells via centrifugation. Insulin concentration was measured using quantitative mouse/rat insulin ELISA kit (paragraph 2.2.6.2), whereas the concentration of cholesterol and glucose were measured by the Institute for Clinical Chemistry and Pathobiochemistry of the Otto-von-Guericke University of Magdeburg. ns = non-significant versus control, by two-way ANOVA followed by Bonferroni's post hoc test. Data are presented as the mean ± s.e.m.

First, the cytotoxicity of MLN-4924 was evaluated *in vivo*. To this end, the body weight of the mice was measured before the first and after the last injection (Figure 33 A) and a slight decrease of the body weight of MLN-4924 injected mice was observed. This is consistent with what reported from some authors who observed a similar effect of the drug in injected mice (Park et al., 2016). Nevertheless, this reduction is not significantly higher than in the animals injected with vehicle suggesting that MLN-4924 is not toxic *in vivo*. Thus, the reduction in the body weight observed cannot be attributed to a direct

effect of MLN-4924 on MetS. Next, the possibility that MLN-4924 counteracts IR at the peripheral level was assayed. Therefore, after the end of the treatment, animals were tested for the glucose tolerance test and the peripheral markers of IR were checked. Both +/+ and +/Tg mice, injected with MLN-4924, showed a tendency to better clear up the circulating glucose in the glucose tolerance test (Figure 33 B). However, in contrast to this, the concentration of glucose in the serum, as well as for other markers of IR like cholesterol and insulin are not changed as compared to control HFD animals injected with vehicle (Figure 33 C-E). No final conclusions can be taken from these experiments yet because of the limited N number but is seems that MLN-4924 potentially has effects as glucose sensitizer in peripheral tissues, which nevertheless did not result in amelioration of peripheral IR *in vivo*.

3.5.2. HFD-induced synaptic IR is prevented in +/+ TBA2.1 mice after MLN-4924 injection

We next examined whether the inhibition of neddylation by MLN-4924 injection prevents IRS degradation *in vivo*. After 14 days of daily injection with MLN-4924, TBA2.1 HFD mice were sacrificed and hippocampi and cortex were dissected. Proteins were extracted from the tissues and quantitative immunoblotting was performed. Interestingly, MLN-4924 elicited significant abolishment of IRS1 and IRS2 degradation in the hippocampus of +/+ HFD mice as compared to those who received the vehicle, whereas no significant effect was detected in +/Tg mice (Figure 34 A and D-E). The rescue of IRS1 and IRS2 levels was accompanied by increased phosphorylation of AKT (Figure 34 C). Only a modest IRS1 and IRS2 rescue was detected in the total homogenate from cortex samples (Figure 34 B and G-H), although a significant increased phosphorylated AKT was observed (Figure 34 B and F).

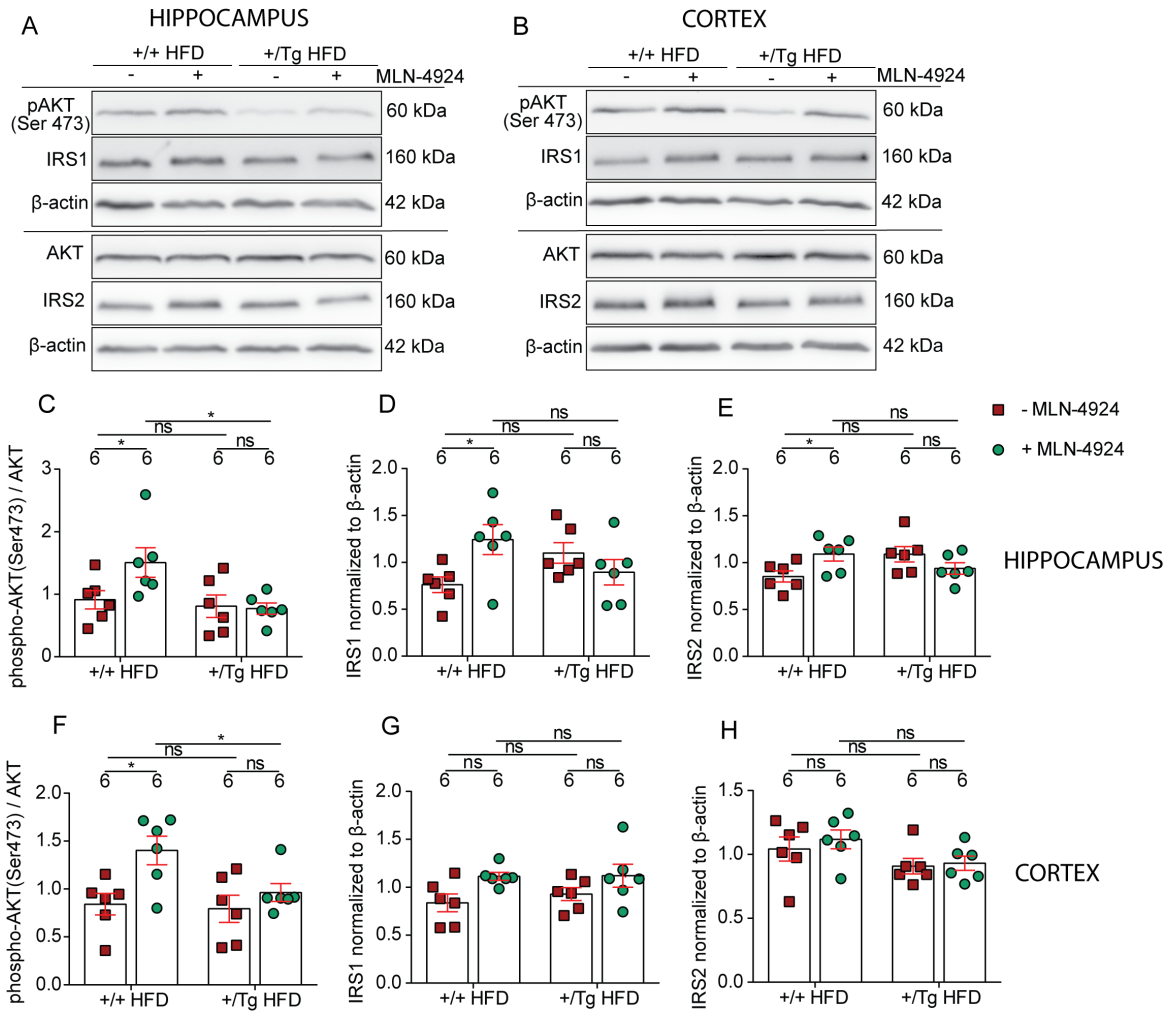

Figure 34: HFD-induced IRS1/2 degradation and AKT de-phosphorylation are attenuated in +/+ but not +/Tg TBA2.1 mice by MLN-4924 injection. (A-B) Representative pictures of immunoblot of total protein extracts from hippocampus (A) and cortex (B) of TBA2.1 injected with vehicle or MLN-4924. Membranes were probed with antibodies detecting phospho-AKT (Ser473), AKT, IRS1 and IRS2. Each blot was furthermore probed with β-actin antibody used as loading control. Quantification of the normalized western blots is plotted in scatter dot plot. MLN-4924 injection resulted in rescued levels of IRS1 and IRS2 in hippocampus (D-E) and in higher phosphorylated AKT (C). Increase phospho-AKT is observed also in cortex (F) whereas the rescue of IRS1 and IRS2 is not significant (G-H). The numbers above each bar indicate the loading of the samples obtained from independent experiments. *p<0.05 versus control, by two-way ANOVA followed by Bonferroni's post hoc test. ns = non-significant. Data are presented as the mean ± s.e.m.

3.5.3. MLN-4924 injection results in a trend to rescue HFD-induced synaptic plasticity impairments

Western blot analysis showed that MLN-4924 protects neurons from IR, at least in the absence of Aβ3(pE)-42. To further investigate the neuroprotective effects of MLN-

4924 *in vivo*, synaptic plasticity was next evaluated in TBA2.1 mice after MLN-4924 injection. To this end, NMDAR-dependent LTD was induced in hippocampal CA1 region with low-frequency stimulation of Schaffer-collaterals (Malenka, 1994) of acute slices from +/+ and +/Tg TBA2.1 mice. Our previous data showed that the most severe LTD impairment in HFD-fed animals occurs in the +/Tg TBA2.1. Given the limited number of animals that could be assayed, we decided in the first attempt to check whether MLN-4924 injection can protect from impaired synaptic plasticity in +/Tg HFD mice. Although the results are very preliminary, a positive trend in recovery of LTD could be spotted in slices from +/Tg animals on HFD injected with MLN-4924 as compared to vehicle (Figure 35 B-C). No changes in the baseline were observed (Figure 35 D).

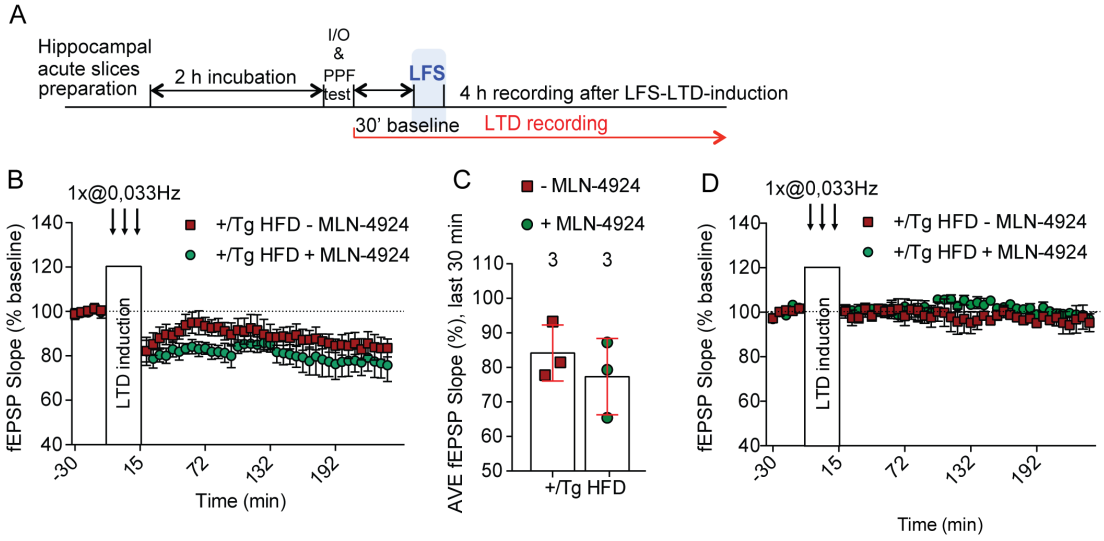

Figure 35: MLN-4924 intraperitoneal injection strengthens LTD in +/Tg TBA2.1 mice. (A) Schematic representation of LTD induction by low-frequency stimulation (LFS) in acute CA1 hippocampal mice slices and experimental design. LFS was applied by a single stimulus with 0.1 ms width every 30 s at 0.0333 Hz, averaged every 3 min. LFS trains were applied after 2 h incubation and 30 min baseline recording. (B) MLN-4924 injection in +/Tg TBA2.1 mice strengthens LTD in +/Tg in TBA2.1 mice fed with HFD. (C) Dot plot graph shows the quantification of averaged fEPSP slopes values measured 210-240 min after LTD induction. (D) Baseline was recorded by second input on the same slice which was induced LTD by the first input. Numbers above the bar graphs refer to the slices used from 1 mouse. Dr. Yuanxiang performed the LTD recordings. ns = non-significant versus control, by two-way ANOVA followed by Bonferroni's post hoc test. Data are presented as the mean ± s.e.m.

In parallel, the effects of bath application of MLN-4924 on the basal level of the LTD were monitored on acute slices of RD +/+ and +/Tg TBA2.1 mice. The idea was to address whether the effect of MLN-4924 observed on synaptic plasticity of intraperitoneally injected mice was specifically consequent to protection of IRS1 degradation that arose only when neddylation was induced by HFD. To this end, 1 µM MLN-4924 was diluted in the aCSF and applied directly on acute slices from +/+ and +/Tg RD TBA2.1 mice for the entire duration of recordings. Measured fEPSP showed clearly no effects of MLN-4924 in both +/+ (Figure 36 A and C) and +/Tg (Figure 36 B and C) mice as compared to DMSO. MLN-4924 did not affect baseline (Figure 36 E-F).

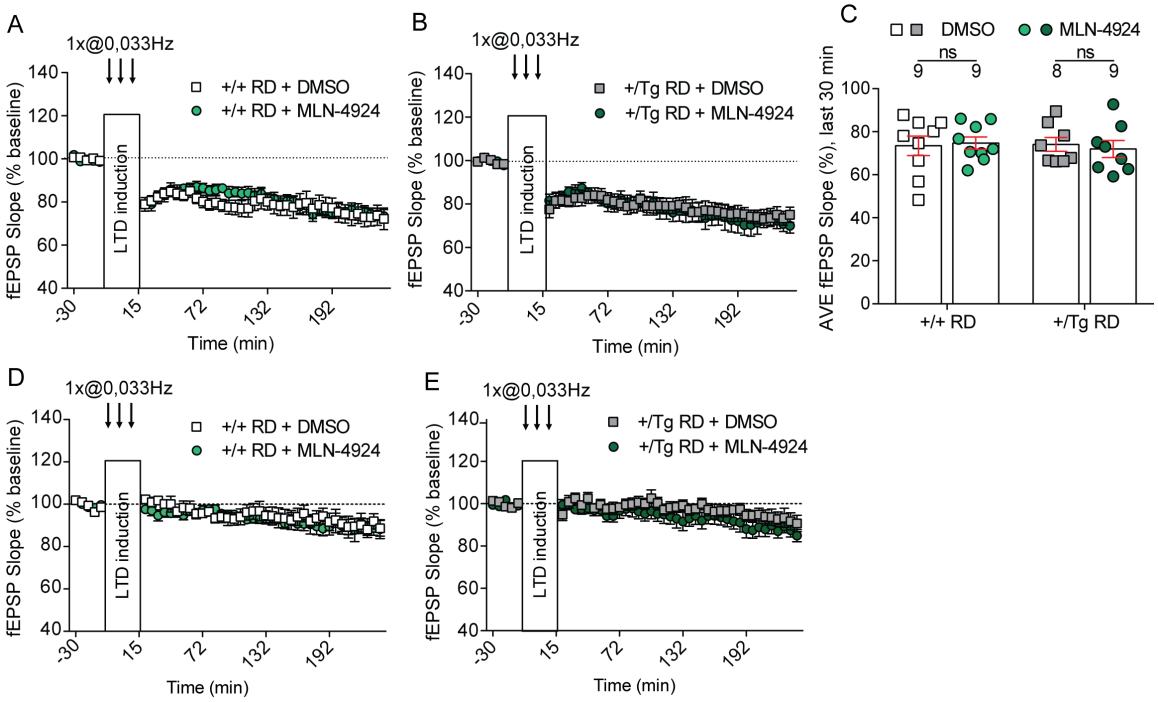

Figure 36: Bath application of MLN-4924 in RD +/+ and +/Tg TBA2.1 mice hippocampal slices did not elicit any effect. (A) Acute CA1 hippocampal mice slices were cut from RD fed animals, both +/+ and +/Tg mice. LFS was applied by a single stimulus with 0.1 ms width every 30 s at 0.0333 Hz, averaged every 3 min. LFS trains were applied after 2 h incubation and 30 min baseline recording. MLN-4924 was diluted in the aCSF buffer at the final concentration of 1 µM and applied on slices during the whole recording. DMSO was used as control. (A-B) Bath application of MLN-4924 1 did not affect LTD in +/+ (A) or +/Tg (B) TBA2.1. (C) Averaged fEPSP slope values measured 210-240 min after LTD induction showed no differences among the groups. (D-E) Baseline was recorded by second input on the same slice which was induced LTD by the first input. Numbers above the bar graphs refer to the slices used from at least 3 mice. Dr. Yuanxiang performed the LTD recordings, ns = non-significant.

3.5.4. MLN-4924 injection improves memory performance in the novel object location/recognition task

Finally, hippocampal CA1-dependent learning and memory performances of TBA2.1 mice fed with HFD were checked after intraperitoneal injection with the specific neddylation inhibitor MLN-4924 for 14 days. Thus, HFD +/+ and +/Tg TBA2.1 animals were tested for novel location and novel object recognition tasks as 24 h after the last MLN-4924 injection in paragraph 3.4.4. The mice were allowed to explore an open field arena and locomotor activity was evaluated revealing no significant difference among the groups (Figure 37 A). Interestingly, the injection of MLN-4924 seems to improve memory performance as evidenced by the enhanced discrimination index in the novel location (Figure 37 C) and novel object recognition task (Figure 37 D) in +/Tg HFD TBA2.1 mice.

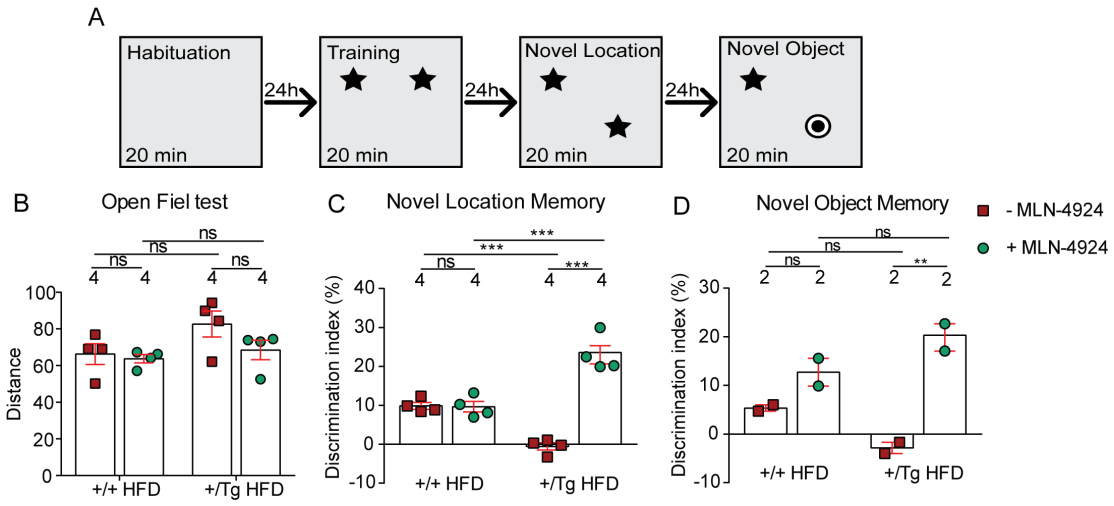

Figure 37: MLN-4924 had trend to strongly enhance HFD-induced memory impairments in the novel object location and recognition task. (A) Schematic representation of the object location and recognition memory experimental protocol. Mice were habituated for 20 min in the open field during which the walked distance was measured. Novel object location and novel object recognition tests were performed 24 h apart from each other. (B-C-D) Scatter dot plot shows the total distance walked during the habituation phase (B), the discrimination index of the new located (C) or replaced object (D) as compared to the old one. The discrimination index shows a significant improvement in the discrimination of the new position or the substitution of one of the two objects in +/Tg TBA2.1 mice on HFD and subsequently injected with MLN-4924. The numbers above the bars indicate the number of mice tested. ***p<0.001, **p<0.01 versus control, by two-way ANOVA followed by Bonferroni's post hoc test. ns = non-significant. Data are presented as the mean ± s.e.m.

4. Discussion

Over the past decades it has been firmly established that the brain is an important target for insulin action. Insulin in the central nervous system (CNS) affects feeding behavior, metabolism of glucose and fats, as well as various aspects of memory and cognition (Gray, Meijer, & Barrett, 2014). The importance of the role of insulin in the CNS is furthermore highlighted by the consequences of the interruption of insulin action on brain performances. IR is defined as a condition in which cells fail to respond properly to the normal actions of circulating insulin (Lebovitz, 2001; Wang, 2014). This pathological condition occurs also in neurons and it has been linked to neurodegenerative diseases (Schubert et al., 2003). IR typically develops with a metabolic disorder known as MetS that characterizes obesity, hypertension and type 2-diabetes. Interestingly, MetS has been confirmed to be a major contributor also for cognitive impairments in aged individuals (Frisardi et al., 2010). This is caused by impairments in insulin signaling that affect particularly some brain regions, which are more "metabolically" active and important for learning and memory, such as the hippocampus and the prefrontal cortex (Crawley, 1999; Wiedenmann & Franke, 1985). Currently there is widening recognition that AD is closely associated with impaired insulin signaling and glucose metabolism in brain (Gupta et al., 2018). MetS, in the interaction with amyloidosis, is considered nowadays as an important risk factor for sporadic AD (Pasinetti & Eberstein, 2008). Subjects with IR and MetS have a roughly 10 times higher likelihood to develop AD (Sikkes et al., 2010; Vanhanen et al., 2006).

AD is a neurodegenerative decline that is characterized by increased deposition in the extracellular environment of neurotoxic amyloid-β oligomers (Aβos) that are the major responsible for synaptic degeneration (Selkoe, 2002). However, about 30 % of the healthy aged population is amyloid positive and shows no symptoms of the disease. Therefore, it is reasonable to believe that diet-induced MetS represents a second hit driving to AD onset in amyloid positive people. Thus, MetS induces cognitive decline during normal aging via synaptic IR and amyloid loads worsen cognitive decline probably via a facilitation of IR. The estimated incidence of the MetS in adults aged 60 to

70 years in the western countries is about 25% (Scuteri et al., 2015). Together with the constant worldwide increase of the lifespan of the population, it becomes clear that the number of potentially concerned people is big. However, it is important to state that the nature of the molecular mechanism driving from IR to synaptic alterations is not yet well understood. Therefore, the study of detailed pathways is crucial for a deep understanding of synaptic dysfunction in these diseases and it may provide novel targets for pharmaceutical intervention.

4.1. Insulin and TNFα induce neuronal IR *in vitro* by means of IRS1 degradation and phosphorylation, respectively

Pro-inflammatory cytokines have profound impact on the onset and progression of AD (Floden et al., 2005; Heneka et al., 2015; Johnston et al., 2011; Meraz-Ríos et al., 2013). Aβ internalization leads to microglia activation, which in turn produce pro-inflammatory chemokines and cytokines, including TNFα (He et al., 2007; Heneka et al., 2015; Heppner et al., 2015; Meraz-Ríos et al., 2013; Wang et al., 2004). Additionally, several authors reported that an abnormal neuroinflammatory mechanism has a major contribution to the onset of IR (Borst, 2004; Moller, 2000; Plomgaard et al., 2005).

In the first part of the thesis major insights were gained related to the mechanisms underlying the role of insulin and TNFα on the onset of synaptic IR *in vitro*. It was demonstrated that cultivated primary cortical and hippocampal neurons chronically exposed to TNFα and high concentration of insulin become insulin resistant as outlined by the reduced phosphorylation and activation of AKT, a fundamental and ubiquitous expressed cytosolic effectors of the InsR cascade. The InsR and the other insulin signaling cascade protein members, including AKT, are known to be a component of synapses of hippocampal neurons (Abbott et al., 1999; Chiu & Cline, 2010). Reduced responsiveness to the hormone was also observed in dendrites of hippocampal primary neurons and in isolated synaptosomes, meaning that the neurons undergo synaptic IR. Moreover, dephosphorylation of AKT and InsR were associated to increased inhibitory serine-phosphorylation of IRS1 as well as protein degradation of IRS1, IRS2 and InsR. In summary, our experiments showed that cultivated neurons treated with insulin and TNFα

develop synaptic IR after 24 h thus severely impacting the IRS proteins content and regulation. Lacking the activity of IRS1 and IRS2, neurons undergo deregulation of the downstream effector AKT in synapses.

We further went into deeper investigation of the pathological effects of insulin and TNFα in neurons. The contribution of the two drugs was evaluated individually and compared to the effects that the two drugs elicit together. Interestingly, while insulin administration clearly elicits IRS1 degradation, TNFα alone increases the serine-phosphorylation of the leftover pool of IRS1, without further affecting the degradation. However, the deregulation of the insulin pathway in terms of activation of AKT is reduced to a greater extend when insulin and TNFα were applied together. As a confirmation of such a divergence in the molecular mechanism, co-application of TNFα-neutralizing antibody on glia-containing neuronal cultures treated with pyro-glutamylated Aβ3(pE)-42 inhibits the hyper-phosphorylation of IRS1 but not its degradation. Phosphorylation of AKT was neither fully rescued by TNFα-neutralizing antibody. This suggests that insulin-induced IRS1 degradation has a major contribution on IR onset than TNFα-induced IRS1 hyper-phosphorylation.

These findings stress out the necessity of the presence of both insulin and TNFα to induce IR and raise important questions about the molecular mechanism behind IR. It seems therefore that, consistently acknowledged data in the field (De Felice, 2013; Kim et al., 2012; Lourenco et al., 2013; Tremblay et al., 2007), high concentration of insulin and exposure to pro-inflammatory cytokines are both important to cause IR. However, they elicit a stronger effect when acting in concert.

4.2. Insulin-induced IRS1 degradation is neddylation dependent and the inhibition of neddylation rescues neuronal IR *in vitro*

Hyper-serine/threonine phosphorylation of IRS1 has been extensively explored and linked to IR in many cell types, including neurons (Mayer & Belsham, 2010; Talbot et al., 2012), as well as to the neuropathology of AD (Yarchoan et al., 2014). In a similar fashion, decreased cellular levels of IRS1 and IRS2 have been shown to be associated with IR (Tamemoto et al., 1994; Zhande et al., 2002), and it is known that IRS1 down-regulation can lead alone to IR and development of diabetes and MetS (Hartley et al.,

2006; Kerouz et al., 1997; Kido et al., 2000). However, the molecular mechanism triggering the neuropathological activation of IRS1 degradation is far from being understood.

Interesting insights were gained into this thesis about the mechanism underlying the active degradation of proteins of the insulin cascade pathway. Taking advantage of the usage of the potent and selective neddylation inhibitor MLN-4924, it was possible to demonstrate that this phenomenon is neddylation-dependent. NEDD8 is a ubiquitin-like protein that activates by covalent bound to specific lysine the cullins E3-ubiquitin ligases (Pan et al., 2004; Petroski & Deshaies, 2005). Once neddylated, cullins ubiquitinate proteins and lead them to proteasome-dependent degradation. We showed that application of MLN-4924 to cultivated cortical and hippocampal neurons treated with insulin and TNFα rescues the total level of IRS1 and InsR proteins that were reduced by IR treatment. MLN-4924 showed trend to rescue also IRS2, which is down regulated by IR treatment as well, but had no effect on the protein level of IRSp53, an insulin-insensitive isoform belonging to IRS family. These findings highlighted that neddylation process specifically involves IRS isoforms that are implicated in the insulin transmission and subjected to IR. Moreover, interestingly, the inhibition of neddylation by MLN-4924 resulted into the restoration of hippocampal and cortical neurons responsiveness to insulin of the downstream effector AKT. Unlike the bath application of TNFα neutralizing antibody, MLN-4924 significantly recovers phospho-AKT levels in IR-induced neurons, as a consequence of the rescued IRS1 and InsR levels. These findings suggest that, although TNFα-dependent IRS1 hyper-phosphorylation and the neddylation-dependent proteasomal degradation of IRS1 work in concert to elicit synaptic IR, the neddylation has a major contribution to the onset of synaptic IR.

The cullin family counts several members expressed almost ubiquitously. It is known that, among the other cullins, CUL7 has an important role in the ubiquitin-dependent degradation of IRS1 in non-neuronal cells (Xu et al., 2008). Notably, it has been recently demonstrated that mTORC1 and its downstream target S6K regulate this process. mTORC1/S6K phosphorylate IRS1 at specific serine residues (Ser422) making IRS1 more prone to be ubiquitinated and degraded (Yoneyama et al., 2018). Nevertheless, it is not excluded that other isoforms could also be in complex with IRS1 and have a possible

role in its degradation. In accordance with the mentioned studies, in this thesis we could show that CUL7 indeed co-immunoprecipitated with IRS1 from HEK293T cell lysate. However, our experiments also depicted that CUL7 is not the only isoform forming a complex with IRS1, but also CUL1, CUL3 and CUL4A can do so. Nevertheless, only the co-expression of IRS1 and CUL7, but not the other isoforms, resulted in massive ubiquitination of the substrate. Even so, the role of NEDD8 in this process remains so far still undisclosed. Neddylation has been extensively investigated in tumor cells (Vanderdys et al., 2018; Xie et al., 2017) and the neddylation inhibitor MLN-4924 is currently in the phase II of clinical investigation as tumor suppressor drug (Bailly et al., 2016; Tong et al., 2017). However, very little is known about its function in neurons and even less about a possible role of neddylation into AD onset. Notably, we could show that the CUL7-dependent IRS1 ubiquitination is NEDD8 dependent as outlined by the reduced ubiquitination of IRS1 in HEK293T cells treated with MLN-4924.

Nevertheless, given the relative high number of cullins expressed in neurons, it is unluckily very challenging to address the specific role of one specific cullin and to exclude the participation of any other isoform in the neddylation-dependent IRS1 degradation. Ponyeam and Hagen suggested that CUL7 promotes the ubiquitination of CUL1 by forming a complex with CUL1 in HEK293T cells via heterodimerization of Fbxw8, the most studied interacting partner of CUL7. The formation of this complex is likely to increase poly-ubiquitination efficiency of IRS1 (Ponyeam & Hagen, 2012). The preliminary data obtained from experiments performed in neuronal cultures, in which the over-expression of HA-tagged NEDD8 was induced using AAV9 virus, showed that CUL7 co-immunoprecipitates with NEDD8 from neuronal cytosolic extract. The idea behind the development of HA-NEDD8 AAV9 virus is to use it as a tool to immunoprecipitate all the neddylated protein in synapses. With this, we eventually could identify proteins that are neddylated in synaptic IR and to nail down quantitative and qualitative changes of these proteins.

4.3. MetS and amyloidosis cause synaptic plasticity and memory impairments in TBA2.1 mice through neuronal IR and neuroinflammation

The *in vitro* experimental work allowed us to generate hypotheses about the molecular mechanism of IR, highlighting the dual effects of high insulin levels, amyloid-β and neuroinflammation on the onset of neuronal IR. Following these hypotheses, the relationship between those factors was next investigated *in vivo* using the novel transgenic mouse model TBA2.1. TBA2.1 mice express human pyro-glutamylated Aβ3(pE)-42 specifically in the brain under the neuronal-specific murine Thy1 promoter. Aβ3(pE)-42 peptide is further secreted in the extracellular environment via the Golgi secretory pathway. Aβ3(pE)-42 is one of the major constituents of Aβ deposits in human AD brain (Harigaya et al., 2000; Portelius et al., 2010; Russo et al., 1997; Saido et al., 1995; Wirths et al., 2010) and it has potent effect in the induction of glial release of TNFα after the uptake from astrocytes (Grochowska et al., 2017). The massive expression of Aβ3(pE)-42 in homozygous (Tg/Tg) TBA2.1 mice lead to severe AD-like symptoms such as neuroinflammation, hippocampal degeneration and motor-coordination problems at early stages of life (3-5 months old) (Alexandru et al., 2011). On the other hand, heterozygous mice (+/Tg TBA2.1), which express lower amount of Aβ3(pE)-42 peptides, do not show the same phenotype (Alexandru et al., 2011). Among the many mouse models for AD that researchers developed over the years, +/+ TBA2.1 mice have been selected for this project because of their asymptomatic expression of Aβos, representing an ideal mouse model for a high-risk population with amyloidosis. This is of relevance because it is nowadays well established that in many cases Aβ deposition in human brain does not overlap with clinical AD manifestations (Davis & Chisholm, 1999; Matthews et al., 2009; Perez-Nievas et al., 2013; Price et al., 2009). Therefore, usage of +/Tg TBA2.1 allowed us to investigate whether the relationship between amyloid burden and IR is of relevance for the onset of cognitive impairments.

To this end, MetS was induced in TBA2.1 mice by means of a high fat/calorie diet (HFD) and mice were tested for experiments once they developed MetS (defined threshold of 70% body weight increase). First, and in order to ensure that the diet successfully induced

MetS, peripheral markers of MetS such as serum insulin, cholesterol and glucose were evaluated. As expected the concentrations of these factors were sensibly higher in mice fed with the HFD. Development of MetS after 14 to 24 weeks of diet showed the same entity in both genotypes of TBA2.1 mice. Additionally, the glucose tolerance test confirmed the greater insulin-insensitivity in peripheral tissues of animals on HFD as compared to controls. Furthermore, the contribution of HFD in the outbreak of IR in neurons and synapses was rated by means of immunoblot analysis of total hippocampus and cortex homogenate, as well as in isolated synaptosomes. Consistent with the *in vitro* experiments, western blots of the total homogenates proved that HFD lowered the total IRS1 and IRS2 levels in both hippocampus and cortex, which was followed by striking reduction of the basal phosphorylation of AKT in both +/+ and +/Tg TBA2.1 mice. Surprisingly, no significant difference in terms of de-phosphorylation of AKT was observed between the two genotypes. However, it would be interesting in the near future to check the serine-phosphorylation levels of IRS1 that we expect to be increased in +/Tg TBA2.1 in agreement with the *in vitro* model. In a similar fashion, the *ex vivo* insulin stimulation of the isolated synaptosomes showed a reduction of the phospho-InsR in +/+ and +/Tg TBA2.1 on HFD as compared to RD mice.

Moreover, we next have correlated the deregulation of the insulin cascade to synaptic processes and learning and memory performance. Over the past decades it has been established that insulin elicits LTD in hippocampal CA1 (Labouèbe et al., 2013). We found that TBA2.1 mice fed with HFD undergo impairments of LTD, as evidenced by measures of fEPSP slope on hippocampal acute slices. Intriguingly, the effects of the diet were more pronounced in +/Tg TBA2.1 as compared to +/+ mice. On the other hand, it is well established that Aβos induce LTP impairment (Cullen et al., 1997; Jo et al., 2011; Kamenetz et al., 2003; Lambert et al., 1998; Shankar et al., 2007; Walsh et al., 2002). Consistent with that, we found that Aβ3(pE)-42 expression in +/Tg TBA2.1 mice caused impaired LTP as compared to slices from +/+ mice. No further reduction was observed in HFD animals compared to RD of the same genotype. However, although it was not statistically significant, the HFD had a tendency to impair LTP also in +/+ TBA2.1 mice. This can be interpreted like a potential negative effect of synaptic IR that is elicited not only on LTD but also on LTP. These impairments in synaptic plasticity can occur even in

amyloid-negative individuals, but the combinatory effect of HFD and amyloidosis worsen the phenotype. Impairment of CA1-dependent memory was furthermore confirmed by novel object location/recognition experiments, by which we showed severe consequences of HFD in animals, with a stronger effect in +/Tg TBA2.1 mice in the recognition of newly located object.

These findings raised the question of how the disruption of the synaptic insulin-signaling cascade can correlate to synaptic plasticity impairments. Crucial component of the insulin pathway are PI3K proteins, known to be required for various forms of LTD in the hippocampus (Daw et al., 2002; Hou & Klann, 2004; van der Heide et al., 2005). Selective activation of mGluR1 induces LTD in CA1 by recruiting the PI3K/AKT/mTOR signaling pathway (Daw et al., 2002). Interestingly, it has been found the Class IB PI3Kγ isoform has the most crucial role in NMDA receptor-mediated synaptic plasticity at mouse Schaffer collateral-CA1 synapses (Kim et al., 2011). These authors proved that pharmacological blockade or genetic knockout of PI3Kγ result in impairment of NMDAR-dependent LTD and learning. Consistent with that, we could show that PI3Kγ activity is highly reduced by the HFD in TBA2.1 mice. Notably, these results were also confirmed *in vitro* on cortical culture treated with insulin and TNFα 24 h to induce IR. Unlike the ubiquitous-expressed Class IA PI3Ks, which are activated by tyrosine-kinase receptors such as the InsR, the Class IB PI3Kγ usually responds to GPCRs. However, once activated PI3Kγ produces $PI(3,4,5)P_3$, important for the phosphorylation of AKT. Albeit it is not clear whether PI3Kγ directly participates or not to the insulin signaling, it is not excluded that the synaptic IR could affect PI3Kγ activity, resulting therefore in NMDAR-dependent LTD and learning impairments observed in TBA2.1 mice.

Our results showed altogether that prolonged HFD causes peripheral IR, which results in neuronal and synaptic IR, impacting the functionality of the neuronal insulin signaling of both +/+ and +/Tg TB2.1 mice. Moreover, these findings stressed out the importance of the combined noxious actions of both over-exposure to insulin in over-fed animals and Aβ expression to affect memory *in vivo* (Figure 38).

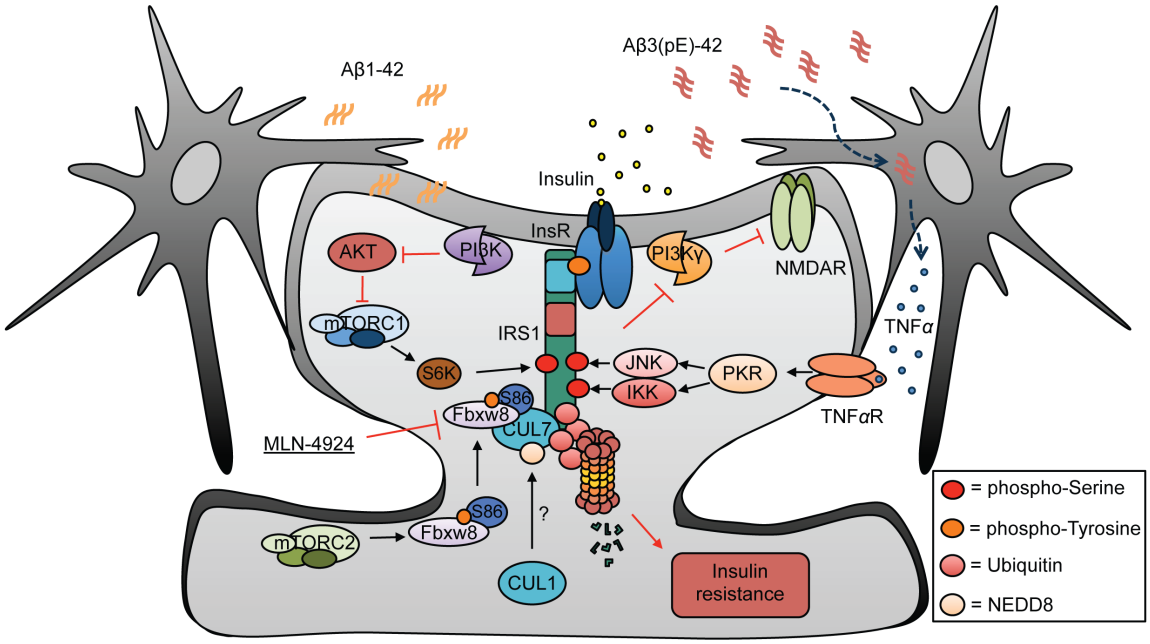

Figure 38: Scheme representing the proposed molecular mechanism for synaptic IR, caused by diet-induced MetS and Aβ3(pE)-42-driven TNFα release. Aβ3(pE)-42-mediates TNFα release from astrocytes and neuroinflammation induces IRS1 serine-phosphorylation via activation of stress-induced kinases such as PKR, JNK or IKK. Phosphorylation of IRS1 (Ser422) by mTORC1/S6K makes IRS1 more susceptible to ubiquitination (Yoneyama et al., 2018). mTORC2 phosphorylates and activates Fbxw8 (Kim et al., 2012), which is a crucial and specific member of CUL7 CRL. Neddylation of CUL7, maybe via the formation of a complex with CUL1 (Ponyeam & Hagen, 2012), activates finally the CRL, leading to IRS1 ubiquitination and degradation. IRS1 degradation and serine-phosphorylation altogether inhibit the PI3K/AKT/mTORC1 pathway. IR finally alters the activity of PI3Kγ causing NMDAR-dependent synaptic plasticity impairments.

Last, and in order to validate the hypothesis that Aβ3(pE)-42 acts in the interplay with neuronal IR via pro-inflammatory mechanism, the markers for astrogliosis and microgliosis were investigated in hippocampal slices. Hippocampal CA1 region is one of the first regions of the brain affected by neurodegeneration in AD (Casas et al., 2004), and astroglia activation is believed to be one of the earliest hallmarks of the disease (DaRocha-Souto et al., 2011; Heneka et al., 2015; Simpson et al., 2011; Tuppo & Arias, 2005). Here we showed that slices from +/Tg TBA2.1 on HFD, stained for activated microglia marker Iba1, have overall major activation of microglia in CA1 region. Immunostaining against the astrocytic marker GFAP showed an increased number of positive cells in +/Tg TBA2.1, becoming significant in HFD-fed animals as compared to those in RD. Increased activation of astrocytes in +/Tg TBA2.1 mice resulted also in

increased levels of total TNFα measured by quantitative ELISA in the total homogenate from cortices of TBA2.1 mice. Astrogliosis and enhanced TNFα release in +/Tg TBA2.1 mice are presumably due to the expression of Aβ3(pE)-42. However, surprisingly, the ELISA assay did not show any significant difference between RD and HFD +/Tg mice. One can speculate that the HFD-induced IR affects primarily the CA1 region of the hippocampus, where it causes a further increase in the activation of astrocytes as compared to RD +/Tg mice. This hypothesis must be further investigated by the quantification of TNFα levels in hippocampus. Additionally, probably as result of the increased neuroinflammation, +/Tg TBA2.1 HFD mice consistently showed significant neuronal cell loss in the molecular layer of CA1 area.

4.4. MLN-4924 injection in TBA2.1 mice showed potential as a therapy against neuronal IR *in vivo*

Finally, in the last part of the thesis we gained insights related to the pharmacological inhibition of neddylation *in vivo*. Bath application of MLN-4924 in neuronal culture showed positive effects in counteracting neuronal IR via inhibition of IRS1 and InsR degradation. Thus, we tried to demonstrate that MLN-4924 indeed leads to restoration of the neuronal insulin signaling pathway and synaptic plasticity and it improves cognitive performance in mice with neuroinflammation and MetS. Previously fed with HFD, TBA2.1 mice were injected with an intraperitoneal dose of MLN-4924 for 14 days, one time per day. Importantly, we first made sure that MLN-4924 is not cytotoxic *in vivo* and does not cause drastic variations of the total body mass of the mice. Although no real conclusions can be taken yet from the preliminary experiments performed because of the limited N numbers, it seems that MLN-4924 has effects as glucose sensitizer in peripheral tissues, but however does not affect the circulating levels of insulin, glucose and fats. If confirmed, this outcome would be the confirmation that the effects of MLN-4924 on neuronal IR that hereafter will be discussed, are not a consequence of the dropped concentration of the peripheral insulin, glucose or fats, but rather a specific neuronal intracellular mechanism.

Albeit once again from limited N number, we were encouraged to observe that MLN-4924 injection has a trend to positively restore synaptic plasticity and memory in TBA2.1 +/Tg HFD mice. In parallel, bath application of MLN-4924 on acute slices of RD +/+ and +/Tg TBA2.1 mice had no effect at basal level on LTD. This allowed us to conclude that the effect of MLN-4924 on synaptic plasticity in intraperitoneally injected HFD mice could be addressed specifically to the inhibition of neddylation, which caused HFD-induced IRS1 degradation. Moreover, we could demonstrate that 14 days-long daily MLN-4924 intraperitoneal injection prevented IRS1 degradation in total homogenate of hippocampus and cortex. Surprisingly this effect was only observed on the +/+ TBA2.1 HFD, but not on the +/Tg HFD mice. A possible interpretation is that, as evidenced by the *in vitro* experiments, IRS1 degradation and serine-phosphorylation have collective roles in the onset of neuronal IR. Therefore, it can be speculated that neddylation inhibition helps to restore neuronal IR in animals that do not express amyloid-β; however it is not enough in the presence of Aβ3(pE)-42, which induces neuroinflammation and hyper phosphorylation of IRS1. In order to address these questions, an interesting experiment that we currently consider to do is to inject TBA2.1 mice with both MLN-4924 and TNFα-neutralizing antibody. A hypothetical rescue of neuronal IR also in +/Tg TBA2.1 mice fed with HFD would be a confirmation of dual action of HFD-induced MetS and neuroinflammation.

5. References

Abbott, M. A., Wells, D. G., & Fallon, J. R. (1999). The insulin receptor tyrosine kinase substrate p58/53 and the insulin receptor are components of CNS synapses. *The Journal of Neuroscience: The Official Journal of the Society for Neuroscience*, *19*(17), 7300–7308.

Abramov, E., Dolev, I., Fogel, H., Ciccotosto, G. D., Ruff, E., & Slutsky, I. (2009). Amyloid-beta as a positive endogenous regulator of release probability at hippocampal synapses. *Nature Neuroscience*, *12*(12), 1567–1576. https://doi.org/10.1038/nn.2433

Adamo, M., Raizada, M. K., & LeRoith, D. (1989). Insulin and insulin-like growth factor receptors in the nervous system. *Molecular Neurobiology*, *3*(1–2), 71–100.

Agostinone, J., Alarcon-Martinez, L., Gamlin, C., Yu, W.-Q., Wong, R. O. L., & Di Polo, A. (2018). Insulin signalling promotes dendrite and synapse regeneration and restores circuit function after axonal injury. *Brain: A Journal of Neurology*, *141*(7), 1963–1980. https://doi.org/10.1093/brain/awy142

Aguirre, V., Uchida, T., Yenush, L., Davis, R., & White, M. F. (2000). The c-Jun NH(2)-terminal kinase promotes insulin resistance during association with insulin receptor substrate-1 and phosphorylation of Ser(307). *The Journal of Biological Chemistry*, *275*(12), 9047–9054.

Alexandru, A., Jagla, W., Graubner, S., Becker, A., Bäuscher, C., Kohlmann, S., … von Hörsten, S. (2011). Selective hippocampal neurodegeneration in transgenic mice expressing small amounts of truncated Aβ is induced by pyroglutamate-Aβ formation. *The Journal of Neuroscience: The Official Journal of the Society for Neuroscience*, *31*(36), 12790–12801. https://doi.org/10.1523/JNEUROSCI.1794-11.2011

Amato, S., & Man, H.-Y. (2012). AMPK signaling in neuronal polarization: Putting the brakes on axonal traffic of PI3-Kinase. *Communicative & Integrative Biology*, *5*(2), 152–155. https://doi.org/10.4161/cib.18968

Andrews, S., Stephens, L. R., & Hawkins, P. T. (2007). PI3K class IB pathway. *Science's STKE: Signal Transduction Knowledge Environment*, *2007*(407), cm2. https://doi.org/10.1126/stke.4072007cm2

Apostolatos, A., Song, S., Acosta, S., Peart, M., Watson, J. E., Bickford, P., … Patel, N. A. (2012). Insulin promotes neuronal survival via the alternatively spliced protein kinase CδII isoform. *The Journal of Biological Chemistry*, *287*(12), 9299–9310. https://doi.org/10.1074/jbc.M111.313080

Arai, T., Kasper, J. S., Skaar, J. R., Ali, S. H., Takahashi, C., & DeCaprio, J. A. (2003). Targeted disruption of p185/Cul7 gene results in abnormal vascular morphogenesis. *Proceedings of the National Academy of Sciences of the United States of America*, *100*(17), 9855–9860. https://doi.org/10.1073/pnas.1733908100

Arnold, S. E., Lucki, I., Brookshire, B. R., Carlson, G. C., Browne, C. A., Kazi, H., … Kim, S. F. (2014). High fat diet produces brain insulin resistance, synaptodendritic abnormalities and altered behavior in mice. *Neurobiology of Disease*, *67*, 79–87. https://doi.org/10.1016/j.nbd.2014.03.011

Artinian, J., McGauran, A.-M. T., De Jaeger, X., Mouledous, L., Frances, B., & Roullet, P. (2008). Protein degradation, as with protein synthesis, is required during not only long-term spatial memory consolidation but also reconsolidation. *The European Journal of Neuroscience*, *27*(11), 3009–3019. https://doi.org/10.1111/j.1460-9568.2008.06262.x

Assini, F. L., Duzzioni, M., & Takahashi, R. N. (2009). Object location memory in mice: pharmacological validation and further evidence of hippocampal CA1 participation. *Behavioural Brain Research*, *204*(1), 206–211. https://doi.org/10.1016/j.bbr.2009.06.005

Bailly, A., Perrin, A., Bou Malhab, L. J., Pion, E., Larance, M., Nagala, M., … Xirodimas, D. P. (2016). The NEDD8 inhibitor MLN4924 increases the size of the nucleolus and activates p53 through the ribosomal-Mdm2 pathway. *Oncogene*, *35*(4), 415–426. https://doi.org/10.1038/onc.2015.104

Barber, D. F., Bartolomé, A., Hernandez, C., Flores, J. M., Redondo, C., Fernandez-Arias, C., … Carrera, A. C. (2005). PI3Kgamma inhibition blocks glomerulonephritis and extends lifespan in a mouse model of systemic lupus. *Nature Medicine*, *11*(9), 933–935. https://doi.org/10.1038/nm1291

Baskin, D. G., Figlewicz Lattemann, D., Seeley, R. J., Woods, S. C., Porte, D., & Schwartz, M. W. (1999). Insulin and leptin: dual adiposity signals to the brain for the regulation of food intake and body weight. *Brain Research*, *848*(1–2), 114–123.

Bateman, R. J., Xiong, C., Benzinger, T. L. S., Fagan, A. M., Goate, A., Fox, N. C., … Dominantly Inherited Alzheimer Network. (2012). Clinical and biomarker changes in dominantly inherited Alzheimer's disease. *The New England Journal of Medicine*, *367*(9), 795–804. https://doi.org/10.1056/NEJMoa1202753

Bayer, T. A., & Wirths, O. (2014). Focusing the amyloid cascade hypothesis on N-truncated Abeta peptides as drug targets against Alzheimer's disease. *Acta Neuropathologica*, *127*(6), 787–801. https://doi.org/10.1007/s00401-014-1287-x

Behnisch, T., Yuanxiang, P., Bethge, P., Parvez, S., Chen, Y., Yu, J., … Kreutz, M. R. (2011). Nuclear translocation of jacob in hippocampal neurons after stimuli inducing long-term potentiation but not long-term depression. *PloS One*, *6*(2), e17276. https://doi.org/10.1371/journal.pone.0017276

Biessels, G. J., Staekenborg, S., Brunner, E., Brayne, C., & Scheltens, P. (2006). Risk of dementia in diabetes mellitus: a systematic review. *The Lancet. Neurology*, *5*(1), 64–74. https://doi.org/10.1016/S1474-4422(05)70284-2

Blázquez, E., Velázquez, E., Hurtado-Carneiro, V., & Ruiz-Albusac, J. M. (2014). Insulin in the brain: its pathophysiological implications for States related with central insulin resistance, type 2 diabetes and Alzheimer's disease. *Frontiers in Endocrinology*, *5*, 161. https://doi.org/10.3389/fendo.2014.00161

Bocarsly, M. E., Fasolino, M., Kane, G. A., LaMarca, E. A., Kirschen, G. W., Karatsoreos, I. N., … Gould, E. (2015). Obesity diminishes synaptic markers, alters microglial morphology, and impairs cognitive function. *Proceedings of the National Academy of Sciences of the United States of America*, *112*(51), 15731–15736. https://doi.org/10.1073/pnas.1511593112

Bomfim, T. R., Forny-Germano, L., Sathler, L. B., Brito-Moreira, J., Houzel, J.-C., Decker, H., … De Felice, F. G. (2012). An anti-diabetes agent protects the mouse brain from defective insulin signaling caused by Alzheimer's disease- associated

Aβ oligomers. *The Journal of Clinical Investigation*, *122*(4), 1339–1353. https://doi.org/10.1172/JCI57256

Borrie, S. C., Brems, H., Legius, E., & Bagni, C. (2017). Cognitive Dysfunctions in Intellectual Disabilities: The Contributions of the Ras-MAPK and PI3K-AKT-mTOR Pathways. *Annual Review of Genomics and Human Genetics*, *18*, 115–142. https://doi.org/10.1146/annurev-genom-091416-035332

Borst, S. E. (2004). The role of TNF-alpha in insulin resistance. *Endocrine*, *23*(2–3), 177–182. https://doi.org/10.1385/ENDO:23:2-3:177

Brewer, P. D., Habtemichael, E. N., Romenskaia, I., Mastick, C. C., & Coster, A. C. F. (2014). Insulin-regulated Glut4 translocation: membrane protein trafficking with six distinctive steps. *The Journal of Biological Chemistry*, *289*(25), 17280–17298. https://doi.org/10.1074/jbc.M114.555714

Bronzuoli, M. R., Iacomino, A., Steardo, L., & Scuderi, C. (2016). Targeting neuroinflammation in Alzheimer's disease. *Journal of Inflammation Research*, *9*, 199–208. https://doi.org/10.2147/JIR.S86958

Burette, A. C., Park, H., & Weinberg, R. J. (2014). Postsynaptic distribution of IRSp53 in spiny excitatory and inhibitory neurons. *The Journal of Comparative Neurology*, *522*(9), 2164–2178. https://doi.org/10.1002/cne.23526

Byrne, J. H., Baxter D. A., Buonomano, D. V., Cleary, L. J., Eskin, A., Goldsmith, J. R., McClendon, E., Nazif, F. A., Noel, F., Scholz, K. P. (1998). Neural and molecular bases of nonassociative and associative learning in Aplysia. *Annals of the New York Academy of Science.* 627: 124-149.

Cai, D., Dhe-Paganon, S., Melendez, P. A., Lee, J., & Shoelson, S. E. (2003). Two new substrates in insulin signaling, IRS5/DOK4 and IRS6/DOK5. *The Journal of Biological Chemistry*, *278*(28), 25323–25330. https://doi.org/10.1074/jbc.M212430200

Calsolaro, V., & Edison, P. (2016). Neuroinflammation in Alzheimer's disease: Current evidence and future directions. *Alzheimer's & Dementia: The Journal of the Alzheimer's Association*, *12*(6), 719–732. https://doi.org/10.1016/j.jalz.2016.02.010

Casas, C., Sergeant, N., Itier, J.-M., Blanchard, V., Wirths, O., van der Kolk, N., … Pradier, L. (2004). Massive CA1/2 neuronal loss with intraneuronal and N-terminal truncated Abeta42 accumulation in a novel Alzheimer transgenic model. *The American Journal of Pathology*, *165*(4), 1289–1300.

Chen, T., Ueda, Y., Xie, S., & Li, E. (2002). A novel Dnmt3a isoform produced from an alternative promoter localizes to euchromatin and its expression correlates with active de novo methylation. *The Journal of Biological Chemistry*, *277*(41), 38746–38754. https://doi.org/10.1074/jbc.M205312200

Cheng, Z., Tseng, Y., & White, M. F. (2010). Insulin signaling meets mitochondria in metabolism. *Trends in Endocrinology and Metabolism: TEM*, *21*(10), 589–598. https://doi.org/10.1016/j.tem.2010.06.005

Chiu, S.-L., & Cline, H. T. (2010). Insulin receptor signaling in the development of neuronal structure and function. *Neural Development*, *5*, 7. https://doi.org/10.1186/1749-8104-5-7

Correia, S. C., Santos, R. X., Perry, G., Zhu, X., Moreira, P. I., & Smith, M. A. (2011). Insulin-resistant brain state: the culprit in sporadic Alzheimer's disease? *Ageing Research Reviews*, *10*(2), 264–273. https://doi.org/10.1016/j.arr.2011.01.001

Craft, S., Baker, L. D., Montine, T. J., Minoshima, S., Watson, G. S., Claxton, A., … Gerton, B. (2012). Intranasal insulin therapy for Alzheimer disease and amnestic mild cognitive impairment: a pilot clinical trial. *Archives of Neurology*, *69*(1), 29–38. https://doi.org/10.1001/archneurol.2011.233

Crawley, J. N. (1999). Behavioral phenotyping of transgenic and knockout mice: experimental design and evaluation of general health, sensory functions, motor abilities, and specific behavioral tests. *Brain Research*, *835*(1), 18–26.

Cullen, W. K., Suh, Y. H., Anwyl, R., & Rowan, M. J. (1997). Block of LTP in rat hippocampus in vivo by beta-amyloid precursor protein fragments. *Neuroreport*, *8*(15), 3213–3217.

Cynis, H., Schilling, S., Bodnár, M., Hoffmann, T., Heiser, U., Saido, T. C., & Demuth, H.-U. (2006). Inhibition of glutaminyl cyclase alters pyroglutamate formation in mammalian cells. *Biochimica Et Biophysica Acta*, *1764*(10), 1618–1625. https://doi.org/10.1016/j.bbapap.2006.08.003

da Costa, R. M., Neves, K. B., Mestriner, F. L., Louzada-Junior, P., Bruder-Nascimento, T., & Tostes, R. C. (2016). TNF-α induces vascular insulin resistance via positive modulation of PTEN and decreased Akt/eNOS/NO signaling in high fat diet-fed mice. *Cardiovascular Diabetology*, *15*(1), 119. https://doi.org/10.1186/s12933-016-0443-0

D'Amelio, M., Cavallucci, V., Middei, S., Marchetti, C., Pacioni, S., Ferri, A., … Cecconi, F. (2011). Caspase-3 triggers early synaptic dysfunction in a mouse model of Alzheimer's disease. *Nature Neuroscience*, *14*(1), 69–76. https://doi.org/10.1038/nn.2709

DaRocha-Souto, B., Scotton, T. C., Coma, M., Serrano-Pozo, A., Hashimoto, T., Serenó, L., … Gómez-Isla, T. (2011). Brain oligomeric β-amyloid but not total amyloid plaque burden correlates with neuronal loss and astrocyte inflammatory response in amyloid precursor protein/tau transgenic mice. *Journal of Neuropathology and Experimental Neurology*, *70*(5), 360–376. https://doi.org/10.1097/NEN.0b013e318217a118

D'Arrigo, C., Tabaton, M., & Perico, A. (2009). N-terminal truncated pyroglutamyl beta amyloid peptide Abetapy3-42 shows a faster aggregation kinetics than the full-length Abeta1-42. *Biopolymers*, *91*(10), 861–873. https://doi.org/10.1002/bip.21271

Davis, J. N., & Chisholm, J. C. (1999). Alois Alzheimer and the amyloid debate. *Nature*, *400*(6747), 810. https://doi.org/10.1038/23571

Daw, M. I., Bortolotto, Z. A., Saulle, E., Zaman, S., Collingridge, G. L., & Isaac, J. T. R. (2002). Phosphatidylinositol 3 kinase regulates synapse specificity of hippocampal long-term depression. *Nature Neuroscience*, *5*(9), 835–836. https://doi.org/10.1038/nn903

De Felice, F. G. (2013). Alzheimer's disease and insulin resistance: translating basic science into clinical applications. *The Journal of Clinical Investigation*, *123*(2), 531–539. https://doi.org/10.1172/JCI64595

De Felice, F. G., & Benedict, C. (2015). A Key Role of Insulin Receptors in Memory. *Diabetes*, *64*(11), 3653–3655. https://doi.org/10.2337/dbi15-0011

De Felice, F. G., Vieira, M. N. N., Bomfim, T. R., Decker, H., Velasco, P. T., Lambert, M. P., … Klein, W. L. (2009). Protection of synapses against Alzheimer's-linked toxins: insulin signaling prevents the pathogenic binding of Abeta oligomers.

Proceedings of the National Academy of Sciences of the United States of America, *106*(6), 1971–1976. https://doi.org/10.1073/pnas.0809158106

de la Monte, S. M. (2009). Insulin resistance and Alzheimer's disease. *BMB Reports*, *42*(8), 475–481.

DeFronzo, R. A. (2010). Insulin resistance, lipotoxicity, type 2 diabetes and atherosclerosis: the missing links. The Claude Bernard Lecture 2009. *Diabetologia*, *53*(7), 1270–1287. https://doi.org/10.1007/s00125-010-1684-1

Deshaies, R. J., Emberley, E. D., & Saha, A. (2010). Control of cullin-ring ubiquitin ligase activity by nedd8. *Sub-Cellular Biochemistry*, *54*, 41–56. https://doi.org/10.1007/978-1-4419-6676-6_4

Dias, D. C., Dolios, G., Wang, R., & Pan, Z.-Q. (2002). CUL7: A DOC domain-containing cullin selectively binds Skp1.Fbx29 to form an SCF-like complex. *Proceedings of the National Academy of Sciences of the United States of America*, *99*(26), 16601–16606. https://doi.org/10.1073/pnas.252646399

Doble, B. W., & Woodgett, J. R. (2003). GSK-3: tricks of the trade for a multi-tasking kinase. *Journal of Cell Science*, *116*(Pt 7), 1175–1186.

Dong, C., Bach, S. V., Haynes, K. A., & Hegde, A. N. (2014). Proteasome modulates positive and negative translational regulators in long-term synaptic plasticity. *The Journal of Neuroscience: The Official Journal of the Society for Neuroscience*, *34*(9), 3171–3182. https://doi.org/10.1523/JNEUROSCI.3291-13.2014

Egawa, K., Nakashima, N., Sharma, P. M., Maegawa, H., Nagai, Y., Kashiwagi, A., … Olefsky, J. M. (2000). Persistent activation of phosphatidylinositol 3-kinase causes insulin resistance due to accelerated insulin-induced insulin receptor substrate-1 degradation in 3T3-L1 adipocytes. *Endocrinology*, *141*(6), 1930–1935. https://doi.org/10.1210/endo.141.6.7516

Fairaq, A., Goc, A., Artham, S., Sabbineni, H., & Somanath, P. R. (2015). TNFα induces inflammatory stress response in microvascular endothelial cells via Akt- and P38 MAP kinase-mediated thrombospondin-1 expression. *Molecular and Cellular Biochemistry*, *406*(1–2), 227–236. https://doi.org/10.1007/s11010-015-2440-0

Ferri, C. P., Prince, M., Brayne, C., Brodaty, H., Fratiglioni, L., Ganguli, M., … Alzheimer's Disease International. (2005). Global prevalence of dementia: a Delphi consensus study. *Lancet (London, England)*, *366*(9503), 2112–2117. https://doi.org/10.1016/S0140-6736(05)67889-0

Floden, A. M., Li, S., & Combs, C. K. (2005). Beta-amyloid-stimulated microglia induce neuron death via synergistic stimulation of tumor necrosis factor alpha and NMDA receptors. *The Journal of Neuroscience: The Official Journal of the Society for Neuroscience*, *25*(10), 2566–2575. https://doi.org/10.1523/JNEUROSCI.4998-04.2005

Fogel, H., Frere, S., Segev, O., Bharill, S., Shapira, I., Gazit, N., … Slutsky, I. (2014). APP homodimers transduce an amyloid-β-mediated increase in release probability at excitatory synapses. *Cell Reports*, *7*(5), 1560–1576. https://doi.org/10.1016/j.celrep.2014.04.024

Franklin, W., & Taglialatela, G. (2016). A method to determine insulin responsiveness in synaptosomes isolated from frozen brain tissue. *Journal of Neuroscience Methods*, *261*, 128–134. https://doi.org/10.1016/j.jneumeth.2016.01.006

Friedman, T. C., Loh, Y. P., Cawley, N. X., Birch, N. P., Huang, S. S., Jackson, I. M., & Nillni, E. A. (1995). Processing of prothyrotropin-releasing hormone (Pro-TRH)

by bovine intermediate lobe secretory vesicle membrane PC1 and PC2 enzymes. *Endocrinology*, *136*(10), 4462–4472. https://doi.org/10.1210/endo.136.10.7664666

Frisardi, V., Solfrizzi, V., Seripa, D., Capurso, C., Santamato, A., Sancarlo, D., … Panza, F. (2010). Metabolic-cognitive syndrome: a cross-talk between metabolic syndrome and Alzheimer's disease. *Ageing Research Reviews*, *9*(4), 399–417. https://doi.org/10.1016/j.arr.2010.04.007

Ghasemi, R., Haeri, A., Dargahi, L., Mohamed, Z., & Ahmadiani, A. (2013). Insulin in the brain: sources, localization and functions. *Molecular Neurobiology*, *47*(1), 145–171. https://doi.org/10.1007/s12035-012-8339-9

Giraud, J., Leshan, R., Lee, Y.-H., & White, M. F. (2004). Nutrient-dependent and insulin-stimulated phosphorylation of insulin receptor substrate-1 on serine 302 correlates with increased insulin signaling. *The Journal of Biological Chemistry*, *279*(5), 3447–3454. https://doi.org/10.1074/jbc.M308631200

Gray, S. M., Meijer, R. I., & Barrett, E. J. (2014). Insulin regulates brain function, but how does it get there? *Diabetes*, *63*(12), 3992–3997. https://doi.org/10.2337/db14-0340

Grochowska, K. M., Yuanxiang, P., Bär, J., Raman, R., Brugal, G., Sahu, G., … Kreutz, M. R. (2017). Posttranslational modification impact on the mechanism by which amyloid-β induces synaptic dysfunction. *EMBO Reports*, *18*(6), 962–981. https://doi.org/10.15252/embr.201643519

Gross, C., & Bassell, G. J. (2014). Neuron-specific regulation of class I PI3K catalytic subunits and their dysfunction in brain disorders. *Frontiers in Molecular Neuroscience*, *7*, 12. https://doi.org/10.3389/fnmol.2014.00012

Gual, P., Le Marchand-Brustel, Y., & Tanti, J.-F. (2005). Positive and negative regulation of insulin signaling through IRS-1 phosphorylation. *Biochimie*, *87*(1), 99–109. https://doi.org/10.1016/j.biochi.2004.10.019

Gupta, S., Yadav, K., Mantri, S. S., Singhal, N. K., Ganesh, S., & Sandhir, R. (2018). Evidence for Compromised Insulin Signaling and Neuronal Vulnerability in Experimental Model of Sporadic Alzheimer's Disease. *Molecular Neurobiology*, *55*(12), 8916–8935. https://doi.org/10.1007/s12035-018-0985-0

Haettig, J., Sun, Y., Wood, M. A., & Xu, X. (2013). Cell-type specific inactivation of hippocampal CA1 disrupts location-dependent object recognition in the mouse. *Learning & Memory (Cold Spring Harbor, N.Y.)*, *20*(3), 139–146. https://doi.org/10.1101/lm.027847.112

Hämäläinen, M., Nieminen, R., Vuorela, P., Heinonen, M., & Moilanen, E. (2007). Anti-inflammatory effects of flavonoids: genistein, kaempferol, quercetin, and daidzein inhibit STAT-1 and NF-kappaB activations, whereas flavone, isorhamnetin, naringenin, and pelargonidin inhibit only NF-kappaB activation along with their inhibitory effect on iNOS expression and NO production in activated macrophages. *Mediators of Inflammation*, *2007*, 45673. https://doi.org/10.1155/2007/45673

Harigaya, Y., Saido, T. C., Eckman, C. B., Prada, C. M., Shoji, M., & Younkin, S. G. (2000). Amyloid beta protein starting pyroglutamate at position 3 is a major component of the amyloid deposits in the Alzheimer's disease brain. *Biochemical and Biophysical Research Communications*, *276*(2), 422–427. https://doi.org/10.1006/bbrc.2000.3490

Harrington, L. S., Findlay, G. M., Gray, A., Tolkacheva, T., Wigfield, S., Rebholz, H., … Lamb, R. F. (2004). The TSC1-2 tumor suppressor controls insulin-PI3K signaling via regulation of IRS proteins. *The Journal of Cell Biology*, *166*(2), 213–223. https://doi.org/10.1083/jcb.200403069

Hartley, M., Thomsett, M. J., & Cotterill, A. M. (2006). Mini-dose glucagon rescue for mild hypoglycaemia in children with type 1 diabetes: the Brisbane experience. *Journal of Paediatrics and Child Health*, *42*(3), 108–111. https://doi.org/10.1111/j.1440-1754.2006.00807.x

Hawkins, P. T., Anderson, K. E., Davidson, K., & Stephens, L. R. (2006). Signalling through Class I PI3Ks in mammalian cells. *Biochemical Society Transactions*, *34*(Pt 5), 647–662. https://doi.org/10.1042/BST0340647

He, P., Zhong, Z., Lindholm, K., Berning, L., Lee, W., Lemere, C., … Shen, Y. (2007). Deletion of tumor necrosis factor death receptor inhibits amyloid beta generation and prevents learning and memory deficits in Alzheimer's mice. *The Journal of Cell Biology*, *178*(5), 829–841. https://doi.org/10.1083/jcb.200705042

Hebert, L. E., Weuve, J., Scherr, P. A., & Evans, D. A. (2013). Alzheimer disease in the United States (2010-2050) estimated using the 2010 census. *Neurology*, *80*(19), 1778–1783. https://doi.org/10.1212/WNL.0b013e31828726f5

Heinonen, O., Soininen, H., Sorvari, H., Kosunen, O., Paljärvi, L., Koivisto, E., & Riekkinen, P. J. (1995). Loss of synaptophysin-like immunoreactivity in the hippocampal formation is an early phenomenon in Alzheimer's disease. *Neuroscience*, *64*(2), 375–384.

Heneka, M. T., Carson, M. J., El Khoury, J., Landreth, G. E., Brosseron, F., Feinstein, D. L., … Kummer, M. P. (2015). Neuroinflammation in Alzheimer's disease. *The Lancet. Neurology*, *14*(4), 388–405. https://doi.org/10.1016/S1474-4422(15)70016-5

Heppner, F. L., Ransohoff, R. M., & Becher, B. (2015). Immune attack: the role of inflammation in Alzheimer disease. *Nature Reviews. Neuroscience*, *16*(6), 358–372. https://doi.org/10.1038/nrn3880

Heung, M.-Y., Visegrady, B., Fütterer, K., & Machesky, L. M. (2008). Identification of the insulin-responsive tyrosine phosphorylation sites on IRSp53. *European Journal of Cell Biology*, *87*(8–9), 699–708. https://doi.org/10.1016/j.ejcb.2008.02.010

Hirosumi, J., Tuncman, G., Chang, L., Görgün, C. Z., Uysal, K. T., Maeda, K., … Hotamisligil, G. S. (2002). A central role for JNK in obesity and insulin resistance. *Nature*, *420*(6913), 333–336. https://doi.org/10.1038/nature01137

Hirsch, E., Katanaev, V. L., Garlanda, C., Azzolino, O., Pirola, L., Silengo, L., … Wymann, M. P. (2000). Central role for G protein-coupled phosphoinositide 3-kinase gamma in inflammation. *Science (New York, N.Y.)*, *287*(5455), 1049–1053.

Hori, K., Yasuda, H., Konno, D., Maruoka, H., Tsumoto, T., & Sobue, K. (2005). NMDA receptor-dependent synaptic translocation of insulin receptor substrate p53 via protein kinase C signaling. *The Journal of Neuroscience: The Official Journal of the Society for Neuroscience*, *25*(10), 2670–2681. https://doi.org/10.1523/JNEUROSCI.3638-04.2005

Hosoda, R., Saido, T. C., Otvos, L., Arai, T., Mann, D. M., Lee, V. M., … Iwatsubo, T. (1998). Quantification of modified amyloid beta peptides in Alzheimer disease

and Down syndrome brains. *Journal of Neuropathology and Experimental Neurology*, *57*(11), 1089–1095.

Hotamisligil, G. S., Peraldi, P., Budavari, A., Ellis, R., White, M. F., & Spiegelman, B. M. (1996). IRS-1-mediated inhibition of insulin receptor tyrosine kinase activity in TNF-alpha- and obesity-induced insulin resistance. *Science (New York, N.Y.)*, *271*(5249), 665–668.

Hou, L., & Klann, E. (2004). Activation of the phosphoinositide 3-kinase-Akt-mammalian target of rapamycin signaling pathway is required for metabotropic glutamate receptor-dependent long-term depression. *The Journal of Neuroscience: The Official Journal of the Society for Neuroscience*, *24*(28), 6352–6361. https://doi.org/10.1523/JNEUROSCI.0995-04.2004

Hoxhaj, G., Dissanayake, K., & MacKintosh, C. (2013). Effect of IRS4 levels on PI 3-kinase signalling. *PloS One*, *8*(9), e73327. https://doi.org/10.1371/journal.pone.0073327

Hoyer, S., Henneberg, N., Knapp, S., Lannert, H., & Martin, E. (1996). Brain glucose metabolism is controlled by amplification and desensitization of the neuronal insulin receptor. *Annals of the New York Academy of Sciences*, *777*, 374–379.

Ikink, G. J., Boer, M., Bakker, E. R. M., & Hilkens, J. (2016). IRS4 induces mammary tumorigenesis and confers resistance to HER2-targeted therapy through constitutive PI3K/AKT-pathway hyperactivation. *Nature Communications*, *7*, 13567. https://doi.org/10.1038/ncomms13567

Ingelsson, M., Fukumoto, H., Newell, K. L., Growdon, J. H., Hedley-Whyte, E. T., Frosch, M. P., … Irizarry, M. C. (2004). Early Abeta accumulation and progressive synaptic loss, gliosis, and tangle formation in AD brain. *Neurology*, *62*(6), 925–931.

Jack, C. R., Knopman, D. S., Jagust, W. J., Petersen, R. C., Weiner, M. W., Aisen, P. S., … Trojanowski, J. Q. (2013). Tracking pathophysiological processes in Alzheimer's disease: an updated hypothetical model of dynamic biomarkers. *The Lancet. Neurology*, *12*(2), 207–216. https://doi.org/10.1016/S1474-4422(12)70291-0

Jarome, T. J., Werner, C. T., Kwapis, J. L., & Helmstetter, F. J. (2011). Activity dependent protein degradation is critical for the formation and stability of fear memory in the amygdala. *PloS One*, *6*(9), e24349. https://doi.org/10.1371/journal.pone.0024349

Jawhar, S., Wirths, O., & Bayer, T. A. (2011). Pyroglutamate amyloid-β (Aβ): a hatchet man in Alzheimer disease. *The Journal of Biological Chemistry*, *286*(45), 38825–38832. https://doi.org/10.1074/jbc.R111.288308

Jo, J., Whitcomb, D. J., Olsen, K. M., Kerrigan, T. L., Lo, S.-C., Bru-Mercier, G., … Cho, K. (2011). Aβ(1-42) inhibition of LTP is mediated by a signaling pathway involving caspase-3, Akt1 and GSK-3β. *Nature Neuroscience*, *14*(5), 545–547. https://doi.org/10.1038/nn.2785

Johnston, H., Boutin, H., & Allan, S. M. (2011). Assessing the contribution of inflammation in models of Alzheimer's disease. *Biochemical Society Transactions*, *39*(4), 886–890. https://doi.org/10.1042/BST0390886

Jonas, E. A., Knox, R. J., Smith, T. C., Wayne, N. L., Connor, J. A., & Kaczmarek, L. K. (1997). Regulation by insulin of a unique neuronal Ca2+ pool and of neuropeptide secretion. *Nature*, *385*(6614), 343–346. https://doi.org/10.1038/385343a0

Kamenetz, F., Tomita, T., Hsieh, H., Seabrook, G., Borchelt, D., Iwatsubo, T., … Malinow, R. (2003). APP processing and synaptic function. *Neuron*, *37*(6), 925–937.

Kamitani, T., Kito, K., Nguyen, H. P., & Yeh, E. T. (1997). Characterization of NEDD8, a developmentally down-regulated ubiquitin-like protein. *The Journal of Biological Chemistry*, *272*(45), 28557–28562.

Karnieli, E., Zarnowski, M. J., Hissin, P. J., Simpson, I. A., Salans, L. B., & Cushman, S. W. (1981). Insulin-stimulated translocation of glucose transport systems in the isolated rat adipose cell. Time course, reversal, insulin concentration dependency, and relationship to glucose transport activity. *The Journal of Biological Chemistry*, *256*(10), 4772–4777.

Karpova, A., Mikhaylova, M., Bera, S., Bär, J., Reddy, P. P., Behnisch, T., … Kreutz, M. R. (2013). Encoding and transducing the synaptic or extrasynaptic origin of NMDA receptor signals to the nucleus. *Cell*, *152*(5), 1119–1133. https://doi.org/10.1016/j.cell.2013.02.002

Karpova, A., Mikhaylova, M., Thomas, U., Knöpfel, T., & Behnisch, T. (2006). Involvement of protein synthesis and degradation in long-term potentiation of Schaffer collateral CA1 synapses. *The Journal of Neuroscience: The Official Journal of the Society for Neuroscience*, *26*(18), 4949–4955. https://doi.org/10.1523/JNEUROSCI.4573-05.2006

Kerouz, N. J., Hörsch, D., Pons, S., & Kahn, C. R. (1997). Differential regulation of insulin receptor substrates-1 and -2 (IRS-1 and IRS-2) and phosphatidylinositol 3-kinase isoforms in liver and muscle of the obese diabetic (ob/ob) mouse. *The Journal of Clinical Investigation*, *100*(12), 3164–3172. https://doi.org/10.1172/JCI119872

Kido, Y., Burks, D. J., Withers, D., Bruning, J. C., Kahn, C. R., White, M. F., & Accili, D. (2000). Tissue-specific insulin resistance in mice with mutations in the insulin receptor, IRS-1, and IRS-2. *The Journal of Clinical Investigation*, *105*(2), 199–205. https://doi.org/10.1172/JCI7917

Kim, A., Nam, Y. J., Shin, Y. K., Lee, M. S., Sohn, D. S., & Lee, C. S. (2017). Rotundarpene inhibits TNF-α-induced activation of the Akt, mTOR, and NF-κB pathways, and the JNK and p38 associated with production of reactive oxygen species. *Molecular and Cellular Biochemistry*, *434*(1–2), 113–125. https://doi.org/10.1007/s11010-017-3041-x

Kim, J.-I., Lee, H.-R., Sim, S., Baek, J., Yu, N.-K., Choi, J.-H., … Kaang, B.-K. (2011). PI3Kγ is required for NMDA receptor-dependent long-term depression and behavioral flexibility. *Nature Neuroscience*, *14*(11), 1447–1454. https://doi.org/10.1038/nn.2937

Kim, S. J., DeStefano, M. A., Oh, W. J., Wu, C., Vega-Cotto, N. M., Finlan, M., … Jacinto, E. (2012). mTOR complex 2 regulates proper turnover of insulin receptor substrate-1 via the ubiquitin ligase subunit Fbw8. *Molecular Cell*, *48*(6), 875–887. https://doi.org/10.1016/j.molcel.2012.09.029

Kleiger, G., Saha, A., Lewis, S., Kuhlman, B., & Deshaies, R. J. (2009). Rapid E2-E3 assembly and disassembly enable processive ubiquitylation of cullin-RING ubiquitin ligase substrates. *Cell*, *139*(5), 957–968. https://doi.org/10.1016/j.cell.2009.10.030

Klein, W. L. (2002). Abeta toxicity in Alzheimer's disease: globular oligomers (ADDLs) as new vaccine and drug targets. *Neurochemistry International*, *41*(5), 345–352.

Koenig, A. M., Mechanic-Hamilton, D., Xie, S. X., Combs, M. F., Cappola, A. R., Xie, L., … Arnold, S. E. (2017). Effects of the Insulin Sensitizer Metformin in Alzheimer Disease: Pilot Data From a Randomized Placebo-controlled Crossover Study. *Alzheimer Disease and Associated Disorders*, *31*(2), 107–113. https://doi.org/10.1097/WAD.0000000000000202

Kuljiš, R. O., & Salković-Petrišić, M. (2011). Dementia, diabetes, Alzheimer's disease, and insulin resistance in the brain: progress, dilemmas, new opportunities, and a hypothesis to tackle intersecting epidemics. *Journal of Alzheimer's Disease: JAD*, *25*(1), 29–41. https://doi.org/10.3233/JAD-2011-101392

Kummer, M. P., & Heneka, M. T. (2014). Truncated and modified amyloid-beta species. *Alzheimer's Research & Therapy*, *6*(3), 28. https://doi.org/10.1186/alzrt258

Labouèbe, G., Liu, S., Dias, C., Zou, H., Wong, J. C. Y., Karunakaran, S., … Borgland, S. L. (2013). Insulin induces long-term depression of ventral tegmental area dopamine neurons via endocannabinoids. *Nature Neuroscience*, *16*(3), 300–308. https://doi.org/10.1038/nn.3321

Lacor, P. N., Buniel, M. C., Furlow, P. W., Clemente, A. S., Velasco, P. T., Wood, M., … Klein, W. L. (2007). Abeta oligomer-induced aberrations in synapse composition, shape, and density provide a molecular basis for loss of connectivity in Alzheimer's disease. *The Journal of Neuroscience: The Official Journal of the Society for Neuroscience*, *27*(4), 796–807. https://doi.org/10.1523/JNEUROSCI.3501-06.2007

Lambert, M. P., Barlow, A. K., Chromy, B. A., Edwards, C., Freed, R., Liosatos, M., … Klein, W. L. (1998). Diffusible, nonfibrillar ligands derived from Abeta1-42 are potent central nervous system neurotoxins. *Proceedings of the National Academy of Sciences of the United States of America*, *95*(11), 6448–6453.

Lavan, B. E., Fantin, V. R., Chang, E. T., Lane, W. S., Keller, S. R., & Lienhard, G. E. (1997). A novel 160-kDa phosphotyrosine protein in insulin-treated embryonic kidney cells is a new member of the insulin receptor substrate family. *The Journal of Biological Chemistry*, *272*(34), 21403–21407.

Lazarevic, V., Fieńko, S., Andres-Alonso, M., Anni, D., Ivanova, D., Montenegro-Venegas, C., … Fejtova, A. (2017). Physiological Concentrations of Amyloid Beta Regulate Recycling of Synaptic Vesicles via Alpha7 Acetylcholine Receptor and CDK5/Calcineurin Signaling. *Frontiers in Molecular Neuroscience*, *10*, 221. https://doi.org/10.3389/fnmol.2017.00221

Lebovitz, H. E. (2001). Insulin resistance: definition and consequences. *Experimental and Clinical Endocrinology & Diabetes: Official Journal, German Society of Endocrinology [and] German Diabetes Association*, *109 Suppl 2*, S135-148. https://doi.org/10.1055/s-2001-18576

Lebovitz, Harold E. (2006). Insulin resistance--a common link between type 2 diabetes and cardiovascular disease. *Diabetes, Obesity & Metabolism*, *8*(3), 237–249. https://doi.org/10.1111/j.1463-1326.2005.00521.x

Lee, C.-C., Huang, C.-C., & Hsu, K.-S. (2011). Insulin promotes dendritic spine and synapse formation by the PI3K/Akt/mTOR and Rac1 signaling pathways. *Neuropharmacology*, *61*(4), 867–879. https://doi.org/10.1016/j.neuropharm.2011.06.003

Leino, R. L., Gerhart, D. Z., van Bueren, A. M., McCall, A. L., & Drewes, L. R. (1997). Ultrastructural localization of GLUT 1 and GLUT 3 glucose transporters in rat brain. *Journal of Neuroscience Research*, *49*(5), 617–626. https://doi.org/10.1002/(SICI)1097-4547(19970901)49:5<617::AID-JNR12>3.0.CO;2-S

Liu, Y.-F., Herschkovitz, A., Boura-Halfon, S., Ronen, D., Paz, K., Leroith, D., & Zick, Y. (2004). Serine phosphorylation proximal to its phosphotyrosine binding domain inhibits insulin receptor substrate 1 function and promotes insulin resistance. *Molecular and Cellular Biology*, *24*(21), 9668–9681. https://doi.org/10.1128/MCB.24.21.9668-9681.2004

Lopez-Salon, M., Alonso, M., Vianna, M. R., Viola, H., Mello e Souza, T., Izquierdo, I., … Medina, J. H. (2001). The ubiquitin-proteasome cascade is required for mammalian long-term memory formation. *The European Journal of Neuroscience*, *14*(11), 1820–1826.

Lourenco, M. V., Clarke, J. R., Frozza, R. L., Bomfim, T. R., Forny-Germano, L., Batista, A. F., … De Felice, F. G. (2013). TNF-α mediates PKR-dependent memory impairment and brain IRS-1 inhibition induced by Alzheimer's β-amyloid oligomers in mice and monkeys. *Cell Metabolism*, *18*(6), 831–843. https://doi.org/10.1016/j.cmet.2013.11.002

Luo, M., Langlais, P., Yi, Z., Lefort, N., De Filippis, E. A., Hwang, H., … Mandarino, L. J. (2007). Phosphorylation of human insulin receptor substrate-1 at Serine 629 plays a positive role in insulin signaling. *Endocrinology*, *148*(10), 4895–4905. https://doi.org/10.1210/en.2007-0049

Lüthi, A., Van der Putten, H., Botteri, F. M., Mansuy, I. M., Meins, M., Frey, U., … Monard, D. (1997). Endogenous serine protease inhibitor modulates epileptic activity and hippocampal long-term potentiation. *The Journal of Neuroscience: The Official Journal of the Society for Neuroscience*, *17*(12), 4688–4699.

Lutski, M., Weinstein, G., Goldbourt, U., & Tanne, D. (2017). Insulin Resistance and Future Cognitive Performance and Cognitive Decline in Elderly Patients with Cardiovascular Disease. *Journal of Alzheimer's Disease: JAD*, *57*(2), 633–643. https://doi.org/10.3233/JAD-161016

Ma, Q.-L., Yang, F., Rosario, E. R., Ubeda, O. J., Beech, W., Gant, D. J., … Cole, G. M. (2009). Beta-amyloid oligomers induce phosphorylation of tau and inactivation of insulin receptor substrate via c-Jun N-terminal kinase signaling: suppression by omega-3 fatty acids and curcumin. *The Journal of Neuroscience: The Official Journal of the Society for Neuroscience*, *29*(28), 9078–9089. https://doi.org/10.1523/JNEUROSCI.1071-09.2009

Malenka, R. C. (1994). Synaptic plasticity in the hippocampus: LTP and LTD. *Cell*, *78*(4), 535–538.

Mandler, M., Walker, L., Santic, R., Hanson, P., Upadhaya, A. R., Colloby, S. J., … Attems, J. (2014). Pyroglutamylated amyloid-β is associated with hyperphosphorylated tau and severity of Alzheimer's disease. *Acta Neuropathologica*, *128*(1), 67–79. https://doi.org/10.1007/s00401-014-1296-9

Mandolesi, L., Polverino, A., Montuori, S., Foti, F., Ferraioli, G., Sorrentino, P., & Sorrentino, G. (2018). Effects of Physical Exercise on Cognitive Functioning and Wellbeing: Biological and Psychological Benefits. *Frontiers in Psychology*, *9*, 509. https://doi.org/10.3389/fpsyg.2018.00509

Mardilovich, K., Pankratz, S. L., & Shaw, L. M. (2009). Expression and function of the insulin receptor substrate proteins in cancer. *Cell Communication and Signaling: CCS*, *7*, 14. https://doi.org/10.1186/1478-811X-7-14

Matthews, F. E., Brayne, C., Lowe, J., McKeith, I., Wharton, S. B., & Ince, P. (2009). Epidemiological pathology of dementia: attributable-risks at death in the Medical Research Council Cognitive Function and Ageing Study. *PLoS Medicine*, *6*(11), e1000180. https://doi.org/10.1371/journal.pmed.1000180

Mayer, C. M., & Belsham, D. D. (2010). Central insulin signaling is attenuated by long-term insulin exposure via insulin receptor substrate-1 serine phosphorylation, proteasomal degradation, and lysosomal insulin receptor degradation. *Endocrinology*, *151*(1), 75–84. https://doi.org/10.1210/en.2009-0838

McCall, A. L., Van Bueren, A. M., Moholt-Siebert, M., Cherry, N. J., & Woodward, W. R. (1994). Immunohistochemical localization of the neuron-specific glucose transporter (GLUT3) to neuropil in adult rat brain. *Brain Research*, *659*(1–2), 292–297.

McNay, E. C., & Recknagel, A. K. (2011). Brain insulin signaling: a key component of cognitive processes and a potential basis for cognitive impairment in type 2 diabetes. *Neurobiology of Learning and Memory*, *96*(3), 432–442. https://doi.org/10.1016/j.nlm.2011.08.005

Meraz-Ríos, M. A., Toral-Rios, D., Franco-Bocanegra, D., Villeda-Hernández, J., & Campos-Peña, V. (2013). Inflammatory process in Alzheimer's Disease. *Frontiers in Integrative Neuroscience*, *7*, 59. https://doi.org/10.3389/fnint.2013.00059

Moller, D. E. (2000). Potential role of TNF-alpha in the pathogenesis of insulin resistance and type 2 diabetes. *Trends in Endocrinology and Metabolism: TEM*, *11*(6), 212–217.

Moloney, A. M., Griffin, R. J., Timmons, S., O'Connor, R., Ravid, R., & O'Neill, C. (2010). Defects in IGF-1 receptor, insulin receptor and IRS-1/2 in Alzheimer's disease indicate possible resistance to IGF-1 and insulin signalling. *Neurobiology of Aging*, *31*(2), 224–243. https://doi.org/10.1016/j.neurobiolaging.2008.04.002

Motta, K., Barbosa, A. M., Bobinski, F., Boschero, A. C., & Rafacho, A. (2015). JNK and IKKβ phosphorylation is reduced by glucocorticoids in adipose tissue from insulin-resistant rats. *The Journal of Steroid Biochemistry and Molecular Biology*, *145*, 1–12. https://doi.org/10.1016/j.jsbmb.2014.09.024

Nielsen, H. M., Mulder, S. D., Beliën, J. A. M., Musters, R. J. P., Eikelenboom, P., & Veerhuis, R. (2010). Astrocytic A beta 1-42 uptake is determined by A beta-aggregation state and the presence of amyloid-associated proteins. *Glia*, *58*(10), 1235–1246. https://doi.org/10.1002/glia.21004

Nussbaum, J. M., Schilling, S., Cynis, H., Silva, A., Swanson, E., Wangsanut, T., … Bloom, G. S. (2012). Prion-like behaviour and tau-dependent cytotoxicity of pyroglutamylated amyloid-β. *Nature*, *485*(7400), 651–655. https://doi.org/10.1038/nature11060

Oh, W. J., & Jacinto, E. (2011). mTOR complex 2 signaling and functions. *Cell Cycle (Georgetown, Tex.)*, *10*(14), 2305–2316. https://doi.org/10.4161/cc.10.14.16586

Oudit, G. Y., Sun, H., Kerfant, B.-G., Crackower, M. A., Penninger, J. M., & Backx, P. H. (2004). The role of phosphoinositide-3 kinase and PTEN in cardiovascular

physiology and disease. *Journal of Molecular and Cellular Cardiology*, *37*(2), 449–471. https://doi.org/10.1016/j.yjmcc.2004.05.015

Pan, Z.-Q., Kentsis, A., Dias, D. C., Yamoah, K., & Wu, K. (2004). Nedd8 on cullin: building an expressway to protein destruction. *Oncogene*, *23*(11), 1985–1997. https://doi.org/10.1038/sj.onc.1207414

Park, H.-S., Ju, U.-I., Park, J.-W., Song, J. Y., Shin, D. H., Lee, K.-H., … Chun, Y.-S. (2016). PPARγ neddylation essential for adipogenesis is a potential target for treating obesity. *Cell Death and Differentiation*, *23*(8), 1296–1311. https://doi.org/10.1038/cdd.2016.6

Pasinetti, G. M., & Eberstein, J. A. (2008). Metabolic syndrome and the role of dietary lifestyles in Alzheimer's disease. *Journal of Neurochemistry*, *106*(4), 1503–1514. https://doi.org/10.1111/j.1471-4159.2008.05454.x

Paz, K., Liu, Y. F., Shorer, H., Hemi, R., LeRoith, D., Quan, M., … Zick, Y. (1999). Phosphorylation of insulin receptor substrate-1 (IRS-1) by protein kinase B positively regulates IRS-1 function. *The Journal of Biological Chemistry*, *274*(40), 28816–28822.

Pearson, H. A., & Peers, C. (2006). Physiological roles for amyloid beta peptides. *The Journal of Physiology*, *575*(Pt 1), 5–10. https://doi.org/10.1113/jphysiol.2006.111203

Perez-Nievas, B. G., Stein, T. D., Tai, H.-C., Dols-Icardo, O., Scotton, T. C., Barroeta-Espar, I., … Gómez-Isla, T. (2013). Dissecting phenotypic traits linked to human resilience to Alzheimer's pathology. *Brain: A Journal of Neurology*, *136*(Pt 8), 2510–2526. https://doi.org/10.1093/brain/awt171

Petrella, J. R. (2013). Neuroimaging and the search for a cure for Alzheimer disease. *Radiology*, *269*(3), 671–691. https://doi.org/10.1148/radiol.13122503

Petroski, M. D., & Deshaies, R. J. (2005). Function and regulation of cullin-RING ubiquitin ligases. *Nature Reviews. Molecular Cell Biology*, *6*(1), 9–20. https://doi.org/10.1038/nrm1547

Petrov, D., Pedrós, I., Artiach, G., Sureda, F. X., Barroso, E., Pallàs, M., … Camins, A. (2015). High-fat diet-induced deregulation of hippocampal insulin signaling and mitochondrial homeostasis deficiences contribute to Alzheimer disease pathology in rodents. *Biochimica Et Biophysica Acta*, *1852*(9), 1687–1699. https://doi.org/10.1016/j.bbadis.2015.05.004

Plomgaard, P., Bouzakri, K., Krogh-Madsen, R., Mittendorfer, B., Zierath, J. R., & Pedersen, B. K. (2005). Tumor necrosis factor-alpha induces skeletal muscle insulin resistance in healthy human subjects via inhibition of Akt substrate 160 phosphorylation. *Diabetes*, *54*(10), 2939–2945.

Plum, L., Schubert, M., & Brüning, J. C. (2005). The role of insulin receptor signaling in the brain. *Trends in Endocrinology and Metabolism: TEM*, *16*(2), 59–65. https://doi.org/10.1016/j.tem.2005.01.008

Pomel, V., Klicic, J., Covini, D., Church, D. D., Shaw, J. P., Roulin, K., … Rückle, T. (2006). Furan-2-ylmethylene thiazolidinediones as novel, potent, and selective inhibitors of phosphoinositide 3-kinase gamma. *Journal of Medicinal Chemistry*, *49*(13), 3857–3871. https://doi.org/10.1021/jm0601598

Ponyeam, W., & Hagen, T. (2012). Characterization of the Cullin7 E3 ubiquitin ligase--heterodimerization of cullin substrate receptors as a novel mechanism to regulate

cullin E3 ligase activity. *Cellular Signalling*, *24*(1), 290–295. https://doi.org/10.1016/j.cellsig.2011.08.020

Portelius, E., Bogdanovic, N., Gustavsson, M. K., Volkmann, I., Brinkmalm, G., Zetterberg, H., … Blennow, K. (2010). Mass spectrometric characterization of brain amyloid beta isoform signatures in familial and sporadic Alzheimer's disease. *Acta Neuropathologica*, *120*(2), 185–193. https://doi.org/10.1007/s00401-010-0690-1

Price, J. L., McKeel, D. W., Buckles, V. D., Roe, C. M., Xiong, C., Grundman, M., … Morris, J. C. (2009). Neuropathology of nondemented aging: presumptive evidence for preclinical Alzheimer disease. *Neurobiology of Aging*, *30*(7), 1026–1036. https://doi.org/10.1016/j.neurobiolaging.2009.04.002

Profenno, L. A., Porsteinsson, A. P., & Faraone, S. V. (2010). Meta-analysis of Alzheimer's disease risk with obesity, diabetes, and related disorders. *Biological Psychiatry*, *67*(6), 505–512. https://doi.org/10.1016/j.biopsych.2009.02.013

Raichle, M. E., & Gusnard, D. A. (2002). Appraising the brain's energy budget. *Proceedings of the National Academy of Sciences of the United States of America*, *99*(16), 10237–10239. https://doi.org/10.1073/pnas.172399499

Reaven, G. M. (1988). Banting lecture 1988. Role of insulin resistance in human disease. *Diabetes*, *37*(12), 1595–1607.

Russo, C., Saido, T. C., DeBusk, L. M., Tabaton, M., Gambetti, P., & Teller, J. K. (1997). Heterogeneity of water-soluble amyloid beta-peptide in Alzheimer's disease and Down's syndrome brains. *FEBS Letters*, *409*(3), 411–416.

Saez, I., Duran, J., Sinadinos, C., Beltran, A., Yanes, O., Tevy, M. F., … Guinovart, J. J. (2014). Neurons have an active glycogen metabolism that contributes to tolerance to hypoxia. *Journal of Cerebral Blood Flow and Metabolism: Official Journal of the International Society of Cerebral Blood Flow and Metabolism*, *34*(6), 945–955. https://doi.org/10.1038/jcbfm.2014.33

Saido, T. C., Iwatsubo, T., Mann, D. M., Shimada, H., Ihara, Y., & Kawashima, S. (1995). Dominant and differential deposition of distinct beta-amyloid peptide species, A beta N3(pE), in senile plaques. *Neuron*, *14*(2), 457–466.

Saido, T. C., Yamao-Harigaya, W., Iwatsubo, T., & Kawashima, S. (1996). Amino- and carboxyl-terminal heterogeneity of beta-amyloid peptides deposited in human brain. *Neuroscience Letters*, *215*(3), 173–176.

Sarikas, A., Hartmann, T., & Pan, Z.-Q. (2011). The cullin protein family. *Genome Biology*, *12*(4), 220. https://doi.org/10.1186/gb-2011-12-4-220

Schilling, S., Lauber, T., Schaupp, M., Manhart, S., Scheel, E., Böhm, G., & Demuth, H.-U. (2006). On the seeding and oligomerization of pGlu-amyloid peptides (in vitro). *Biochemistry*, *45*(41), 12393–12399. https://doi.org/10.1021/bi0612667

Schilling, S., Zeitschel, U., Hoffmann, T., Heiser, U., Francke, M., Kehlen, A., … Rossner, S. (2008). Glutaminyl cyclase inhibition attenuates pyroglutamate Abeta and Alzheimer's disease-like pathology. *Nature Medicine*, *14*(10), 1106–1111. https://doi.org/10.1038/nm.1872

Schlenzig, D., Manhart, S., Cinar, Y., Kleinschmidt, M., Hause, G., Willbold, D., … Demuth, H.-U. (2009). Pyroglutamate formation influences solubility and amyloidogenicity of amyloid peptides. *Biochemistry*, *48*(29), 7072–7078. https://doi.org/10.1021/bi900818a

Schubert, M., Brazil, D. P., Burks, D. J., Kushner, J. A., Ye, J., Flint, C. L., … White, M. F. (2003). Insulin receptor substrate-2 deficiency impairs brain growth and promotes tau phosphorylation. *The Journal of Neuroscience: The Official Journal of the Society for Neuroscience*, *23*(18), 7084–7092.

Scott, P. H., Brunn, G. J., Kohn, A. D., Roth, R. A., & Lawrence, J. C. (1998). Evidence of insulin-stimulated phosphorylation and activation of the mammalian target of rapamycin mediated by a protein kinase B signaling pathway. *Proceedings of the National Academy of Sciences of the United States of America*, *95*(13), 7772–7777.

Scuteri, A., Laurent, S., Cucca, F., Cockcroft, J., Cunha, P. G., Mañas, L. R., … Metabolic Syndrome and Arteries Research (MARE) Consortium. (2015). Metabolic syndrome across Europe: different clusters of risk factors. *European Journal of Preventive Cardiology*, *22*(4), 486–491. https://doi.org/10.1177/2047487314525529

Seidenbecher, C. I., Landwehr, M., Smalla, K.-H., Kreutz, M., Dieterich, D. C., Zuschratter, W., … Kreutz, M. R. (2004). Caldendrin but not calmodulin binds to light chain 3 of MAP1A/B: an association with the microtubule cytoskeleton highlighting exclusive binding partners for neuronal Ca(2+)-sensor proteins. *Journal of Molecular Biology*, *336*(4), 957–970. https://doi.org/10.1016/j.jmb.2003.12.054

Selkoe, D. J. (2002). Alzheimer's disease is a synaptic failure. *Science (New York, N.Y.)*, *298*(5594), 789–791. https://doi.org/10.1126/science.1074069

Sergeant, N., Bombois, S., Ghestem, A., Drobecq, H., Kostanjevecki, V., Missiaen, C., … Delacourte, A. (2003). Truncated beta-amyloid peptide species in pre-clinical Alzheimer's disease as new targets for the vaccination approach. *Journal of Neurochemistry*, *85*(6), 1581–1591.

Sevillano, J., de Castro, J., Bocos, C., Herrera, E., & Ramos, M. P. (2007). Role of insulin receptor substrate-1 serine 307 phosphorylation and adiponectin in adipose tissue insulin resistance in late pregnancy. *Endocrinology*, *148*(12), 5933–5942. https://doi.org/10.1210/en.2007-0352

Shah, O. J., & Hunter, T. (2006). Turnover of the active fraction of IRS1 involves raptor-mTOR- and S6K1-dependent serine phosphorylation in cell culture models of tuberous sclerosis. *Molecular and Cellular Biology*, *26*(17), 6425–6434. https://doi.org/10.1128/MCB.01254-05

Shankar, G. M., Bloodgood, B. L., Townsend, M., Walsh, D. M., Selkoe, D. J., & Sabatini, B. L. (2007). Natural oligomers of the Alzheimer amyloid-beta protein induce reversible synapse loss by modulating an NMDA-type glutamate receptor-dependent signaling pathway. *The Journal of Neuroscience: The Official Journal of the Society for Neuroscience*, *27*(11), 2866–2875. https://doi.org/10.1523/JNEUROSCI.4970-06.2007

Shankar, G. M., Li, S., Mehta, T. H., Garcia-Munoz, A., Shepardson, N. E., Smith, I., … Selkoe, D. J. (2008). Amyloid-beta protein dimers isolated directly from Alzheimer's brains impair synaptic plasticity and memory. *Nature Medicine*, *14*(8), 837–842. https://doi.org/10.1038/nm1782

Shankar, G. M., & Walsh, D. M. (2009). Alzheimer's disease: synaptic dysfunction and Abeta. *Molecular Neurodegeneration*, *4*, 48. https://doi.org/10.1186/1750-1326-4-48

Sikkes, S. A. M., van den Berg, M. T., Knol, D. L., de Lange-de Klerk, E. S. M., Scheltens, P., Uitdehaag, B. M. J., … Pijnenburg, Y. A. L. (2010). How useful is the IQCODE for discriminating between Alzheimer's disease, mild cognitive impairment and subjective memory complaints? *Dementia and Geriatric Cognitive Disorders*, *30*(5), 411–416. https://doi.org/10.1159/000321697

Simpson, J. E., Ince, P. G., Shaw, P. J., Heath, P. R., Raman, R., Garwood, C. J., … MRC Cognitive Function and Ageing Neuropathology Study Group. (2011). Microarray analysis of the astrocyte transcriptome in the aging brain: relationship to Alzheimer's pathology and APOE genotype. *Neurobiology of Aging*, *32*(10), 1795–1807. https://doi.org/10.1016/j.neurobiolaging.2011.04.013

Sinadinos, C., Valles-Ortega, J., Boulan, L., Solsona, E., Tevy, M. F., Marquez, M., … Guinovart, J. J. (2014). Neuronal glycogen synthesis contributes to physiological aging. *Aging Cell*, *13*(5), 935–945. https://doi.org/10.1111/acel.12254

Smalla, K.-H., Seidenbecher, C. I., Tischmeyer, W., Schicknick, H., Wyneken, U., Böckers, T. M., … Kreutz, M. R. (2003). Kainate-induced epileptic seizures induce a recruitment of caldendrin to the postsynaptic density in rat brain. *Brain Research. Molecular Brain Research*, *116*(1–2), 159–162.

Sonar, S. A., & Lal, G. (2017). Differentiation and Transmigration of CD4 T Cells in Neuroinflammation and Autoimmunity. *Frontiers in Immunology*, *8*, 1695. https://doi.org/10.3389/fimmu.2017.01695

Soucy, T. A., Smith, P. G., Milhollen, M. A., Berger, A. J., Gavin, J. M., Adhikari, S., … Langston, S. P. (2009). An inhibitor of NEDD8-activating enzyme as a new approach to treat cancer. *Nature*, *458*(7239), 732–736. https://doi.org/10.1038/nature07884

Stoyanov, B., Volinia, S., Hanck, T., Rubio, I., Loubtchenkov, M., Malek, D., … Nürnberg, B. (1995). Cloning and characterization of a G protein-activated human phosphoinositide-3 kinase. *Science (New York, N.Y.)*, *269*(5224), 690–693.

Stuart, C. A., Lee, M. L., South, M. A., Howell, M. E. A., & Stone, M. H. (2017). Muscle hypertrophy in prediabetic men after 16 wk of resistance training. *Journal of Applied Physiology (Bethesda, Md.: 1985)*, *123*(4), 894–901. https://doi.org/10.1152/japplphysiol.00023.2017

Sun, X. J., Goldberg, J. L., Qiao, L. Y., & Mitchell, J. J. (1999). Insulin-induced insulin

receptor substrate-1 degradation is mediated by the proteasome degradation pathway. *Diabetes*, *48*(7), 1359–1364.

Tai, H.-C., & Schuman, E. M. (2008). Ubiquitin, the proteasome and protein degradation in neuronal function and dysfunction. *Nature Reviews. Neuroscience*, *9*(11), 826–838. https://doi.org/10.1038/nrn2499

Talbot, K., Wang, H.-Y., Kazi, H., Han, L.-Y., Bakshi, K. P., Stucky, A., … Arnold, S. E. (2012). Demonstrated brain insulin resistance in Alzheimer's disease patients is associated with IGF-1 resistance, IRS-1 dysregulation, and cognitive decline. *The Journal of Clinical Investigation*, *122*(4), 1316–1338. https://doi.org/10.1172/JCI59903

Tamemoto, H., Kadowaki, T., Tobe, K., Yagi, T., Sakura, H., Hayakawa, T., … Satoh, S. (1994). Insulin resistance and growth retardation in mice lacking insulin receptor substrate-1. *Nature*, *372*(6502), 182–186. https://doi.org/10.1038/372182a0

Taniguchi, C. M., Emanuelli, B., & Kahn, C. R. (2006). Critical nodes in signalling pathways: insights into insulin action. *Nature Reviews. Molecular Cell Biology*, *7*(2), 85–96. https://doi.org/10.1038/nrm1837

Thrower, J. S., Hoffman, L., Rechsteiner, M., & Pickart, C. M. (2000). Recognition of the polyubiquitin proteolytic signal. *The EMBO Journal*, *19*(1), 94–102. https://doi.org/10.1093/emboj/19.1.94

Tiwari, P. C., & Pal, R. (2017). The potential role of neuroinflammation and transcription factors in Parkinson disease. *Dialogues in Clinical Neuroscience*, *19*(1), 71–80.

Tong, S., Si, Y., Yu, H., Zhang, L., Xie, P., & Jiang, W. (2017). MLN4924 (Pevonedistat), a protein neddylation inhibitor, suppresses proliferation and migration of human clear cell renal cell carcinoma. *Scientific Reports*, *7*(1), 5599. https://doi.org/10.1038/s41598-017-06098-y

Tremblay, F., Brûlé, S., Hee Um, S., Li, Y., Masuda, K., Roden, M., … Marette, A. (2007). Identification of IRS-1 Ser-1101 as a target of S6K1 in nutrient- and obesity-induced insulin resistance. *Proceedings of the National Academy of Sciences of the United States of America*, *104*(35), 14056–14061. https://doi.org/10.1073/pnas.0706517104

Tsuriel, S., Geva, R., Zamorano, P., Dresbach, T., Boeckers, T., Gundelfinger, E. D., … Ziv, N. E. (2006). Local sharing as a predominant determinant of synaptic matrix molecular dynamics. *PLoS Biology*, *4*(9), e271. https://doi.org/10.1371/journal.pbio.0040271

Tuppo, E. E., & Arias, H. R. (2005). The role of inflammation in Alzheimer's disease. *The International Journal of Biochemistry & Cell Biology*, *37*(2), 289–305. https://doi.org/10.1016/j.biocel.2004.07.009

Uemura, E., & Greenlee, H. W. (2006). Insulin regulates neuronal glucose uptake by promoting translocation of glucose transporter GLUT3. *Experimental Neurology*, *198*(1), 48–53. https://doi.org/10.1016/j.expneurol.2005.10.035

Um, S. H., Frigerio, F., Watanabe, M., Picard, F., Joaquin, M., Sticker, M., … Thomas, G. (2004). Absence of S6K1 protects against age- and diet-induced obesity while enhancing insulin sensitivity. *Nature*, *431*(7005), 200–205. https://doi.org/10.1038/nature02866

Unger, J., McNeill, T. H., Moxley, R. T., White, M., Moss, A., & Livingston, J. N. (1989). Distribution of insulin receptor-like immunoreactivity in the rat forebrain. *Neuroscience*, *31*(1), 143–157.

van der Heide, L. P., Kamal, A., Artola, A., Gispen, W. H., & Ramakers, G. M. J. (2005). Insulin modulates hippocampal activity-dependent synaptic plasticity in a N-methyl-d-aspartate receptor and phosphatidyl-inositol-3-kinase-dependent manner. *Journal of Neurochemistry*, *94*(4), 1158–1166. https://doi.org/10.1111/j.1471-4159.2005.03269.x

Vanderdys, V., Allak, A., Guessous, F., Benamar, M., Read, P. W., Jameson, M. J., & Abbas, T. (2018). The Neddylation Inhibitor Pevonedistat (MLN4924) Suppresses and Radiosensitizes Head and Neck Squamous Carcinoma Cells and Tumors. *Molecular Cancer Therapeutics*, *17*(2), 368–380. https://doi.org/10.1158/1535-7163.MCT-17-0083

Vanhanen, M., Koivisto, K., Moilanen, L., Helkala, E. L., Hänninen, T., Soininen, H., … Kuusisto, J. (2006). Association of metabolic syndrome with Alzheimer disease: a

population-based study. *Neurology*, *67*(5), 843–847. https://doi.org/10.1212/01.wnl.0000234037.91185.99

Vannucci, S. J., Maher, F., & Simpson, I. A. (1997). Glucose transporter proteins in brain: delivery of glucose to neurons and glia. *Glia*, *21*(1), 2–21.

Varshavsky, A. (2017). The Ubiquitin System, Autophagy, and Regulated Protein Degradation. *Annual Review of Biochemistry*, *86*, 123–128. https://doi.org/10.1146/annurev-biochem-061516-044859

Viola, K. L., & Klein, W. L. (2015). Amyloid β oligomers in Alzheimer's disease pathogenesis, treatment, and diagnosis. *Acta Neuropathologica*, *129*(2), 183–206. https://doi.org/10.1007/s00401-015-1386-3

Vogl, A. M., Brockmann, M. M., Giusti, S. A., Maccarrone, G., Vercelli, C. A., Bauder, C. A., … Refojo, D. (2015). Neddylation inhibition impairs spine development, destabilizes synapses and deteriorates cognition. *Nature Neuroscience*, *18*(2), 239–251. https://doi.org/10.1038/nn.3912

Walsh, D. M., Klyubin, I., Fadeeva, J. V., Rowan, M. J., & Selkoe, D. J. (2002). Amyloid-beta oligomers: their production, toxicity and therapeutic inhibition. *Biochemical Society Transactions*, *30*(4), 552–557. https://doi.org/10.1042/

Wan, Q., Xiong, Z. G., Man, H. Y., Ackerley, C. A., Braunton, J., Lu, W. Y., … Wang, Y. T. (1997). Recruitment of functional GABA(A) receptors to postsynaptic domains by insulin. *Nature*, *388*(6643), 686–690. https://doi.org/10.1038/41792

Wang, G. (2014). Raison d'être of insulin resistance: the adjustable threshold hypothesis. *Journal of the Royal Society, Interface*, *11*(101), 20140892. https://doi.org/10.1098/rsif.2014.0892

Wang, Q., Walsh, D. M., Rowan, M. J., Selkoe, D. J., & Anwyl, R. (2004). Block of long-term potentiation by naturally secreted and synthetic amyloid beta-peptide in hippocampal slices is mediated via activation of the kinases c-Jun N-terminal kinase, cyclin-dependent kinase 5, and p38 mitogen-activated protein kinase as well as metabotropic glutamate receptor type 5. *The Journal of Neuroscience: The Official Journal of the Society for Neuroscience*, *24*(13), 3370–3378. https://doi.org/10.1523/JNEUROSCI.1633-03.2004

Wang, S. H., Morris, R. G. (2010). Hippocampal-neocortical interactions in memory formation, consolidation and reconsolidation. *Annual review of psychology.* 10.1146/annurev.psych.093008.100523

Werner, E. D., Lee, J., Hansen, L., Yuan, M., & Shoelson, S. E. (2004). Insulin resistance due to phosphorylation of insulin receptor substrate-1 at serine 302. *The Journal of Biological Chemistry*, *279*(34), 35298–35305. https://doi.org/10.1074/jbc.M405203200

Wheatcroft, S. B., Williams, I. L., Shah, A. M., & Kearney, M. T. (2003). Pathophysiological implications of insulin resistance on vascular endothelial function. *Diabetic Medicine: A Journal of the British Diabetic Association*, *20*(4), 255–268.

White, J. A., Manelli, A. M., Holmberg, K. H., Van Eldik, L. J., & Ladu, M. J. (2005). Differential effects of oligomeric and fibrillar amyloid-beta 1-42 on astrocyte-mediated inflammation. *Neurobiology of Disease*, *18*(3), 459–465. https://doi.org/10.1016/j.nbd.2004.12.013

White, M. F. (2002). IRS proteins and the common path to diabetes. *American Journal of Physiology. Endocrinology and Metabolism*, *283*(3), E413-422. https://doi.org/10.1152/ajpendo.00514.2001

Wiedenmann, B., & Franke, W. W. (1985). Identification and localization of synaptophysin, an integral membrane glycoprotein of Mr 38,000 characteristic of presynaptic vesicles. *Cell*, *41*(3), 1017–1028.

Wirths, O., Bethge, T., Marcello, A., Harmeier, A., Jawhar, S., Lucassen, P. J., … Bayer, T. A. (2010). Pyroglutamate Abeta pathology in APP/PS1KI mice, sporadic and familial Alzheimer's disease cases. *Journal of Neural Transmission (Vienna, Austria: 1996)*, *117*(1), 85–96. https://doi.org/10.1007/s00702-009-0314-x

Wymann, M. P., & Pirola, L. (1998). Structure and function of phosphoinositide 3-kinases. *Biochimica Et Biophysica Acta*, *1436*(1–2), 127–150.

Wyneken, U., Smalla, K. H., Marengo, J. J., Soto, D., de la Cerda, A., Tischmeyer, W., … Gundelfinger, E. D. (2001). Kainate-induced seizures alter protein composition and N-methyl-D-aspartate receptor function of rat forebrain postsynaptic densities. *Neuroscience*, *102*(1), 65–74.

Xie, P., Yang, J.-P., Cao, Y., Peng, L.-X., Zheng, L.-S., Sun, R., … Qian, C.-N. (2017). Promoting tumorigenesis in nasopharyngeal carcinoma, NEDD8 serves as a potential theranostic target. *Cell Death & Disease*, *8*(6), e2834. https://doi.org/10.1038/cddis.2017.195

Xu, X., Sarikas, A., Dias-Santagata, D. C., Dolios, G., Lafontant, P. J., Tsai, S.-C., … Pan, Z.-Q. (2008). The CUL7 E3 ubiquitin ligase targets insulin receptor substrate 1 for ubiquitin-dependent degradation. *Molecular Cell*, *30*(4), 403–414. https://doi.org/10.1016/j.molcel.2008.03.009

Yamada, M., Ohnishi, H., Sano, S. i, Nakatani, A., Ikeuchi, T., & Hatanaka, H. (1997). Insulin receptor substrate (IRS)-1 and IRS-2 are tyrosine-phosphorylated and associated with phosphatidylinositol 3-kinase in response to brain-derived neurotrophic factor in cultured cerebral cortical neurons. *The Journal of Biological Chemistry*, *272*(48), 30334–30339.

Yarchoan, M., Toledo, J. B., Lee, E. B., Arvanitakis, Z., Kazi, H., Han, L.-Y., … Arnold, S. E. (2014). Abnormal serine phosphorylation of insulin receptor substrate 1 is associated with tau pathology in Alzheimer's disease and tauopathies. *Acta Neuropathologica*, *128*(5), 679–689. https://doi.org/10.1007/s00401-014-1328-5

Yoneyama, Y., Inamitsu, T., Chida, K., Iemura, S.-I., Natsume, T., Maeda, T., … Takahashi, S.-I. (2018). Serine Phosphorylation by mTORC1 Promotes IRS-1 Degradation through SCFβ-TRCP E3 Ubiquitin Ligase. *IScience*, *5*, 1–18. https://doi.org/10.1016/j.isci.2018.06.006

Youngren, J. F. (2007). Regulation of insulin receptor function. *Cellular and Molecular Life Sciences: CMLS*, *64*(7–8), 873–891. https://doi.org/10.1007/s00018-007-6359-9

Yuanxiang, P., Bera, S., Karpova, A., Kreutz, M. R., & Mikhaylova, M. (2014). Isolation of CA1 nuclear enriched fractions from hippocampal slices to study activity-dependent nuclear import of synapto-nuclear messenger proteins. *Journal of Visualized Experiments: JoVE*, (90), e51310. https://doi.org/10.3791/51310

Zhande, R., Mitchell, J. J., Wu, J., & Sun, X. J. (2002). Molecular mechanism of insulin-induced degradation of insulin receptor substrate 1. *Molecular and Cellular Biology*, *22*(4), 1016–1026.

Zhang, X., Tang, S., Zhang, Q., Shao, W., Han, X., Wang, Y., & Du, Y. (2016). Endoplasmic reticulum stress mediates JNK-dependent IRS-1 serine phosphorylation and results in Tau hyperphosphorylation in amyloid β oligomer-treated PC12 cells and primary neurons. *Gene*, *587*(2), 183–193. https://doi.org/10.1016/j.gene.2016.05.018

Zhao, W. Q., & Alkon, D. L. (2001). Role of insulin and insulin receptor in learning and memory. *Molecular and Cellular Endocrinology*, *177*(1–2), 125–134.

Zhao, W., Wu, X., Xie, H., Ke, Y., & Yung, W.-H. (2010). Permissive role of insulin in the expression of long-term potentiation in the hippocampus of immature rats. *Neuro-Signals*, *18*(4), 236–245. https://doi.org/10.1159/000324040

Zhao, W.-Q., De Felice, F. G., Fernandez, S., Chen, H., Lambert, M. P., Quon, M. J., … Klein, W. L. (2008). Amyloid beta oligomers induce impairment of neuronal insulin receptors. *FASEB Journal: Official Publication of the Federation of American Societies for Experimental Biology*, *22*(1), 246–260. https://doi.org/10.1096/fj.06-7703com

Zoncu, R., Efeyan, A., & Sabatini, D. M. (2011). mTOR: from growth signal integration to cancer, diabetes and ageing. *Nature Reviews. Molecular Cell Biology*, *12*(1), 21–35. https://doi.org/10.1038/nrm3025

6. Abbreviations

4AP	4-aminopirydine
AAV9	adeno-associated virus-9
aCSF	artificial cerebrospinal fluid
AD	alzheimer's disease
Aβ	amyloid-β
Aβos	amyloid-β oligomers
Aβ3(pE)-42	pyro-glutamylated amyloid-β
AKT	RAC-alpha serine/threonine protein kinase
AMP	adenosine-5'-monophosphate
APP	amyloid precursor protein
ATP	adenosine-5'-triphosphate
B27	serum for neural cells
BAIAP2	brain-specific angiogenesis inhibitor 1-associated protein 2
BDNF	brain derived neurotrophic factor
BSA	bovine serum albumin
CAND1	Cullin-associated NEDD8-dissociated protein 1
cDNA	complementary DNA
CH	cullin homology domain
CNS	central nervous system
Co-IP	co-immunoprecipitation
CRIB	Cdc42 and Rac-interacting binding domain
CRL	cullin-RING ubiquitin ligase
C-terminus	carboxy terminus
CUL	cullin
DAPI	4'-6-Diamidino-2-phenylindole
dH_2O	distilled water
DIV	day(s) *in vitro*
DMEM	Dulbecco's Modified Eagle Medium
DMSO	dimethylsulfoxide
DNA	deoxyribonucleic acid
dNTPs	deoxy-nucleotide-triphosphates
dsRNA	double-stranded RNA
E.coli	Escherichia coli
EDTA	ethylenediaminetetraacetic acid
ELISA	enzyme-linked immunosorbent assay
ERK	extracellular signal-regulated protein kinases
FBS	fetal bovine serum
Fbxw8	F-box/WD repeat-containing protein 8
fEPSPs	field excitatory postsynaptic potentials
GFAP	glial fibrillary acidic protein
GFP	green fluorescent protein
GLUT	glucose transporter
GPCRs	G-protein coupled receptors

GSK3β	glycogen synthase kinase 3 β
HA	high affinity
HBK	HEPES-buffered Krebs-like buffer
HEK293T	human embryonic kidney-293-T
HFD	high fat diet
HFIP	1,1,1,3,3,3-hexafluoro-2-propanol
HRP	horse radish peroxidase
Iba-1	ionized calcium-binding adapter-1
IGFR	insulin-like growth factor receptor
IKK	Ikk-β kinase
InsR	insulin receptor
IRS	insulin receptor substrate
ICC	immunocytochemistry
IHC	immunohistochemistry
IMD	IRSp53/MIM Homology Domain
IR	Insulin resistance
JNK	c-Jun-N-terminal kinase
kDa	kilo Dalton
LB	lysogeny broth
LTD	long-term depression
LTP	long-term potentiation
MAP2	microtubule-associated protein 2
MAPK	mitogen-activated protein kinase
MetS	metabolic syndrome
MLN-4924	Pevonedistat
mRNA	messenger ribonucleic acid
mTOR	mammalian target for rapamycin
mTORC	mammalian target for rapamycin complex
N-terminus	amino terminus
Na_3VO_4	sodium orthovanadate
NAE	NEDD8 –activating enzyme
NB	neurobasal medium
NB+	complete neurobasal medium
NB-	antibiotic-free neurobasal medium
NEDD8	neural precursor cell-expressed developmentally down-regulated gene 8
NeuN	neuronal Nuclear Antigen and Neuron Differentiation Marker
NMDAR	N-methyl D-aspartate receptors
o/n	over night
P2-fraction	crude membrane fraction
PAGE	polyacrylamide gel electrophoresis
PBS	phosphate buffered saline
PC	prohormone convertase
PCR	polymerase chain reaction
PDK1	3-phosphoinositide-dependent protein kinase-1
PDZ	Post-synaptic Density 95/Disc Large/Zonula Occludens-1 domain
PFA	paraformaldehyde
pH	potentium hydrogenii

PH	pleckstrin homology domain
PKC	protein kinase C
PKR	protein kinase R
$PI(3,4,5)P_2$	phosphatidylinositol (3,4)-biphosphate
$PI(3,4,5)P_3$	phosphatidylinositol (3,4,5)-triphosphate
PI3K	phosphatidylinositol-3-kinase
pS	phospho-serine
PSD	postsynaptic density
PSD95	postsynaptic dendisty-95
PTB	phospho-tyrosine binding domain
pY	phospho-tyrosine
QC	glutaminyl cyclase
RD	regular diet
RING	really interesting gene
RIPA	radioimmunoprecipitation assay buffer
ROI	region of interest
RT	room temperature
S6K	ribosomal protein S6 kinase beta-1
s.e.m.	standard error of the mean
SDS	sodium dodecyl sulfate
Ser	serine
SH2	Src-homology domain-2
SH3	Src-homology domain-3
Shank3	SH3 and multiple ankyrin repeat domains protein-3
shRNA	short hairpin RNA
SOC	super optimal broth with catabolite repression
TBS	TRIS buffered saline
TBS-T	TBS-Twin
TEMED	Tetramethylethylenediamine
Thy1	cell surface antigen
TNE	Tris-NaCl-EDT buffer
TNFαR	TNFα receptor
TNFα	tumor necrosis factor α
TRH	thyroliberin
Tyr	tyrosine
Ubiq	Ubiquitin
WB	western blot
+/+	wild-type
+/Tg	heterozygous

Ehrenerklärung

Ich versichere hiermit, dass ich die vorliegende Arbeit ohne unzulässige Hilfe Dritter und ohne Benutzung anderer als der angegebenen Hilfsmittel angefertigt habe; verwendete fremde und eigene Quellen sind als solche kenntlich gemacht.

Ich habe insbesondere nicht wissentlich:
- Ergebnisse erfunden oder widersprüchlich Ergebnisse verschwiegen,
- statistische Verfahren absichtlich missbraucht, um Daten in ungerechtfertigter Weise zu interpretieren,
- fremde Ergebnisse oder Veröffentlichungen plagiiert,
- fremde Forschungsergebnisse verzerrt wiedergegeben.

Mir ist bekannt, dass Verstöße gegen das Urheberrecht Unterlassungs- und Schadensersatzansprüche des Urhebers sowie eine strafrechtliche Ahndung durch die Strafverfolgungsbehörden begründen kann.

Ich erkläre mich damit einverstanden, dass die Arbeit ggf. mit Mitteln der elektronischen Datenverarbeitung auf Plagiate überprüft werden kann.

Die Arbeit wurde bisher weder im Inland noch im Ausland in gleicher oder ähnlicher Form als Dissertation eingereicht und ist als Ganzes auch noch nicht veröffentlicht.

Magdeburg, 05.06.2019

Alessandro Dario Confettura